SPENT FUEL MEASUREMENTS: PASSIVE NEUTRON ALBEDO REACTIVITY (PNAR) AND PHOTON SIGNATURES

A Dissertation

by

JULIA M. EIGENBRODT

Submitted to the Office of Graduate and Professional Studies of
Texas A&M University
in partial fulfillment of the requirements for the degree of

DOCTOR OF PHILOSOPHY

Chair of Committee,	William S. Charlton
Committee Members,	Pavel V. Tsvetkov
	Riccardo Bettati
	Sunil S. Chirayath
Head of Department,	Yassin A. Hassan

May 2016

Major Subject: Nuclear Engineering

ABSTRACT

The International Atomic Energy Agency's (IAEA) safeguards technical objective is the timely detection of a diversion of a significant quantity of nuclear material from peaceful activities to the manufacture of nuclear weapons or of other nuclear explosive devices or for purposes unknown, and deterrence of such diversion by the risk of early detection. An important IAEA task towards meeting this objective is the ability to accurately and reliably measure spent nuclear fuel (SNF) to verify reactor operating parameters and verify that the fuel has not been removed from reactors or SNF storage facilities. This dissertation analyzes a method to improve the state-of-the-art of nuclear material safeguards measurements using two combined measurement techniques: passive neutron albedo reactivity (PNAR) and passive spectral photon measurements.

PNAR was used for measurements of SNF in Japan as well as fresh fuel pins at Los Alamos National Laboratory (LANL). The measured PNAR signal was shown to trend well with neutron multiplication and fissile content of the SNF. The PNAR measurements showed a 73% change in signal for a fuel burnup range of 7.1 to 19.2 GWd/MTHM of spent mixed-oxide (MOX) fuel and a 40% change in signal over a range of initial ^{235}U enrichment from 0.2% to 3.2% in UO_2 fuel.

Photon measurements were performed on a wide range of SNF pins to determine which photon signatures are visible in different sets of fuels. These signatures were then investigated and tested using a sensitivity analysis to determine the spent fuel parameters to which each signal is most sensitive. These photon signatures can be used to determine SNF parameters that can support PNAR determination of SNF fissile content.

Based on the results from these measurements, we have concluded that spectral photon measurements can determine operating parameters to improve the implementation of PNAR. We also concluded that PNAR can accurately measure multiplication and fissile content in SNF with standard deviations of 1% and 4%, respectively. The PNAR and photon measurements can be used together as a powerful tool to support the IAEA safeguards technical objective.

ACKNOWLEDGEMENTS

I would like to thank my advisor, Dr. William Charlton, for the advice and guidance through several years as an undergraduate research assistant and graduate student. I would also like to thank Dr. Sunil Chirayath for his continual insight and encouragement. Thanks to other committee members, Dr. Pavel Tsvetkov, and Dr. Riccardo Bettati, for their time and support.

Several staff members at Los Alamos National Laboratory have also been an invaluable resource during my research and experiments. I would especially like to thank Dr. Howard Menlove and Dr. Stephen Tobin for their support and guidance developing my methods and analyzing experiments. Many thanks to Dr. Johnna Marlow, and Dr. Martyn Swinhoe, Dr. Holly Trellue, Carlos Rael, and Isaac Martinez for help and during my time at LANL and during the PNAR measurements.

Thanks also to Alan Bolind, Inoue-san, and Seya-san, along with the rest of the JAEA and Fugen staff during measurements at Fugen, as well as the ORNL staff support during photon pin measurements.

I would also like to thank my friends and family who have provided continually support. Special thanks and appreciation for my parents and husband, who have been endless sources of encouragement.

Finally, I would like to acknowledge the support of Next Generation Safeguards Initiative (NGSI), Office of Nonproliferation and International Security (NIS), National Nuclear Security Administration (NNSA) and the Ministry of Education, Culture, Sports, Science and Technology (MEXT) of Japan

NOMENCLATURE

ADEPT	Advanced Diagnostics and Evaluation PlaTform
BWR	Boiling Water Reactor
DA	Destructive Analysis
HPGe	High-Purity Germanium
IAEA	International Atomic Energy Agency
LANL	Los Alamos National Laboratory
LEU	Low-Enriched Uranium
LWR	Light Water Reactor
MCNP	Monte Carlo N-Particle
MOX	Mixed Oxide
MTHM	Metric Tons Heavy Metal
NGSI	Next Generation Safeguards Initiative
NDA	Non-destructive Analysis
ORNL	Oak Ridge National Laboratory
PNAR	Passive Neutron Albedo Reactivity
PWR	Pressurized Water Reactor
SNF	Spent Nuclear Fuel
TAMU	Texas A&M University

TABLE OF CONTENTS

Page

Page

LIST OF FIGURES

Page

LIST OF TABLES

Page

1. INTRODUCTION

As of July 2015, there are 438 operating nuclear power reactors in 30 countries providing 10.9% of the world's electricity production. One-hundred and ninety-eight of these reactors are in states that do not possess nuclear weapons[1]. As of 2005, there was roughly 180,000 metric tons of heavy metal (MTHM) in spent nuclear fuel (SNF) worldwide, and the International Atomic Energy Agency (IAEA) estimates that this will grow to 300,000 MTHM by 2020[2]. Part of the mission statement of the IAEA is to "verify through its inspection system that States comply with their commitments, under the Non-Proliferation Treaty and other non-proliferation agreements, to use nuclear material and facilities only for peaceful purposes[3]." Thus, the IAEA has a responsibility to detect and deter the diversion of nuclear material from nuclear power plants to military purposes. The goal of this research is to assess the capability of two SNF nondestructive analysis (NDA) measurement techniques for the purposes of nuclear material safeguards measurements of commercial SNF and fresh fuel: passive neutron albedo reactivity (PNAR) and spectral passive photon measurements.

Accurately measuring nuclear material contained in the SNF for nuclear safeguards purposes is a difficult task. Ideally, the IAEA would be able to determine initial enrichment, burnup, cooling time, and fissile content within acceptable uncertainty from independent measurements. They could then use this information to determine if the operator declarations are accurate and if any of the SNF has been diverted or substituted. Since there are several unknowns, multiple independent signals would be required to fully characterize the items being considered. Currently, the IAEA relies on total neutron and/or

total photon measurements to verify operator declarations. Their current goal is to be able to reliably detect the removal or substitution of 50% or more of the fuel pins in an assembly[4].

When uranium dioxide (UO_2) fuel is exposed to a neutron flux in a reactor, it undergoes transmutation, decay, neutron absorption, etc. This results in a highly radioactive and diverse mix of fission products and actinides in the SNF. Changes in the irradiation history such as changes in power level and irradiation and decay periods, as well as different initial fuel compositions (e.g. enrichment or mixed oxide fuel), will affect these physical processes in different ways for different fission products and actinides. Theoretically, these resulting differences in final fuel composition can be used to provide information about the history and initial enrichment of the fuel. This could be a difficult inverse problem to solve. The inputs for this inverse problem could be acquired from a destructive analysis (DA) and/or non-destructive analysis (NDA) measurements. DA, however, is not a feasible measurement option for the vast majority of SNF, which for safety needs to remain contained in the fuel pins and often is intended to be irradiated further. NDA techniques are feasible, because they rely on signals such as photons and neutrons emitted from the SNF. Even when these signals can be measured accurately in the harsh environment of SNF, they may be affected by dozens of different isotopes in the fuel and the convolution of these different effects can be difficult to unfold.

Spectral passive photon measurements involve measuring the photons (gamma-rays and x-rays) emitted by the fission products (and sometimes actinides) in SNF. Since gamma-rays are emitted at characteristic energies for individual isotopes and x-rays are

emitted at characteristic energies for individual elements, spectral photon measurements can be used to determine absolute or relative quantities of some isotopes or elements in SNF, although this can be complicated by self-attenuation and background.

At reactor sites, it would be desirable to have a technique which can independently identify fuel assemblies with a higher degree of accuracy and reliability than are available with current techniques during regular inspections. Passive photon measurements could also be useful as a means to recover continuity of knowledge[5]. At reactor sites and reprocessing facilities, better characterization of fuel, especially measurements of plutonium (Pu) concentration, would help reduce shipper-receiver differences and optimize fuel loading. It could also help reprocessing plants select fuels for reprocessing to produce optimal materials. For spent fuel storage and repositories, direct measurement of fuel parameters could enable more efficient safe fuel storage through the use of a "burnup credit" system[6].

PNAR is a passive neutron measurement technique which utilizes high and low neutron-multiplying regions within the detector to measure the multiplication of special nuclear material (SNM), such as SNF or fresh fuel. This multiplication is directly related to the nuclear fissile content. Neutron multiplication is useful in terms of reactor safety, spent fuel storage, and spent fuel shipping. If some other information about the fuel is known either through operator declarations or through additional measurements (such as passive photon or total neutron), fissile content potentially could be mapped to plutonium content and used to verify reactor operation parameters such as burnup, initial enrichment, and/or cooling time.

The primary objective of this research was to develop and assess the use of spectral photon measurements and the PNAR technique for nuclear material safeguards measurements of SNF.

This work is part of the Next Generation Safeguards Initiative Spent Fuel (NGSI-SF) Project. In 2009, the U.S. Department of Energy's National Nuclear Security Administration (DOE/NNSA) began the NGSI-SF project as a multi-year effort to research the capability of an integrated nondestructive assay (NDA) system to improve the state-of-the-practice in safeguards technology. The technical safeguards goals of the NGSI-SF Project include (1) measuring the Pu mass in an individual assembly, (2) verifying initial enrichment, burnup, and cooling time and (3) verifying that pins have not been removed or replaced from the fuel[7-9].

1.1 Objectives

Spectral photon measurements were investigated to determine what information could be obtained about (1) SNF irradiation history to improve nuclear material safeguards measurements and/or (2) quantify neutron absorbers in SNF to better inform neutron measurements such as PNAR. Many of the neutron SNF measurement techniques depend on burnup code and fuel history generalizations to estimate the content of several neutron absorbers in SNF which strongly affect the neutron signals. These neutron absorbers are generally stable isotopes, but in some cases they are strongly related to secondary radioactive isotopes. Measurement of these secondary isotopes could provide an indirect measurement of neutron absorbers to better inform the simulations and calculations.

The PNAR technique was tested on SNF to ensure that it would perform in harsh SNF environments and on the complicated isotopics in spent fuel. The objectives of the PNAR measurements and simulations were to optimize the design of the PNAR detector built through LANL to measure Fugen spent fuel, benchmark PNAR simulations in MCNPX, and to verify that the measured PNAR signal can be used to calculate neutron multiplication and fissile content. Fresh fuel measurements were conducted to test PNAR measurement response to axial source location, effective assembly enrichment, position of the assembly within the detector, and distribution of LEU and DU pins within the assembly.

1.2 Previous Work

1.2.1 Current Spent Nuclear Fuel Measurement Techniques

Photon measurements are a well understood technique for estimating burnup and cooling time in SNF. However, at most only a few isotopes are currently analyzed. In current IAEA measurements, only total gamma measurements or low resolution spectral gamma measurements are made[12-14]. Utilizing a larger set of photon signatures as well as including low-energy measurements (around 100 keV) could provide a significant increase in the information gained from such measurements.

Currently, the main techniques used to measure SNF for safeguards purposes are the Digital Cerenkov Viewing Device (DCVD), the Fork Detector (FDET), and the Safeguards MOX Python Detector (SMOPY).

The DCVD measures photon activity using the Cerenkov glow produced by electrons slowing down in water. It uses a charge coupled device camera system with a UV filter to view the Cerenkov light, which is strongest through the water holes in the assembly. The presence and behavior of this light verifies that the assembly is SNF and that fuel rods are not missing from the assembly. The intensity of the light provides some information about spent fuel history. This light intensity is related to many fuel parameters, particularly burnup and cooling time. However, there are many combinations of these parameters which lead to the same DCVD signal. It also requires a known calibration assembly to account for effects such as water quality[15, 16].

The SMOPY and FDET systems use photons (from ^{137}Cs and ^{134}Cs isotopes only) and total neutron signatures to infer burnup, but rely on operator declarations. SMOPY serves three main functions: determining whether a fuel assembly is low-enriched uranium (LEU) or mixed oxide (MOX) fuel, determining the burnup of an assembly, and looking for partial defects within the fuel assembly (removal or replacement of fuel pins with dummy pins). When calculating burnup of an assembly, SMOPY uses a high-efficiency fission chamber neutron detector. This measurement requires an initial measurement of a known assembly to account for measurement geometry. The calculation requires knowledge of reactor type, initial enrichment, irradiation history, and cooling time. If an anomaly is detected, the SMOPY includes a Python script which uses a parametric on-line depletion calculation to determine neutron emission rate as a function of burnup for those parameters and the calibrated measurement geometry in order to determine burnup of the assembly[17].

The FDET is used to verify burnup and look for partial defects. It consists of an ionization chamber for gross gamma measurements and a fission chamber for gross neutron measurements. To calculate burnup, the FDET also requires operator declarations to determine burnup of the assembly. The development of a tool which utilizes more signatures from SNF than FDET has the potential to provide more fuel parameters without relying on operator declarations[18, 19].

A large effort has been funded by the NGSI to improve state-of-the-art SNF measurements and quantify Pu content in SNF. This effort (NGSI-SF) is investigating the integration of complimentary spent fuel nondestructive measurement techniques, including PNAR, in order to best quantify the Pu in the SNF.

There are a total of 14 techniques being researched as part of the NGSI-SF effort. In addition to PNAR, these techniques include Self-Interrogation Neutron Resonance Densitometry (SINRD), Differential Die-Away (DDA), Differential Die-Away Self-Interrogation (DDSI), Californium-Interrogation with Prompt Neutrons (CIPN), Assembly Interrogation with Prompt Neutrons (AIPN), Passive Gamma (PG), Delayed Gamma (DG), Delayed Neutron (DN), Neutron Multiplicity (NM), Lead Slowing Down Spectroscopy (LSDS), Neutron Resonance Transmission Analysis (NRTA), X-ray Fluorescence (XRF), and Nuclear Resonance Fluorescence (NRF). Many of the techniques involved require information about burnup, initial enrichment, and cooling time in order to draw conclusions about the fuel.

Two of the important attributes of each of these measurements in terms of application is whether they are passive or active measurements and how portable they are.

Passive techniques rely on self-interrogation, or using the radiation source naturally produced by the fuel as the source signal. They are generally less expensive to build, and are easier to use and less invasive in current facilities because they do not require procurement, storage, or transportation of large radiation sources or generators. In addition to the distinction between passive and active measurements, some measurement techniques are not portable and require new facilities to be built around them. These un-portable techniques are better suited to specific facilities such as reprocessing plants or long-term storage sites rather than for safeguards purposes at nuclear power reactors around the world.

SINRD is a passive technique which uses multiple sets of fission chambers surrounded by filters of different materials to measure 'windows' of neutron energies. These filter materials are chosen so that the neutron energy windows being measured correspond to neutron absorption resonances in ^{239}Pu to measure ^{239}Pu content[20, 21].

DDA and DDSI rely on the differential die-away of the neutron multiplication in the assembly. DDSI is a passive measurement which uses neutron multiplicity to analyze the Rossi-Alpha distribution of neutrons from the fuel assembly[22, 23]. DDA uses a neutron generator to interrogate the assembly and looks at neutron counts in specific time windows after the neutron pulses[24, 25].

CIPN and AIPN are both active neutron measurements which use an external neutron source to induce fissions in SNF. CIPN uses an external ^{252}Cf source, while AIPN uses one assembly to interrogate another. CIPN has a better known interrogation signal

which leads to better accuracy, although it requires a very large ^{252}Cf source at each facility which can be difficult to obtain, store, and move around a facility[25, 26].

Passive gamma can refer to total or spectral gamma measurements[27, 28]. Delayed gamma measurements involve interrogating the material with pulses from a neutron generator to activate fission products in the fuel, and then measuring the gamma signatures from these activation products[29]. DN is similar to delayed gamma in that it measures fuel between neutron pulses, but it is looking at the total neutron signal rather than spectral gamma[30].

NM measurements use high efficiency banks of detectors to measure neutron singles, doubles, and triples counts to obtain estimates of actinide content for multiplicity data[31].

LSDS is an active time-of-flight measurement technique currently used to measure nuclear cross-sections. It involves using a linear accelerator to inject neutrons into a large mass of lead surrounding the material to be measured[32, 33]. NRTA is another time-of-flight active measurement. It uses a pulsed accelerator on one side of the assembly and measures the neutron through the assembly as a function of time after the pulse to differentiate between neutrons of different energies. Known absorption resonances of isotopes such as ^{239}Pu are used to calculate the mass of those isotopes in the fuel from the attenuation of the original beam[34]. Both of these techniques require large facilities built specifically for their purpose.

XRF is the only technique in this list which directly measures elemental plutonium. In SNF, it is a passive technique which relies on photons from fission products to generate

x-rays in uranium and plutonium which are around 100 keV[35-37]. NRF of SNF involves directing a broad-energy or mono-energetic photon source through the assembly and on to a witness foil. The witness foil creates activation products which are then measured by a gamma detector shielded from the fuel assembly. This is another technique which requires a facility to be built around its use[38, 39].

Another aspect of the NGSI-SF effort has been to develop a spent fuel library in simulation space. This library of spent fuel assemblies has been used in simulations of many of these measurement techniques for comparison to each other[40]. Since each of the techniques has been investigated by different scientists in multiple organizations, this common simulation space has been an important tool to compare the results of these techniques to each other and choose combinations of techniques to investigate further.

While current spent fuel safeguards measurements have room for improvement, PNAR and spectral photon measurements are two of several NDA SNF measurement techniques being investigated to improve the IAEA's capabilities.

1.3 Theory

1.3.1 PNAR Technique

The first paper written about the PNAR technique was published in 1997 by H.O. Menlove and D.H. Beddingfield. This paper demonstrates the proof of concept of a PNAR detector through MCNP simulations and measurements of fresh fuel in a high-efficiency passive neutron multiplicity counter (PSMC) at LANL[41]. PNAR was later selected as one of the NGSI-SF techniques in 2009. Much of the initial PNAR research as part of the

NGSI-SF effort focused on PNAR measurements with He-3 tubes[42], and then switched to PNAR measurements with FCs due to the expense and difficulty of obtaining He-3 tubes. The previous work was entirely simulation based, and focused on PNAR geometries for typical PWR SNF assemblies. This work developed a strong modeling capability for PNAR in MCNPX and investigated the effects of different fuel parameters on the PNAR ratio using the LANL spent fuel library. Previous work has shown that simulations predict that the PNAR ratio trends well with neutron multiplication and fissile content[43-46].

PNAR is a passive neutron measurement technique which utilizes high and low neutron-multiplying regions within the detector to measure multiplication of special nuclear material (SNM). One measurement is taken in a high multiplying region (in this case, with no cadmium liner), and the other in a low multiplying region (in this case, with a cadmium liner between the fuel and the detectors). Cadmium affects the multiplication of the low multiplying region since it is a strong thermal neutron absorber and keeps most thermal neutrons which have left the assembly from returning to the assembly and causing more fissions. The ratio of these two measurements is used as the PNAR ratio and has been shown to scale with multiplication and fissile content[41, 43-46]. The basic geometry for the detector built for this research is shown below in Figure 1.1.

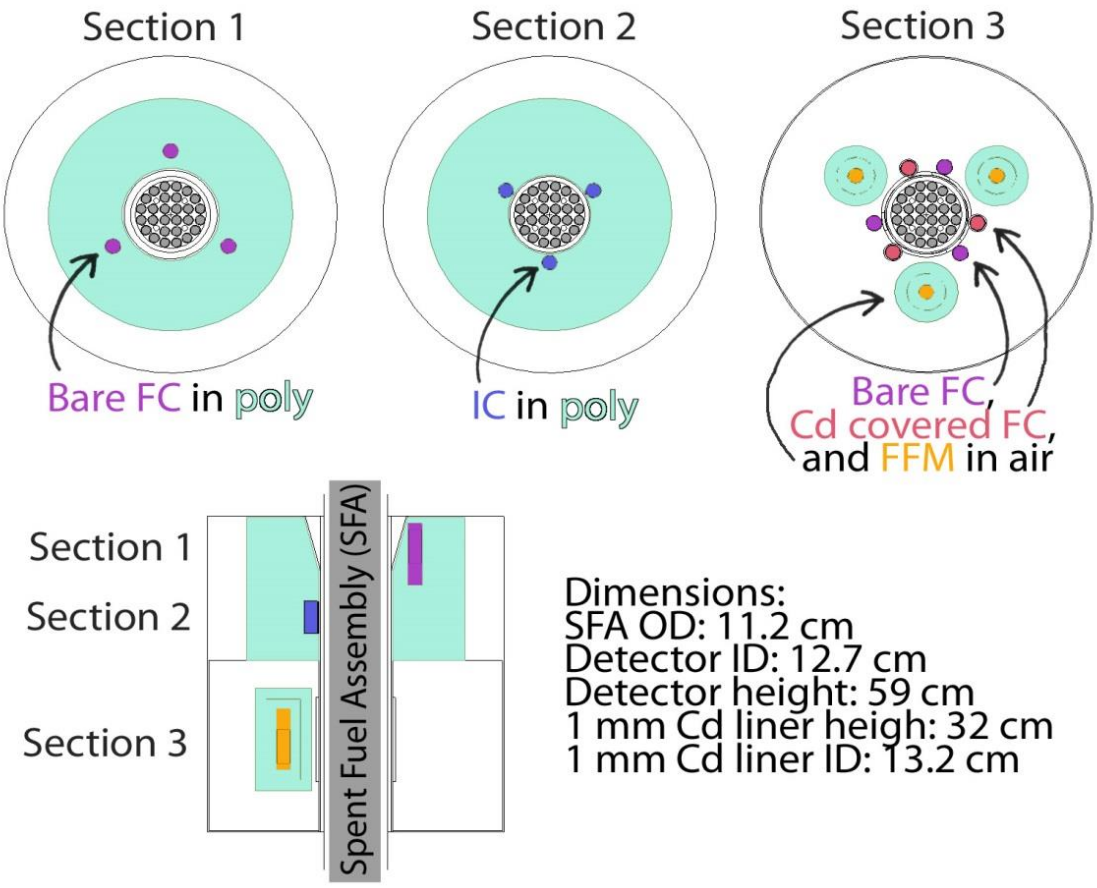

Figure 1.1. Diagram of PNAR detector built for Fugen reactor SNF measurements.

In Figure 1.1, section 1 is the high neutron-multiplying region, where neutrons are free to leave the fuel assembly, slowdown in the water around the assembly or the polyethylene in section 1, and return to the fuel to create more fissions. Section 3 is the low neutron-multiplying region, where a cadmium liner between the detectors and the fuel absorbs many of the neutrons escaping the fuel assembly from returning to cause more fissions. The ion chambers in section 2 are for collecting gross gamma measurements, and the multiple sets of fission chambers in section 3 are for neutron energy measurements in addition to the PNAR signal and will be explained in chapter 2.

Neutron multiplication is useful in terms of reactor safety, spent fuel storage, and spent fuel shipping. If some other information about the fuel is known either through operator declarations or through additional measurements (such as passive gamma or total neutron), multiplication can be mapped to plutonium content and used to verify reactor operation parameters such as burnup, initial enrichment, and/or cooling time.

1.3.2 Plutonium Effective Measurements

The multiplication measured by the PNAR detector is a function of the fissile isotopics in the fuel. The main isotopes contributing to this measurement in uranium dioxide SNF are ^{239}Pu, ^{241}Pu, and ^{235}U. This fissile content can be expressed in units of effective grams of ^{239}Pu, or ^{239}Pu$_{eff}$. This is basically a measurement of how many grams of pure ^{239}Pu would produce the same measured signal as the mixture. ^{239}Pu$_{eff}$ is calculated according to Eq. (1.1):

$$^{239}Pu_{eff} = C_1\,{}^{235}U_m + {}^{239}Pu_m + C_2\,{}^{241}Pu_m, \tag{1.1}$$

where $^{235}U_m$, $^{239}Pu_m$, and $^{241}Pu_m$ are the masses of ^{235}U, ^{239}Pu, and ^{241}Pu, respectively. C_1 and C_2 are weighting constants that are specific to each measurement technique and need to be calculated via simulations. In simulation space, the contribution of fission neutrons from each isotope which cause interactions in the detectors can be tracked. This data is used to calculate the relative effect of a difference in ^{235}U, ^{239}Pu, or ^{241}Pu on the measured signal for each measurement technique. These values can then be used to calculate C_1 and C_2 for each technique. An experimental calibration of C_1 and C_2 would be very

complicated and require making several measurements of samples that are well-known either because of extensive calculations or through performing DA after the NDA measurement.

In a safeguards context, the goal is to measure either grams of plutonium or grams of fissile material. It becomes necessary to be able to split this measured signal into its three isotopic parts. Since there is only one signal which depends on all three of these isotopes, additional knowledge of the relative isotopics is required to calculate the quantity of plutonium in the fuel. If the relative quantities of ^{235}U, ^{239}Pu, and ^{241}Pu are known from burnup and initial enrichment or simulations, the plutonium mass or total fissile mass can be calculated from the measured $^{239}Pu_{eff}$ signal[47].

1.3.3 MONTEBURNS

MONTEBURNS is a reactor physics code that was developed as a master's thesis project by Holly Trellue at the University of New Mexico and is maintained by Los Alamos National Laboratory. It uses a Perl script to link the cross section and flux calculation capability of MCNP with the production and decay calculations of ORIGEN or CINDER. The simulations used for this work used MCNP5 and ORIGEN 2.2. Figure 1.2 shows how MONTEBURNS interacts with both ORIGEN and MCNP to calculate material compositions for each step. For each step, ORIGEN is first used to perform fuel burnup and decay the materials provided by the MCNP input file for half of the step and create a new MCNP deck with these materials. MCNP then uses this information to calculate one-group cross sections and neutron fluxes half way through the step. This information is considered to be valid for the entire step, and is fed into ORIGEN to perform

fuel burnup and decay the materials for the entire step. This process is valid as long as sufficiently small steps are used throughout the calculation (generally less than 2500 MWD/MTU). Especially small steps need to be used at the beginning of each burn cycle to account for initial buildup of neutron absorbing fission products. Decay steps can be considerably longer (years) because the calculations are much simpler and the fuel compositions are changing more predictably.

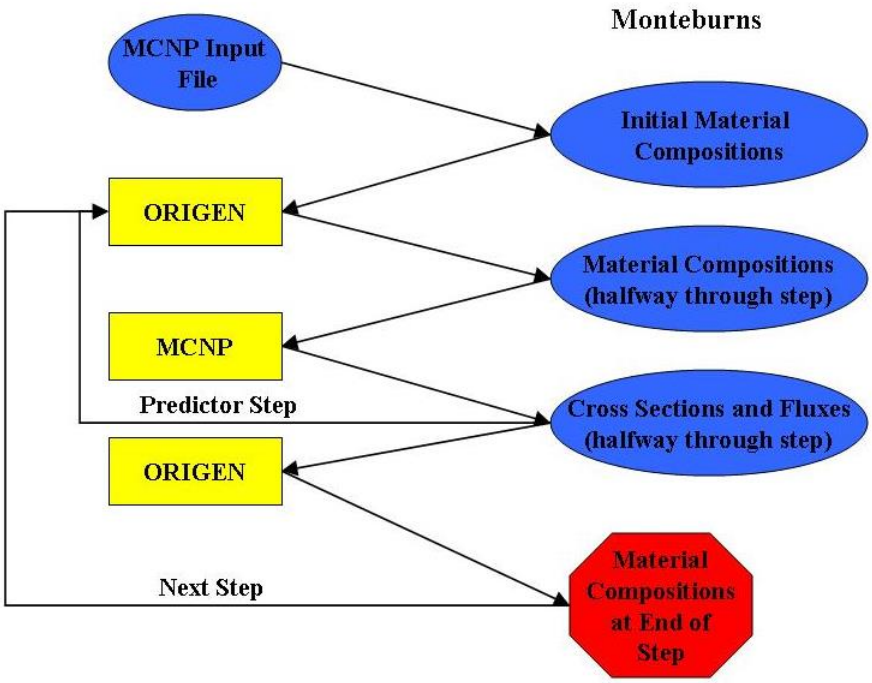

Figure 1.2. Interaction of MONTEBURNS with MCNP and ORIGEN[8].

MONTEBURNS requires both an MCNP input deck and a MONTEBURNS input deck. The MCNP input deck defines the geometry and composition of the simulation, and the MONTEBURNS input deck defines other required parameters such as power level, how many steps to link between ORIGEN and MCNP, which isotopes to keep track of,

and which ORIGEN library to use. There is also an optional feed file which allows for adding or removing materials during the simulation or, as used in this work, for defining a power cycle[8].

While MONTEBURNS takes a considerable period of time to run, depending on how many MCNP steps are included, it is a very powerful code. By using MCNP to input geometry specifications, very complex systems can be simulated, which makes MONTEBURNS a very flexible simulation code.

Since the standard MONTEBURNS output file only has three significant digits, all analysis of material concentrations used data from the mb5tx files saved in the temp folder once MONTEBURNS has finished running. There is an mb5tx file saved for each material which lists the grams of each isotope for each feed step with eight significant digits.

1.3.4 Fission Product Production and Decay

The nuclides present in SNF consist of (1) fission products generated during reactor operation, (2) activation products created by absorption reactions in the cladding or other fuel support structures, and (3) actinides, as well as the decay products of all three categories. The buildup of these nuclides can depend on many fuel parameters, and each measurable nuclide may be able to provide unique information about the history of the fuel based on how it is produced and removed from the fuel during irradiation. Not all of the signatures will be visible in all fuels since some will decay quickly and others take time to build up.

1.3.4.1 Cesium-137

^{137}Cs is produced at a constant rate in nuclear fission systems, almost regardless of the fissioning nuclide because it is rarely produced by anything other than fission and the M=137 mass chain lies almost directly on the intersection between the U and Pu fission product yield curves, as shown in Figure 1.3. This means that ^{137}Cs is produced steadily throughout the burnup of SNF regardless of whether fissions are occurring in U or Pu. It also has a low absorption cross-section. This makes it an especially easy fission product to calculate the quantity of in SNF. It is produced in significant quantities from fission and is radioactive with a relatively long half-life of 30 years. It produces a single 662 keV gamma-ray with an abundance of 85% per decay. This makes it one of the most straight forward fission products to measure in SNF and means that if cooling time is known, an absolute measurement of ^{137}Cs is a fairly direct measurement of burnup.

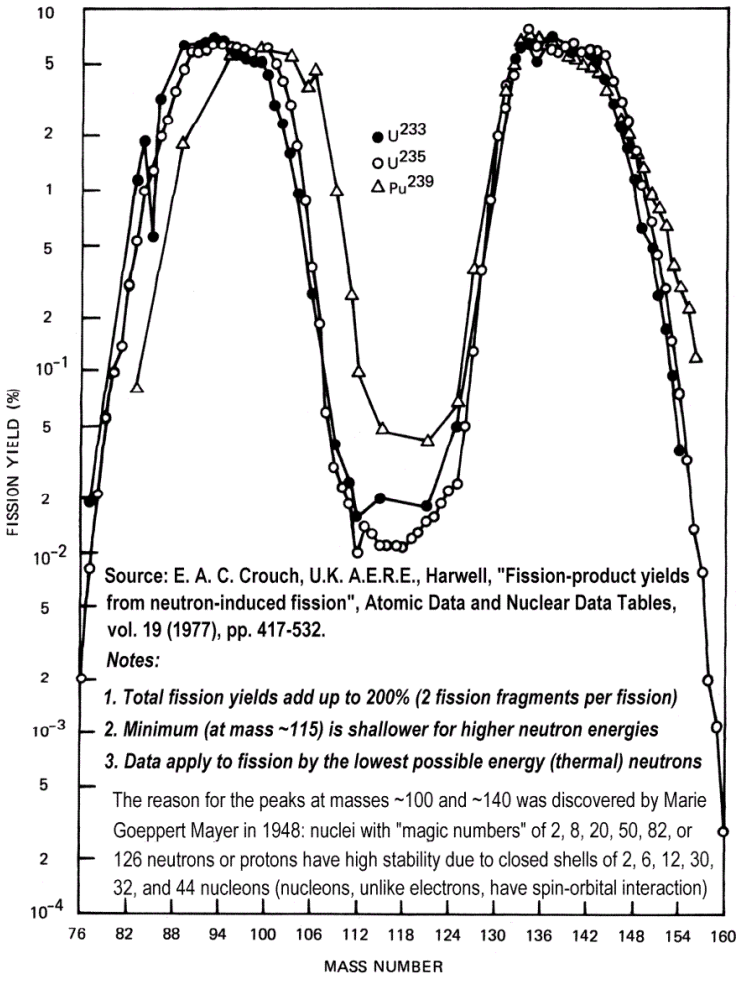

Figure 1.3. Fission Product Yield Curves [48]

^{137}Cs's half-life is 30.1 years, making it typically the longest lived fission product measurable in SNF photon measurements. This combined with the 662 keV photon emitted in every decay makes ^{137}Cs especially useful because it is still clearly measurable in SNF after many of the shorter lived isotopes have decayed past being useful, even in fuel that is many years old. It is linearly dependent on burnup and predictably dependent on cooling time, but is almost insensitive to other fuel parameters[48]. Other studies have used a direct measurement of ^{137}Cs activity to calculate burnup based on a known cooling

time, but this also requires very precise information about the geometry of the measurement and efficiencies of the system in order to translate a count rate into an activity[49]. ^{137}Cs beta decays and produces a 662 keV photon which is emitted in 85% of decays[50].

1.3.4.2 Cesium-134 and Cesium-133

^{133}Cs has a high cumulative fission yield, produced by roughly 7% of fissions in both ^{235}U and ^{239}Pu[51], and it also has a fairly high resonance radiative capture cross section of 390 barns[52]. This makes it a prominent neutron absorber in SNF, and it is thus interesting to several neutron measurement techniques which depend on understanding the neutron absorption environment to quantify Pu content. However, ^{133}Cs is stable and thus impossible to measure directly with photon measurements. Being able to better quantify the ^{133}Cs by understanding its relationship with ^{134}Cs in SNF could help the accuracy of these neutron techniques[8].

Many fission products are produced largely through beta decay chains, where several higher-Z nuclides of the same mass have very short half-lives and quickly decay through beta decay along the mass chain until they reach an isotope in the chain that is either stable or has a longer half-life (around 100+ days). In these cases, it can be assumed that the isotope blocking the fission chain (the first in the mass chain that is stable or has a longer half-life) has a fission yield equivalent to the sum of its own fission yield and the fission yields of the previous isotopes in the decay chain, and this sum of fission yields is referred to as cumulative fission yield. In this way, the direct fission yield of the specific isotope may be low, but the cumulative fission yield may be quite important. This

assumption is generally valid, but can lead to complications in simulations that lead to relatively larger errors in mass estimates for these isotopes. ^{134}Xe, which is stable and is higher in the mass chain than ^{134}Cs, is one of these blocking isotopes. While M=134 is the mass chain with the highest cumulative fission field from ^{235}U, ^{134}Cs is not produced this way because it is blocked within its mass chain by a stable element: ^{134}Xe[52]. Since ^{134}Xe is stable, ^{134}Cs is not produced directly from fission outside of its direct fission yield, which is quite small[51].

Instead, ^{134}Cs is largely produced by radiative capture in ^{133}Cs, which means that it is closely related to ^{133}Cs content and measurement of ^{134}Cs could possibly be used to infer information about the quantity of ^{133}Cs present during measurements. [48].

^{134}Cs is also relatively frequently used in specialized spent fuel photon analysis as a ratio to ^{137}Cs to estimate cooling time. Since it is mostly produced by radiative capture in ^{133}Cs, the production of ^{134}Cs has a roughly quadratic dependence on the neutron flux density, which shows up as a quadratic dependence on burnup. It is one of the strongest photon signals present in fuels with cooling time less than around 15 years, which accounts for most fuel measurements performed by the IAEA, but it becomes unusable at much longer cooling times due to its 2.1 year half-life. It beta decays with several signatures, the strongest of which are 604 keV (98% of decays), 796 keV (86% of decays), and 569 keV (15% of decays)[50].

1.3.4.3 Europium-154

Similar to ^{134}Cs, ^{154}Eu is blocked in its decay chain by ^{154}Sm, which is stable. One prominent production path for ^{154}Eu is through radiative capture in ^{153}Eu. ^{153}Eu is stable,

and has a resonance integral radiative capture cross section of 1,500 barns[52], so even though its cumulative fission yield is more than an order of magnitude lower than the fission yield of ^{133}Cs , it is still one of the important neutron absorbers to quantify for neutron based NDA measurements. ^{154}Eu is an especially complicated fission product to model because it is produced significantly from 20 different paths[48]. CINDER 90 in MCNP allows for the creation of 'chains' files which track how each element is created. This chains file was created with the simulation of the Three Mile Island fuel. Analysis of this file showed that while 97% of ^{154}Eu created was created directly from ^{153}Eu, this ^{153}Eu was created in many ways, a few of which are shown below with their percentage:

$$^{239}Pu \underset{fission}{\rightarrow} {}^{153}Pm \underset{\beta}{\rightarrow} {}^{153}Sm \underset{\beta}{\rightarrow} {}^{153}Eu \quad (30\%)$$

$$^{235}U \underset{fission}{\rightarrow} \left({}^{151}\mathrm{Pr} \underset{\beta}{\rightarrow} \right)^{151} Nd \underset{\beta}{\rightarrow} {}^{151}Pm \underset{\beta}{\rightarrow} {}^{151}Sm + n \rightarrow {}^{152}Sm + n \rightarrow {}^{153}Sm \underset{\beta}{\rightarrow} {}^{153}Eu$$

(14% w/out ^{151}Pr, 3% with ^{151}Pr)

$$^{235}U \underset{fission}{\rightarrow} {}^{152}\mathrm{Pr} \underset{\beta}{\rightarrow} {}^{152}Nd \underset{\beta}{\rightarrow} {}^{152}Pm \underset{\beta}{\rightarrow} {}^{152}Sm + n \rightarrow {}^{153}Sm \underset{\beta}{\rightarrow} {}^{153}Eu \quad (8\%)$$

$$^{235}U \underset{fission}{\rightarrow} \left({}^{153}\mathrm{Pr} \underset{\beta}{\rightarrow} \right)^{153} Nd \underset{\beta}{\rightarrow} {}^{153}Pm \underset{\beta}{\rightarrow} {}^{153}Sm \underset{\beta}{\rightarrow} {}^{153}Eu \quad (7\% \text{ without } {}^{153}\mathrm{Pr}, 4\% \text{ with } {}^{153}\mathrm{Pr})$$

$$^{239}Pu \underset{fission}{\rightarrow} {}^{152}Pm^{*} \underset{\beta}{\rightarrow} {}^{152}Sm + n \rightarrow {}^{153}Sm \underset{\beta}{\rightarrow} {}^{153}Eu \quad (3\%)$$

$$^{239}Pu \underset{fission}{\rightarrow} {}^{152}Pm \underset{\beta}{\rightarrow} {}^{152}Sm + n \rightarrow {}^{153}Sm \underset{\beta}{\rightarrow} {}^{153}Eu \quad (3\%)$$

The relative weights in this simulation are dependent on many fuel parameters and so are just an example for this specific fuel case. This complicated production process makes it relatively difficult to calculate ^{153}Eu or ^{154}Eu with reactor physics codes, especially since some of the nuclides in these chains are not well benchmarked. It also makes any changes in ^{154}Eu production as a result of changes in fuel parameters difficult to predict without measurements or simulations. For this reason, measurements of ^{153}Eu would be especially beneficial. Since the complicated part of this production process lies in the production of ^{153}Eu, quantifying ^{154}Eu content could be directly tied to quantifying ^{153}Eu. ^{154}Eu beta decays with a half-life of 8.6 years, which is the second longest (after ^{137}Cs) of the nuclides visible in the spent fuel measurements at ORNL. Because of this, a ratio of ^{137}Cs and ^{154}Eu would be especially practical since it would be visible in fuels with the longest cooling times, once other isotopes are no longer measurable. ^{154}Eu produces many strong photon signatures over a wide range of energies in SNF, the most intense of which are 123 keV (40% of decays), 1,274 keV (35% of decays), 723 keV (20% of decays), and 1,004 keV (18% of decays)[50].

In some measurements in this work, as many as 26 ^{154}Eu peaks are visible. One benefit of the large quantity and range of photopeaks visible from ^{154}Eu is that this is the only isotope with photopeaks clearly visible in both low-energy planar and broad-energy coaxial measurements. This allows for calculation of relative efficiencies between the two detectors so that ratios can be used between signals visible in the different detector energy regions. The wide range of ^{154}Eu peak energies is beneficial because it provides several options for calculating peak ratios to different nuclides. Ideally, any ratio between two

isotopes would be calculated with photon peaks that are close together in energy so as to reduce errors from detector efficiency and escape ratio differences. With many strong peaks between 123 keV and 1,274 keV, ^{154}Eu has photopeaks close in energy to many of the nuclides being measured.

1.3.4.4 Cerium-144

^{144}Ce is mainly produced by fission, with relatively high fission yields of 5.5% and 3.7% from ^{235}U and ^{239}Pu, respectively[51]. ^{144}Ce beta decays with a half-life of 285 d to ^{144}Pr, which then beta decays with a half-life of 17 minutes. The strongest signal visible in spent fuel photon measurements from this pair is a 2,185 keV photon which is produced in 0.7% of decays[50]. While this is a low emission rate, the very low background at 2,185 keV makes this a viable measurement for fuel with short enough cooling times that ^{144}Ce is still present.

In a reactor, ^{144}Ce will reach an equilibrium concentration over the period of typical power cycle lengths. This equilibrium concentration is dependent on power level, but since most power plants operate in a small range of power levels, this is considered known in some facility measurement situations. When this happens, the concentration of ^{144}Ce in measured fuel is independent of burnup and only on cooling time. This allows ^{144}Ce to be used as a cooling time indicator for young fuel at reprocessing plants by using a ratio of ^{144}Ce with ^{137}Cs or ^{95}Zr[53, 54].

1.3.4.5 Americium-241

^{241}Am is formed in nuclear fuel from ^{241}Pu beta decay, and thus increases in concentration with cooling time and burnup. ^{241}Am has a large resonance radiative capture absorption cross-section of 1,490 barns[52], and thus the ^{241}Am measured in spent fuel is almost entirely from Pu decay once fuel has been removed from the reactor. This makes it a promising cooling time indicator when combined with information about the Pu content. The strongest photon produced by ^{241}Am, at 60 keV, cannot be well discriminated with broad-energy photon measurements. The capability of measuring ^{241}Am with low-energy gamma-ray measurements (such as the thin planar detector used in these measurements) is also of particular interest with respect to neutron measurements attempting to quantify Pu mass because of its large neutron absorption cross section.

^{241}Am alpha decays with a half-life of 432 years and is produced from ^{241}Pu with a half-life of 14.4 years, so it takes several years after discharge from the reactor to build up enough ^{241}Am to have a strong signal. The only photon from ^{241}Am decay visible in the SNF measurements at ORNL is at 60 keV and has an emission rate of 40%[50].

1.3.4.6 Europium-155 and Gadolinium-155

^{155}Eu beta decays with a half-life of 4.8 years with a photon signature at 105 keV clearly visible in the SNF measurements made at ORNL. This is a low enough energy that it is not identifiable in standard broad-energy photon measurements, but it can be resolved in the low-energy measurements done at ORNL with the planar HPGe detector.

^{155}Eu has a fairly complicated production process. It has cumulative fission yields of .03% and 0.17% from ^{235}U and ^{239}Pu fissions, respectively. It is also created through

neutron capture in ^{154}Eu, which has a complicated production history of its own and thermal and resonance radiative capture cross sections of 1,400 barns and 1,600 barns, respectively. It is also produced in considerable quantity through neutron absorption in ^{154}Sm to ^{155}Sm followed by beta decay to ^{155}Eu[55]. This complicated production history makes it difficult to calculate with reactor physics codes. It makes predictions of how it will behave in reaction to changes in fuel parameters difficult as well. The same 'chains' file produced with CINDER 90 discussed in section 1.4.3 was also analyzed for ^{155}Eu. It showed that for the Three Mile Island fuel simulated, 74.9% and 24.8% of ^{155}Eu came directly from ^{154}Eu and ^{155}Sm, respectively. ^{155}Eu is of particular interest to measure in relation to neutron measurements due to its large resonance radiative capture cross section of 16,000 barns and the fact that its stable daughter product, ^{155}Gd, is also a strong neutron absorber in SNF. Since ^{155}Gd has an enormous thermal neutron absorption cross section of 61,000 barns, it can be assumed that all ^{155}Gd in the fuel at the time of measurement has been produced by decay from ^{155}Eu after discharge from the reactor[52]. It would be helpful to the neutron measurement techniques measuring Pu in SNF if measuring ^{155}Eu could provide information about both ^{155}Eu and ^{155}Gd in the fuel.

1.3.4.7 Silver-110m, Ruthenium-106, and Antimony-125

^{110m}Ag, ^{106}Ru, and ^{125}Sb are all of interest primarily because of their potential to provide information about initial enrichment. All three of these nuclides have significantly higher fission yields from Pu than from U[51]. SNF at the same burnup will have more fissions from Pu and fewer fissions from U than if the fresh fuel had a lower initial enrichment. For this reason, quantifying concentrations of isotopes with higher fission

yields from Pu fissions than from U fissions could provide information about the initial enrichment if burnup information is known. Since these isotopes are all produced more through Pu fissions, they could also help indicate whether SNF is MOX or UO_2 fuel[56].

None of these isotopes are used frequently in SNF measurements. Reactor physics codes are tested primarily against fuel parameters of interest to reactor operators and the academic community: thus most reactor physics codes are not as accurate at predicting these lesser studied isotopes as they are at predicting other fission products such as ^{137}Cs and ^{134}Cs. For example, MONTEBURNS, which is used for the sensitivity simulations in this work, does not track ^{110m}Ag, so not many conclusions about ^{110m}Ag are generated in this research.

Of these three nuclides, ^{110m}Ag has the largest difference in fission yields between ^{235}U and ^{239}Pu fissions. It is produced in 0.03% of ^{235}U fissions and 1.5% of ^{239}Pu fissions, with a factor of 47 times difference. ^{110m}Ag is blocked in its mass decay chain in the same manner as ^{134}Cs and ^{154}Eu. It is mostly produced by neutron absorption in ^{109}Ag, which is a stable isotope with a resonance absorption cross section of 1,460 barns[52]. ^{110m}Ag decays with a half-life of 250 days. Several ^{110m}Ag gamma-rays were visible in the measurements of Catawba MOX fuel at ORNL, the strongest of which is at 658 keV which is produced in 95% of decays[50]. Other well-defined gamma-rays from ^{110m}Ag included 884 keV, 937 keV, and 1,384 keV.

^{106}Ru is produced in 4.4% of ^{239}Pu fissions, but only 0.4% of ^{235}U fissions, which differ by a factor of 10.8. The strongest ^{106}Ru photon visible in the measurements at ORNL is at 622 keV and is emitted in 10% of decays. There is a stronger gamma-ray emitted at

511 keV, but since this severely overlaps with the 511 keV escape peak, it is impossible to measure ^{106}Ru using this peak[50]. Other well-defined peaks visible in the Catawba MOX fuel measured at ORNL were at 1,050 keV, 1,128 keV, and 1,562 keV. For MOX fuel, where nearly all fissions are from Pu, ^{106}Ru has been shown to be a good burnup indicator when used with ^{134}Cs and ^{137}Cs due to its low absorption cross section and high production[56]. One issue with measuring ^{106}Ru is that it tends to migrate towards the center of the fuel pellet, with peripheral-to-center concentrations as high as 1:20[57]. The energy of the photon being measured, at 622 keV, is high enough that effects on photon measurements due to this migration should be minimal.

^{125}Sb is produced 3.3 times as much from ^{239}Pu as from ^{235}U, with fission yields of 0.11% and 0.03%, respectively[51]. ^{125}Sb beta decays with a 2.8 year half-life. The strongest photon from ^{125}Sb visible in the photon measurements at ORNL was the 600 keV gamma-ray emitted in 17% of decays. There is a stronger 427.8 keV photon, but it is too close in energy to the 428.4 keV photon emitted by ^{106}Ru to be discriminated[50].

All three of these nuclides, especially ^{110m}Ag and ^{125}Sb because of their relatively low fission yields, are impossible to measure in many fuels because of their short half-lives and low fission yields in ^{235}U. They are only likely to be viable for measurements of fuel with some combination of high burnup, low cooling time, and MOX rather than UO_2 fuel.

1.3.4.8 Uranium and Plutonium

Most of SNF is U. Since SNF has a high photon activity, the U produces strong self-induced x-ray peaks visible clearly even in typical broad-energy HPGe measurements.

Only about 1% of typical SNF is Pu. ^{239}Pu is produced in SNF via the following chain:

$$n + {}^{238}U \rightarrow {}^{239}U \underset{\beta}{\rightarrow} {}^{239}Np \underset{\beta}{\rightarrow} {}^{239}Pu$$

^{240}Pu, ^{241}Pu, and ^{242}Pu are all produced by one or more neutron absorptions from ^{239}Pu. This chain effectively stops, however, at ^{242}Pu because ^{243}Pu has a half-life of 5 hours. The radiative capture and fission cross sections for the main Pu isotopes found in SNF are shown in Table 1.1.

Table 1.1. Plutonium Cross Sections[52]

Isotope	Thermal Radiative Capture Cross Section [barns]	Resonance Radiative Capture Cross Section [barns]	Thermal Fission Cross Section [barns]	Resonance Fission Cross Section [barns]
^{239}Pu	271	200	750	300
^{240}Pu	290	8100	0.05	2.4
^{241}Pu	361	160	1010	570
^{242}Pu	19	1100	0.2	0.2

Both U and Pu x-rays are at a very low energy, around 100 keV. Due to the high density of SNF, the fuel itself acts as a very effective shield for these x-rays, such that they have a mean free path of about 0.05 cm, while the diameter of most PWR fuel pins is around 0.5 cm[36]. This results in the x-ray signal being measured coming only from the U and Pu in the very outer edge of the fuel pin. U is evenly distributed throughout the fuel pin. When Pu is produced in LWR fuel, however, it has a significantly higher concentration on the very outer edge of the fuel pin due to resonance shielding in the fuel[58]. This is convenient for Pu x-ray measurements because only the x-ray signal from the part of the fuel with the highest Pu concentration is reaching the detectors. Even though only the outer edge of the fuel pin is being measured, it has been shown that the Pu/U x-ray ratio is directly proportional to the bulk Pu/U content ratio in the fuel[35, 36, 58, 59].

The U and Pu x-ray peaks scale heavily with background radiation, since they are created primarily when fission product gamma-rays knock electrons from U and Pu atoms. While gamma peaks have a natural Gaussian shape, x-ray peaks have a natural Laurentian shape, which can be more difficult to fit in spectral analysis software. This is addressed further later.

^{239}Pu, ^{240}Pu, and ^{242}Pu have half-lives over 6,000 years, and so are effectively independent of cooling time in reference to the time periods experienced by SNF. ^{241}Pu has a half-life of 14.4 years, but this is long in terms of most fuels measured, and ^{241}Pu is usually only a small portion of the Pu vector, so this results in only a minor dependence of Pu on cooling time.

1.3.4.9 Cobalt-60

^{60}Co is not a fission product, but is formed as an activation product in the cladding and structural materials surrounding the fuel. Most types of nuclear fuel cladding and stainless steel can contain impurities of iron, nickel, and cobalt. Natural cobalt is 100% ^{59}Co, which becomes ^{60}Co when it absorbs a neutron. ^{60}Co can also be formed in a few ways by irradiation of stable isotopes in iron and nickel. Two of these modes of production are:

$$n + {}^{58}Fe \rightarrow {}^{59}Fe \underset{\beta}{\rightarrow} {}^{59}Co + n \rightarrow {}^{60}Co$$

$$n + {}^{58}Ni \rightarrow {}^{59}Ni \underset{EC}{\rightarrow} {}^{59}Co + n \rightarrow {}^{60}Co\,.$$

In theory, activation products could be used to determine cladding composition and/or calculate the fluence experienced by the fuel. However, the exact concentrations of these impurities fluctuate and are too hard to determine for ^{60}Co activation to be useful in either of these capacities.

^{60}Co beta decays with a half-life of 5.2 years, which is relatively long when compared to the other isotopes being considered in this study but not so long that the activity is immeasurably low. ^{60}Co produces two photons from each decay, at 1,173 keV and 1,332 keV. This is a high enough energy that there is very little background noise from other fission products[50].

1.3.4.10 Bismuth-214

^{214}Bi is a decay product of ^{238}U which is created as follows:

$$^{238}U \xrightarrow[\alpha]{} ^{234}Th \xrightarrow[\beta]{} ^{234}Pa \xrightarrow[\beta]{} ^{234}U \xrightarrow[\alpha]{} ^{230}Th \xrightarrow[\alpha]{} ^{226}Ra \xrightarrow[\alpha]{} ^{222}Rn \xrightarrow[\alpha]{} ^{218}Po \xrightarrow[\alpha]{} ^{214}Pb \xrightarrow[\beta]{} ^{214}Bi$$

Many ^{214}Bi peaks are visible in older fuel (with a cooling time of around 30+ years), where background radiation has gone down significantly. In the other fuels, ^{214}Bi is measurable because one of its strongest gamma lines is at 1,764 keV, where there is less background than at lower energies. When there is strong activity from ^{106}Ru, the 1,764 keV peak from ^{214}Bi can be covered up by the ^{106}Ru 1,766 keV peak. However, in the measurements at ORNL, they were easily separated using Genie's interactive peak fitting program. While ^{214}Bi does not provide any information about cooling time, burnup, initial enrichment, or power history, it has the possibility of indicating the time since the U was chemically processed.

2. PNAR MEASUREMENTS

This section describes the Fugen reactor SNF and LANL fresh fuel used in the PNAR measurements, the characteristics of the PNAR detector built, the measurement procedure, and the results from the SNF measurements and the fresh fuel measurements performed.

2.1 Fugen Reactor and Fuel Design

The Fugen reactor is a heavy-water moderated, light-water cooled reactor. It was built as a prototype of an advanced thermal reactor to test the use of mixed oxide (MOX) fuel in a heavy-water moderated nuclear power plant. The core contained 224 fuel assemblies, each of which has an effective fuel length of 3.7 m, a radius of 5.6 cm, and contains 28 fuel pins, as shown below in Figure 2.1. [60]

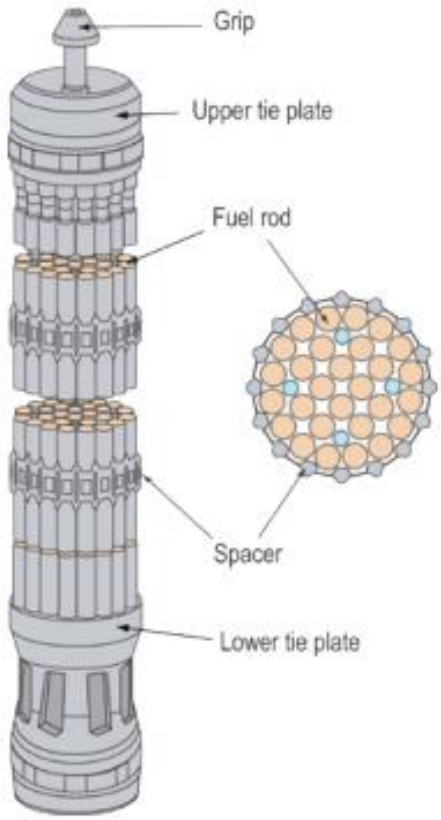

Figure 2.1. Schematic view of a standard Fugen fuel assembly[60].

The Fugen reactor site provided 8 of these assemblies for PNAR measurements. The fuel burnup information and simulated multiplication values for these assemblies are shown below in Table 2.1. The assemblies were irradiated MOX fuel over a range of fuel burnup and cooling time values. Neutron multiplication was not calculated for the LEU assembly since the count rates were too low to get an accurate measurement.

Table 2.1. Fugen Fuel Assemblies Measured

Assembly	Fuel Type	Burnup (GWd/MTHM)	Cooling Time (yrs)	Simulated Neutron Multiplication
M1	MOX	3.7	10	1.74
M2	MOX	7.1	10	1.69
M3	MOX	12.3	10	1.59
M4	MOX	15.2	10	1.55
M5	MOX	15.2	15	1.54
M6	MOX	15.2	20	1.52
M7	MOX	19.2	20	1.48

LANL performed fuel burnup simulations of Fugen MOX fuel assemblies using Monteburns to determine their neutron multiplication. Monteburns is a LANL burn-up calculation code (different from JAEA Fugen's burnup calculation codes). LANL used only the official data they got from a published paper / booklet about the Fugen power plant along with estimated data from LWR burnup calculations. LANL used their own Pu isotopic composition data for LWR fuel with 28 GWD/MTHM for the initial Fugen fresh fuel MOX assembly actinide compositions. This is because the Fugen fresh fuel assemblies use recovered Pu from Tokai Reprocessing Plant (TRP) to make the MOX fuel. Following the fuel burnup simulations, the spent fuel assemblies were simulated inside the detector using MCNPX to predict neutron count rates and prepare for measurements.

2.2 Fresh Fuel Design

The second measurement campaign with the PNAR detector was on fresh fuel with a ^{252}Cf source at LANL. This allowed for more precise measurements in that the isotopics

of the fuel and position of the assembly within the detector were better known. LANL has a variety of fresh PWR fuel pins, as described in Table 2.2.

Table 2.2: LANL Fresh Fuel Pin Inventory

	LEU	DU	Gd rod
Number of rods	204	204	12
Pellet density (g/cm^3)	10.48	10.48	10.48
Pellet O.D. (cm)	0.851	0.851	0.877
Rod O.D. (cm)	1.08	1.08	1.08
Cladding Material	Zr-2	Zr-2	Zr-4
Cladding thickness (cm)	0.115	0.115	0.064
Rod active length (cm)	103.5	103.5	104
U-235 enrichment (wt %)	3.19	0.2	3.28
Gd wt%	0	0	5.12

2.3 PNAR Detector Design

The PNAR detector, as built for measurements of Fugen fuel, is primarily divided into three axial sections, as shown in

Figure 2.2. The detector consists of three ion chambers and twelve fission chambers which combine the following NDA measurements: (1) PNAR ratio, (2) total neutron counts, (3) total gamma counts and (4) counts from three sets of energy filtering fission chambers. Sections 1 and 2 are together considered the high neutron-multiplying region. These sections are filled with polyethylene and have no cadmium (Cd) between the fuel and the detectors, allowing neutrons to reflect back and forth between the fuel assembly and the detector. The polyethylene surrounding the detectors allows the neutrons to thermalize in the detector as if they were in water. Section 3 is considered the low

neutron-multiplying section. In contrast to sections 1 and 2, section 3 is filled with air, which reduces the number of neutrons which will thermalize near the fuel and reflect back to the assembly. Section 3 also has a Cd liner between the fuel and the detectors which prevents thermalized neutrons from returning to the assembly to cause more fissions. This PNAR detector uses the ratio of counts in the fission chambers in the high-multiplying section to counts in the fission chambers in the low-multiplying section to obtain the PNAR ratio, which is a measurement of the neutron multiplication of the assembly.

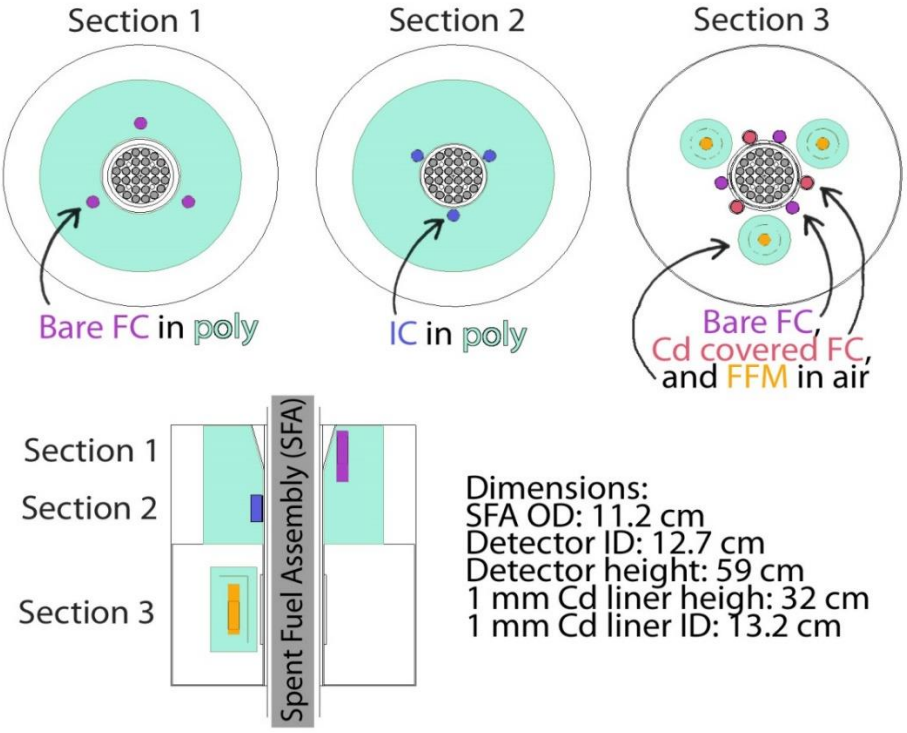

Figure 2.2: PNAR detector system as built for use at the Fugen site in Japan.

Section 1 has three bare fission chambers which are used to obtain the high neutron-multiplying measurement. Section 2 has three ion chambers, which are used to

measure the total gamma dose from which the burnup of the fuel can be inferred. They could also possibly be used for determining the position of the assembly within the detector.

Section 3 has nine fission chambers, divided into three groups of three fission chambers which are each tailored to measure a different energy region of the neutron spectrum from the fuel assembly. The three groups of fission chambers in section 3 are fast-flux monitors (FFM), Cd-covered fission chambers and bare fission chambers. Each of these sets of fission chambers is surrounded with different neutron-absorbing materials in order to tailor them to measure different regions of the neutron-energy spectrum.

The fission chambers in the PNAR detector are 93% ^{235}U. Because of the fission cross-section of ^{235}U, shown in Figure 2.3, these fission chambers are mainly measuring thermal neutrons when left bare.

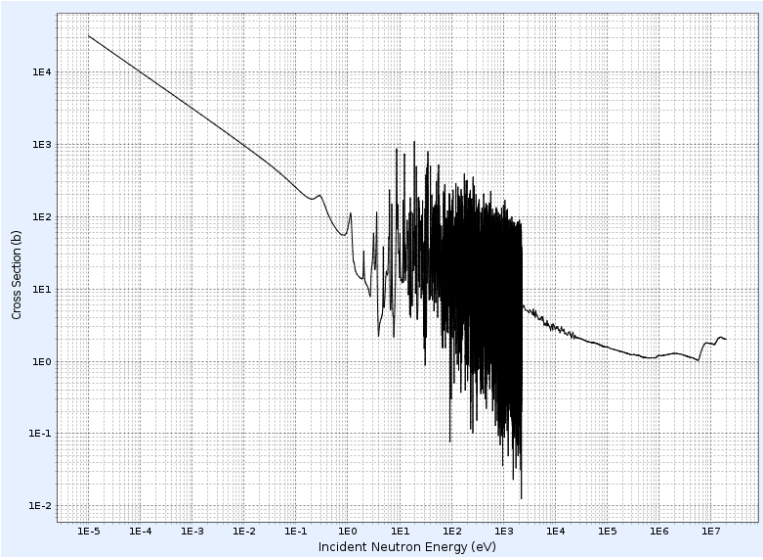

Figure 2.3. Fission cross-section of uranium-235[50].

There is a Cd layer around some sets of fission chambers as well as between the fuel and all but the bare detectors in section 3. This Cd absorbs nearly all of the thermal neutrons, due to its absorption cross-section as shown in Figure 2.4.

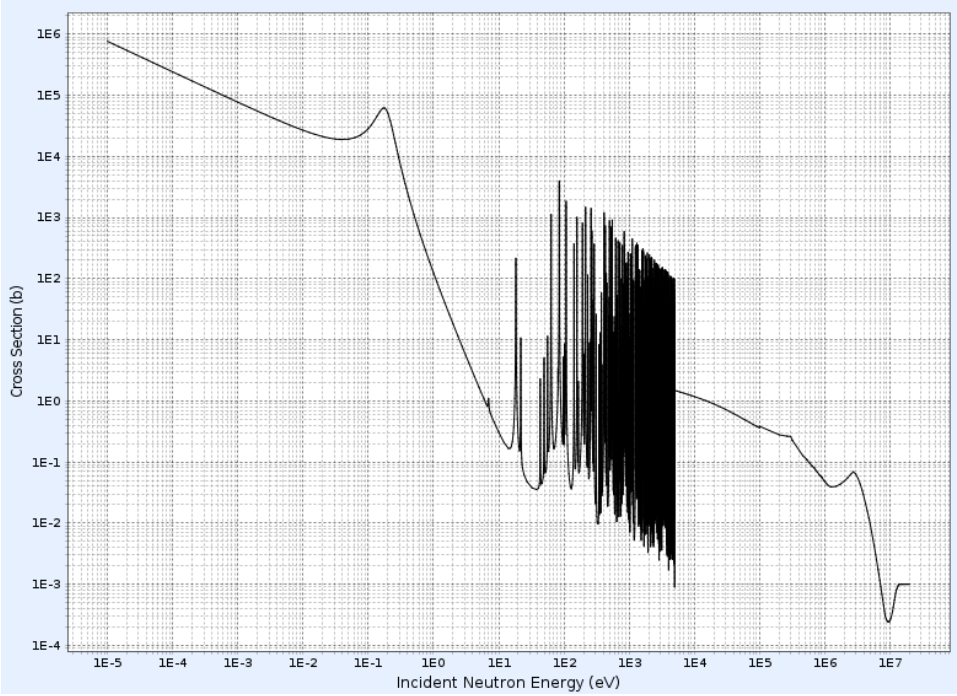

Figure 2.4. Absorption cross-section of ^{113}Cd[50].

The Cd liner between section 3 of the detector and the fuel "bulges out" around the bare fission chambers as shown in Figure 2.5. This allows the bare fission chambers to measure the thermal flux from the fuel, while keeping thermal neutrons from returning to the fuel assembly.

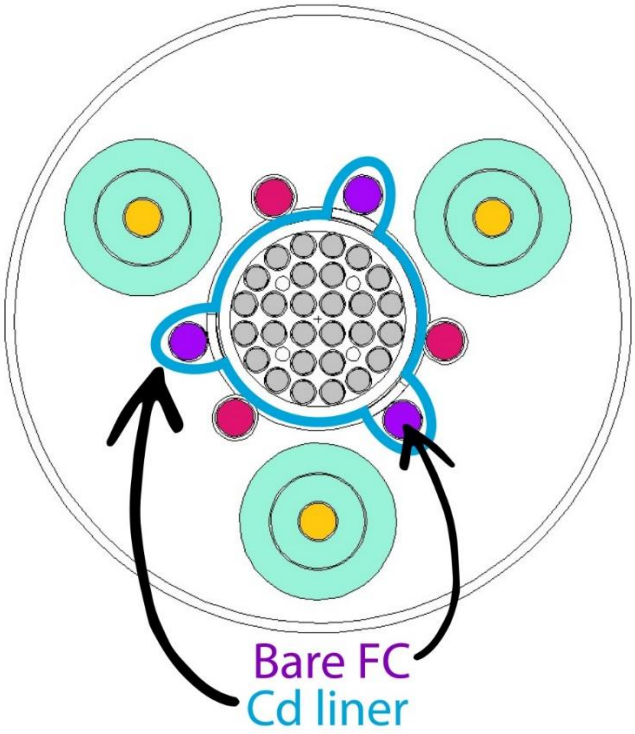

Figure 2.5. Diagram of Cd liner in section 3 of PNAR detector.

Because of the set up shown in Figure 2.5, the bare fission chambers are measuring primarily thermal flux from the fuel. The Cd covered fission chambers are on the other side of this Cd liner from the fuel, and they are also surrounded with an additional thin layer of Cd, which together absorb most of the thermal neutrons. As a result, these detectors primarily measure epithermal neutrons. The fast flux monitors are surrounded by 1.73 cm of polyethylene, 0.1 cm of Cd, and then another 1.9 cm of polyethylene. The goal of these detectors is to detect only neutrons which were fast when they left the fuel assembly. The first layer of polyethylene preferentially slows down lower energy neutrons. The Cd then absorbs the lowest energy neutrons at this point, which were more likely to have been epithermal and thermal when leaving the fuel assembly. The final layer

of polyethylene slows down the remaining neutrons, which were likely fast when they left the fuel, to the thermal region so they can interact in the fission chambers. The fission chambers in Section 3 can also be used to analyse different parts of the neutron energy spectrum. An MCNPX input deck used to simulate fresh fuel measurements in this detector can be found in Appendix A. The detector built for these measurements is shown in Figure 2.6 with the clamp and hose for carrying signal cables above water.

Figure 2.6. Fugen detector built for underwater measurements of Fugen fuel

2.4 Fugen Spent Fuel Measurements

In June 2013, a series of spent fuel measurements were performed in Tsuruga, Japan at the Fugen Power Reactor Site. These measurements were performed to

experimentally assess the capability of PNAR to determine multiplication and fissile content of SNF.

2.4.1 Fugen Spent Fuel Measurement Schedule

The schedule of events during the two weeks of measurements at the Fugen site is shown in Table 2.3. The first three days involved site specific training for LANL staff, as well as background measurements and preparations for measurements by JAEA and Fugen staff. Over the next eight days, each assembly was measured at least once. The measurement plan was drafted in advance based on simulations of PNAR measurements of these assemblies to obtain similar counting statistics amongst the assemblies.

Table 2.3. Preparation and Measurement Schedule

June 17	Overnight background measurement, training and preparation
June 18	Training and preparation
June 19	Training and preparation, overnight background measurement
June 20	Measure M7
June 21	Measure M5, start overnight measurement of U2
June 22	Finish U2 measurement, measure M6, start overnight background measurement
June 23	Continue background measurement from 6/22
June 24	Measure M4, start overnight measurement of M1
June 25	Finish M1 measurement, measure M3
June 26	Measure M2
June 27	Measure M1, M2, M3, M4, M6, and M7 again for comparison to earlier measurements. Also measure M7 3 times to investigate effects of fuel positioning within the detector.

Before long measurements of each assembly, the assembly was scanned axially at a rate of approximately 1 cm per second while collecting 4 second measurements to obtain gamma and neutron profiles of each assembly. After the axial scans, one long measurement was made for each assembly with the bottom of the fuel 2600 mm below the top of the PNAR detector. This position was chosen because it had the highest neutron count rate in the axial scan of the first assembly. The actual count times for each of these long measurements are shown in Table 2.4.

Table 2.4. Measurement Times for Each Assembly June 20-26

Assembly	Measurement Time (hours)
M1	14.0
M2	7.3
M3	7.0
M4	3.2
M5	3.6
M6	3.1
M7	3.7

One concern in these measurements was that the axial offset between sections 1 and 3 (38 cm) would affect the PNAR measurement. To test this, assemblies M4, M5, M6, and M7 also had long measurements with the assembly moved down another 38 cm so that the bottom of the fuel was 2980 mm below the top of the PNAR detector. This allowed for measurements of the same portion of the fuel assembly with section 1 and section 3 fission chambers. It was determined that the PNAR ratio calculated from one measurement location was not significantly different than the PNAR ratio calculated with offset

measurements to measure the same position of each fuel assembly with section 1 and section 3 detectors.

Two systematic concerns inherent in these measurements were 1) how stable the detector response would be over time and 2) how significant would any random changes in lateral position of the fuel assembly within the detector be on the PNAR ratio. To assess these issues, the last day of measurements was spent re-measuring most of the assemblies for comparison to previous measurements. Assemblies M1, M2, M3, M4, and M6 were each measured once more for comparison to measurements made earlier in the week. M7 was measured twice, for comparison to the measurement earlier in the week and to have a set of three measurements to investigate the effects of positioning within the detector. Assembly M7 was returned to the fuel storage rack between these two measurements so that the positioning would be as random as any other two fuel assembly measurements.

The members from LANL and JAEA are shown in Figure 2.7 with many of the Fugen site staff during measurements in the spent fuel pool area at the Fugen reactor site.

Figure 2.7. Measurement team including LANL, JAEA, and Fugen by spent fuel pool during spent fuel measurements.

2.4.2 Fugen Measurement Results

This section includes results and analysis from the Fugen PNAR Measurements.

2.4.2.1 Axial Scans

Each assembly was scanned twice (up and down) before its first long measurement. An example of the total photon and neutron (section 1) counts from assembly M7 is shown in

Figure 2.8, where 0 mm is when the bottom of the fuel assembly is at the top of the PNAR detector. As the plot moves to the right, the assembly is moving downwards through the PNAR detector at roughly 10 mm/sec. The indentions in the photon flux line up axially with the spacer plates in the assembly, and the dip around 2200 mm in the neutron spectrum lines up with a larger spacer grid present in all assemblies.

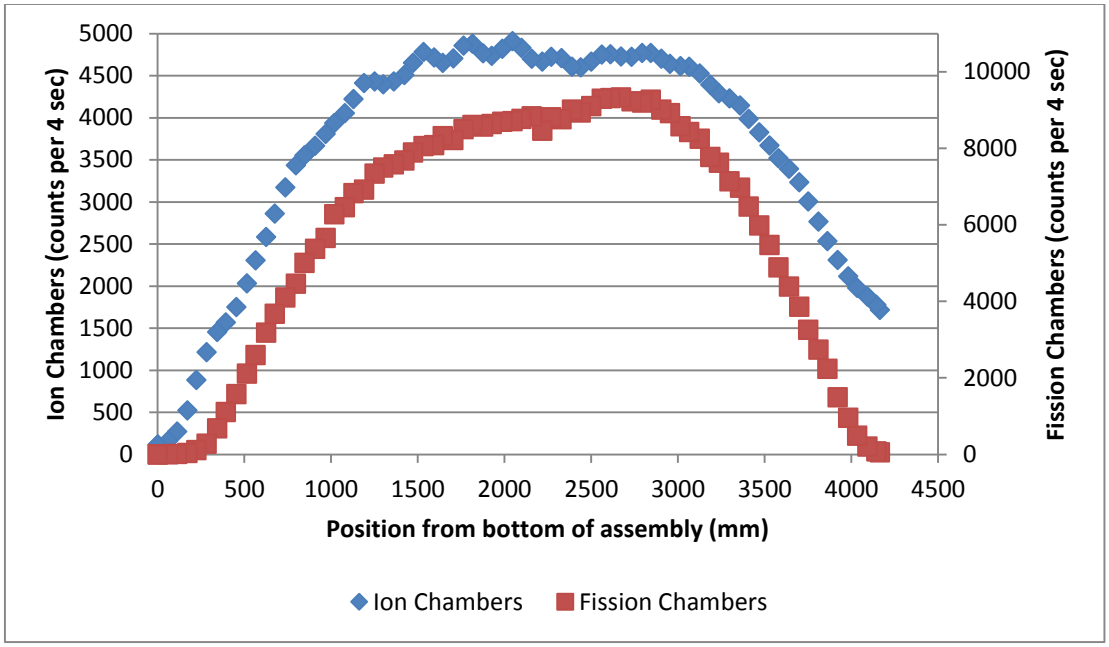

Figure 2.8. Photon and neutron scans of assembly M7 in 4 second increments.

Comparisons between gamma and neutron scans of different assemblies are shown in Figure 2.9 and Figure 2.10. It is clear that they follow the same basic shape but with different magnitudes. Information on each assembly's burnup and cooling time can be found in Table 2.1. Assemblies M1-M4 have the same cooling time and increasing burnup, M4-M6 have the same burnup and increasing cooling time, and M7 has the same cooling time as M6 but a higher burnup. It was expected that the counts in both the ion chambers and fission chambers would increase from M1-M4, decrease from M4-M6, and then for M7 to be higher than M6. This behavior was observed in the measured data.

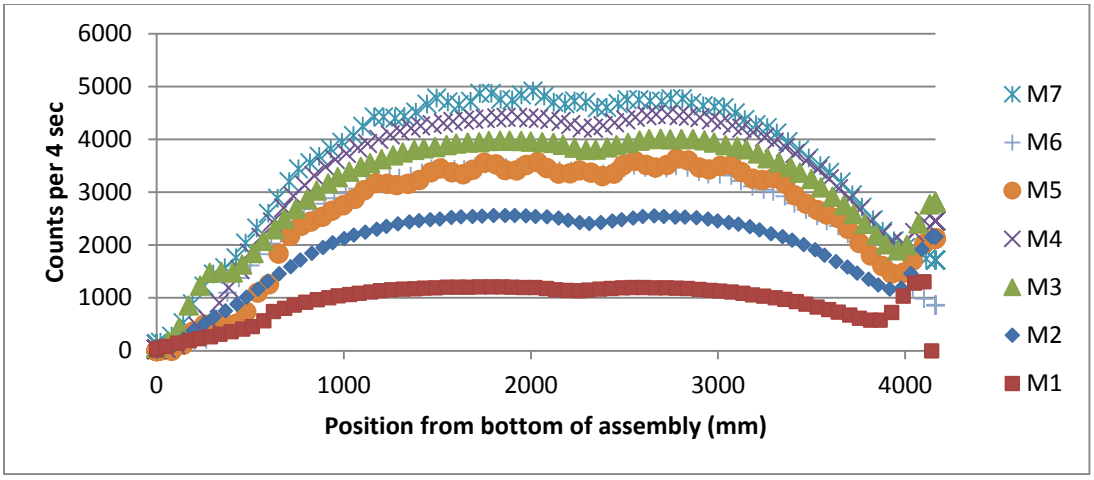

Figure 2.9. Total ion chamber counts from scans of each assembly during first week of measurements.

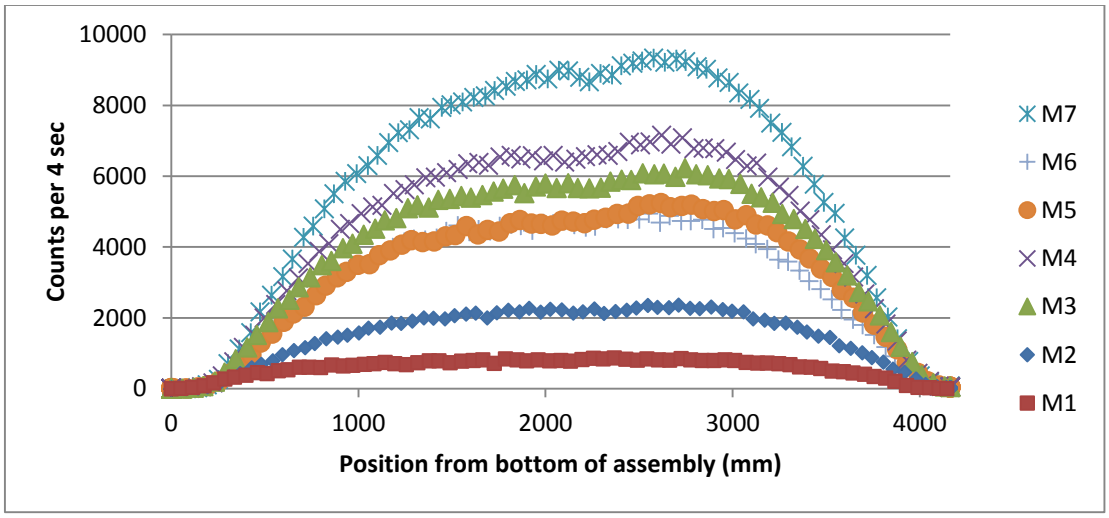

Figure 2.10. Fission chamber scans from each assembly during first week of measurements. Shown here are the total counts for the three fission chambers in section one.

2.4.2.2 Ion Chamber Measurements

The ion chambers functioned well during the measurements except at very low count rates (such as background measurements). The ion chamber count rate of each

assembly versus fuel burnup is shown in Figure 2.11. Ion chamber counts for this plot are used from long measurements of each assembly, and have count rate errors of less than 1% which cannot be seen on this plot. As expected, the ion chamber count rate increases with burnup, but decreases with cooling time. The burnup and cooling time for each assembly can be seen in Table 2.1. The ion chamber was less sensitive than typical ion chambers at low count rates due to the use of an analog-to-digital converter box that was necessary in order to input the ion chamber signal into the data acquisition system designed for neutron detection.

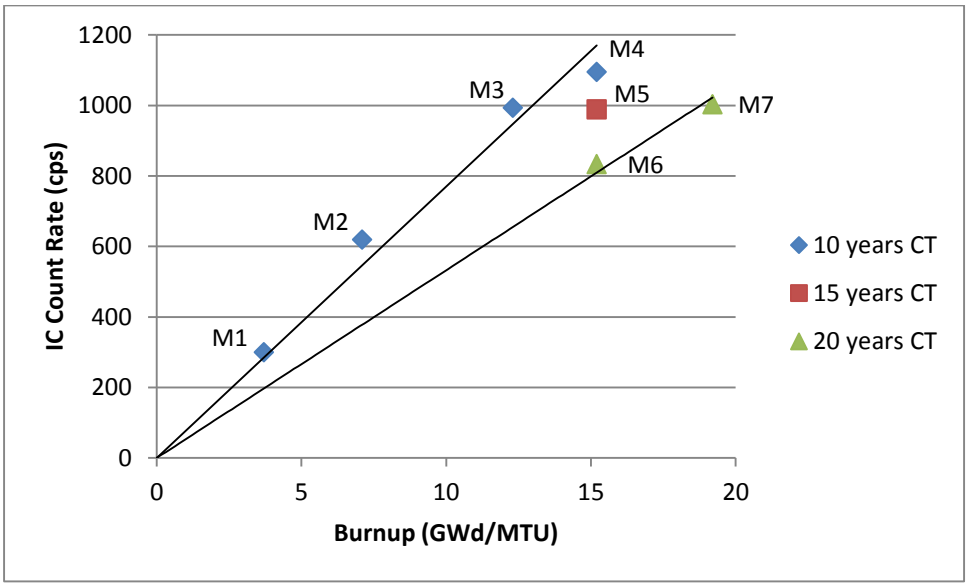

Figure 2.11. Total Ion Chamber counts per second versus burnup for assemblies measured on June 27.

2.4.2.3 PNAR Ratio

Because all three sets of fission chambers in section 3 are in the low multiplying region, the PNAR ratio could be calculated with different sets of section 3 fission chambers. Several combinations were investigated, but the ratio chosen for this research is:

$$PNAR = \frac{\text{Section 1}}{\text{Bare - Cd}} \tag{2.1}$$

It was discovered that by using a difference between the bare and Cd covered tubes, the signal was dependent on epithermal neutrons which created a greater change in signal across the range of fuel measured. The results of PNAR measurements of the Fugen SNF assemblies are shown in Figure 2.12. In Figure 2.12, M1 appears to be a statistical outlier. The cause for this outlier point is undetermined, but appears to be either an assembly misidentification or measurement error. Resolution of this outlier will be left as future work.

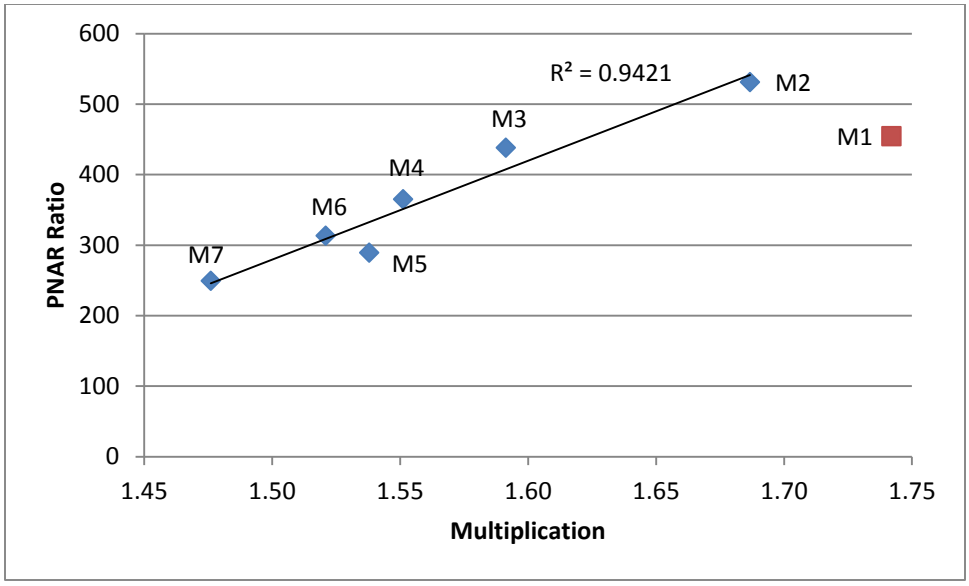

Figure 2.12. PNAR Ratio for Fugen SNF assemblies.

This plot shows a 73% change in measured PNAR signal over the range of fuels measured. The count rate statistics errors on these points are too small to be visible at less than 2%. With the count rate statistics and standard deviation of the line fit to assemblies M2-M7, the multiplication of an assembly can be calculated with a standard deviation of .02, or roughly 1%.

2.4.2.4 Pu Effective

As described in Section 1.3.2, Pu_{eff} is an indirect measurement of the plutonium present in a fuel assembly. In fuel assemblies from the same reactor, the Pu_{eff} value is often directly related to the multiplication, which is what PNAR measures. C_1 and C_2 were calculated using the "MCNPX method" from Hu, 2010[47], which involves using flux multipliers in MCNPX. The values of C_1 and C_2 were calculated to be 0.435 and 1.33, respectively. Figure 2.13 shows the multiplication of the Fugen assemblies as a function

of Pu_{eff}. The isotopics of each assembly were calculated using LANL's burnup simulations, and these isotopics are used to calculate Pu_{eff} and simulate an assembly in MCNPX to determine multiplication. The labels show that Pu_{eff} decreases with an increase in burnup for this fuel, which is expected since it is MOX fuel.

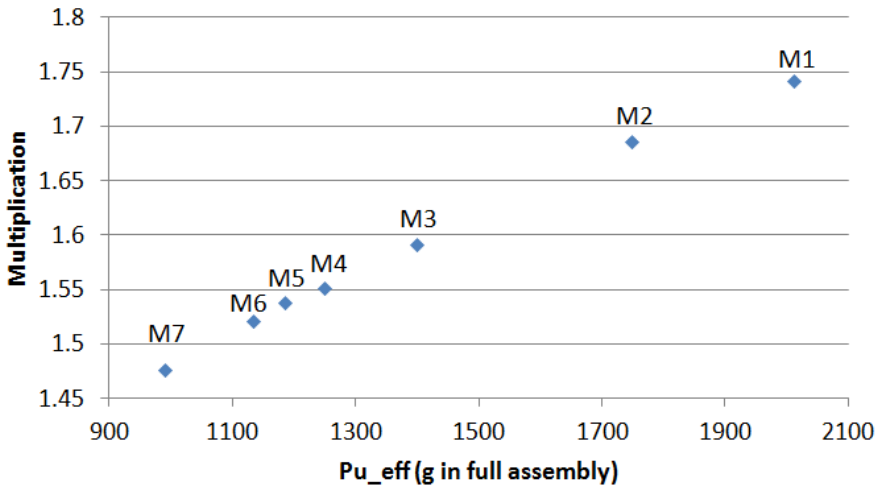

Figure 2.13. Pu_{eff} vs. multiplication in Fugen assemblies

Figure 2.14 shows the PNAR ratio measured from Fugen assemblies as a function of Pu_{eff} in grams in the full assembly. This is a comparison of a simulated value (Pu_{eff} is based on simulated isotopics) to a measured value. They trend quite well, except for the outlier data point of M1. This is a result of the M1 data point being an outlier in Figure 2.12.

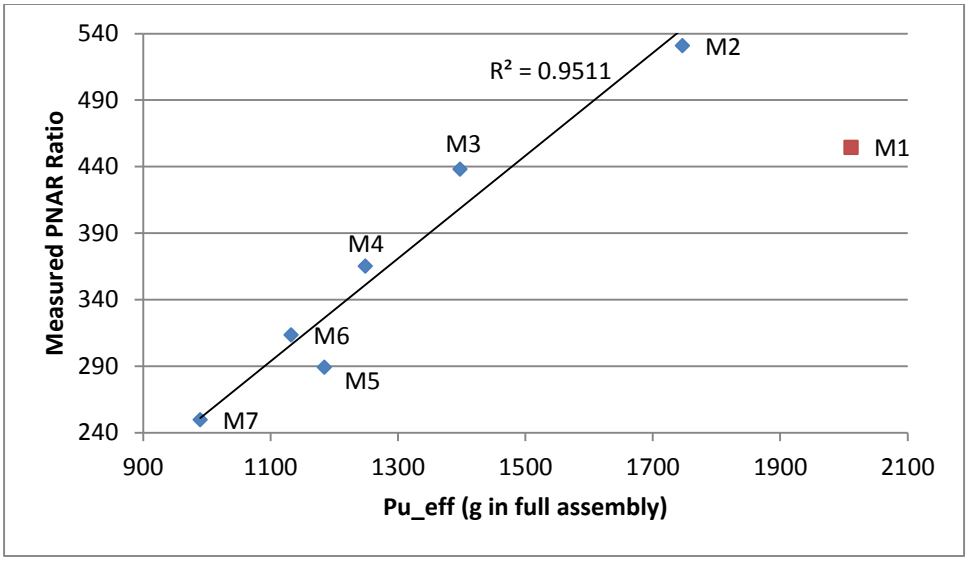

Figure 2.14. Pu_{eff} vs. measured PNAR Ratio

Without the outlier at M1, this plot shows a 77% change in signal over the range of measurements. With the standard deviation of the line fit to assemblies M2-M7, the Pu_{eff} content of an assembly can be calculated to within 54 g, or 4.2%. This number could likely be improved if calibrated with fuel with better known isotopics.

2.5 LANL Fresh Fuel Measurements

2.5.1 Fresh Fuel Measurement Experiments

Fresh fuel racks were built specifically for these measurements since the PNAR detector built for Fugen measurements does not fit typical PWR or BWR assemblies. This rack design is shown in Figure 2.15. There is a solid base plate, two fuel rod spacer plates, and a shaft in the center. The fuel rod spacer plates are attached to each other and the base plate with threaded rods which allow the fuel rod spacer plates to be moved and keep them aligned. The fuel rod spacer plates each have three threaded slots around the perimeter.

Small set screws in these slots allow for precise positioning of the assembly within the detector. The shaft in the center of the assembly racks is for the ^{252}Cf source during measurements.

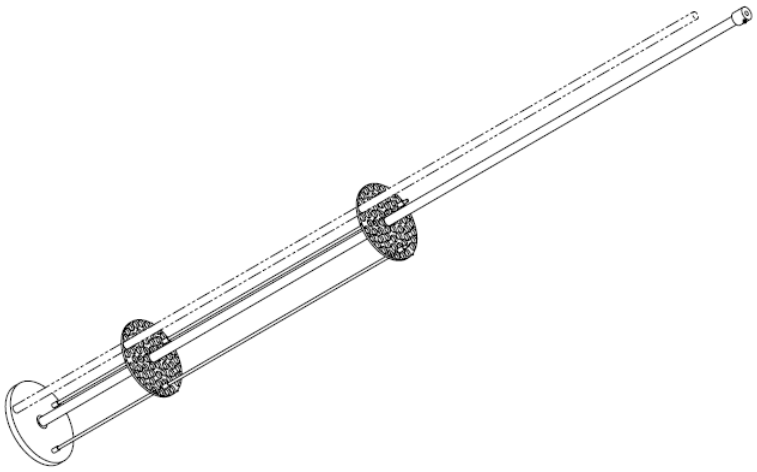

Figure 2.15. Assembly rack design for LANL fresh fuel PNAR measurements.

Two assembly designs were developed. The first design, assembly 1, is similar to Fugen fuel in that it has the same quantity of fuel per unit length and radius as Fugen fuel, but with PWR pins. In order to keep the same mass of fuel per unit length of the assembly, 60 PWR pins were used in this design. The assembly radius was kept the same as the Fugen fuel assemblies – 5.6 cm. The other design, assembly 2, is similar to typical LWR fuel in that it has the same fuel/moderator ratio and a thinner gap between the fuel and the detector. This design was chosen to have a water gap between the fuel of 1/8" – similar to the spacing found in PWR spent fuel storage racks. This resulted in an assembly radius of 6 cm. The assembly was also chosen to have a similar fuel to moderator ratio as typical

PWR fuel, which resulted in having 51 PWR pins. The assembly designs are shown below in Figure 2.16. The rectangular slots around the perimeter of the assemblies are for the set screws which are used to specify the location of the assembly within the detector.

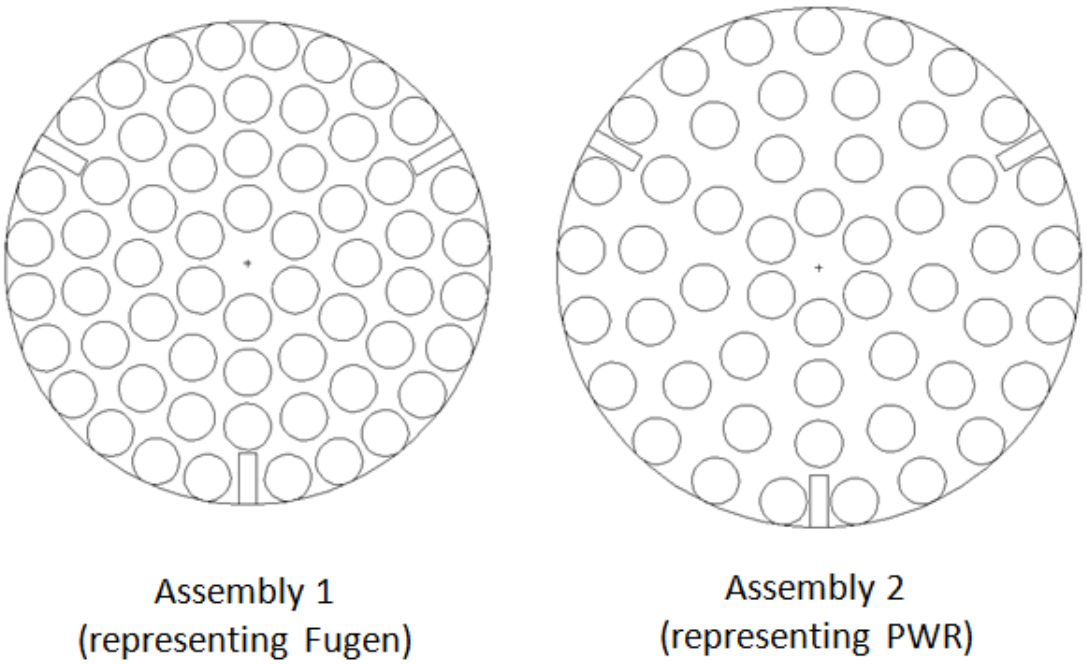

Figure 2.16. Assembly designs

Both of these designs were tested in multiple configurations. For each measurement, the source was placed in three locations: centered on the section one fission chambers, centered on the section three fission chambers, and midway between those two locations. In some configurations, a scan of the entire assembly was taken by moving the source in 2” increments from 4” above the detector lid to 6”below the bottom surface of the detector.

Each assembly was measured at 5 ‘effective enrichments’ obtained by evenly mixing the Depleted Uranium (DU) and LEU pins. Each assembly was measured at different positions within the detector to estimate effects of fuel assembly location on the PNAR ratio. A measurement was also made with LEU and DU pins distributed unevenly throughout the assembly to test the penetrability of the PNAR measurements.

For the effective enrichment measurements, 5 configurations were chosen for each of the two assembly designs. The lowest enrichment was 0.2% ^{235}U, all DU pins. The highest enrichment was 3.19% ^{235}U, all LEU pins. Three other configurations were chosen between those two values by mixing the LEU and DU pins evenly throughout the assembly. These arrangements are shown in Figure 2.17 and Figure 2.18.

One of the concerns in SNF NDA measurements is the precise location of the fuel with respect to the detector. Most owners of SNF will require some gap between the detector and the assembly – they need some space in case the fuel is bowed and would prefer the detector to not touch or rub against the fuel to prevent fuel failure. In most cases, this gap creates some uncertainty about the position of the fuel assembly with respect to the detector. In the PNAR detector specifically, the 120^{o} symmetry could potentially offset any effects of an un-centered fuel assembly. One of the goals of the fresh fuel measurements was to determine if this position uncertainty resulted in a change in the PNAR ratio.

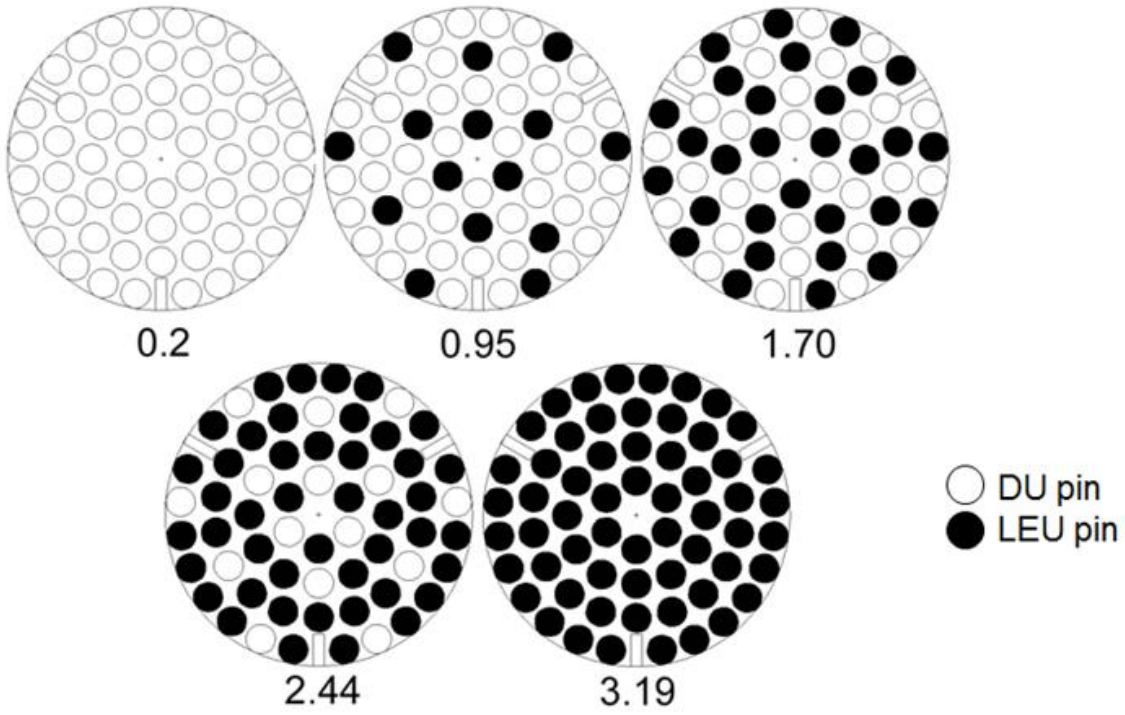

Figure 2.17. Assembly 1 enrichment configurations.

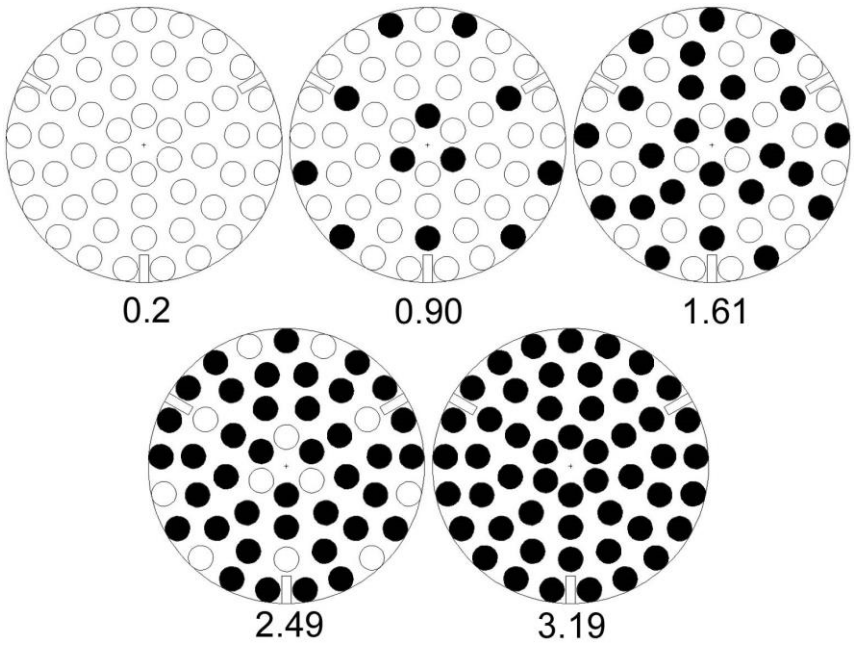

Figure 2.18. Assembly 2 enrichment configurations

In order to test the effect of a change in the position of the assembly within the detector on the PNAR signal, set screws were adjusted in the fresh fuel rack assembly plates to set the assembly at specific locations within the detector. The measured locations are shown below in Figure 2.19. These are worst case scenarios, with the assembly entirely against a wall of the detector. The positions were chosen with respect to the 120° symmetry of the detectors – one off-centered location is towards the FFM, while the other is between two FFMs. Ideally, the higher counts from one or two detectors closest to the assembly would offset the lower counts from one or two detectors farther from the assembly.

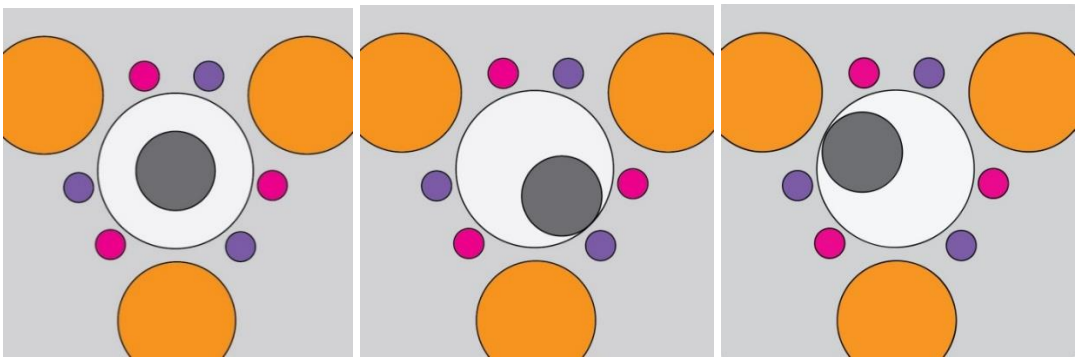

Figure 2.19. Positioning measurements: assembly centered, assembly towards cable port, and assembly away from cable port.

Another concern in general spent fuel measurements is the penetration of the measured signal. Ideally, a SNF NDA measurement would measure an average of the entire fuel assembly. Realistically, some measurements are especially weighted towards one region of the fuel, such as the outer perimeter, and don't effectively measure other parts of the assembly, such as the center. To test the penetrability of the PNAR detector,

the same number of LEU and DU pins from the 2.49% assembly 2 design were arranged unevenly throughout the assembly, with all the LEU pins on the outside edge of the assembly. If PNAR was preferentially measuring the outside of this assembly, the PNAR ratio would indicate a higher enrichment than in the evenly distributed 2.49% case. The assembly configurations for both of these cases are shown in Figure 2.20.

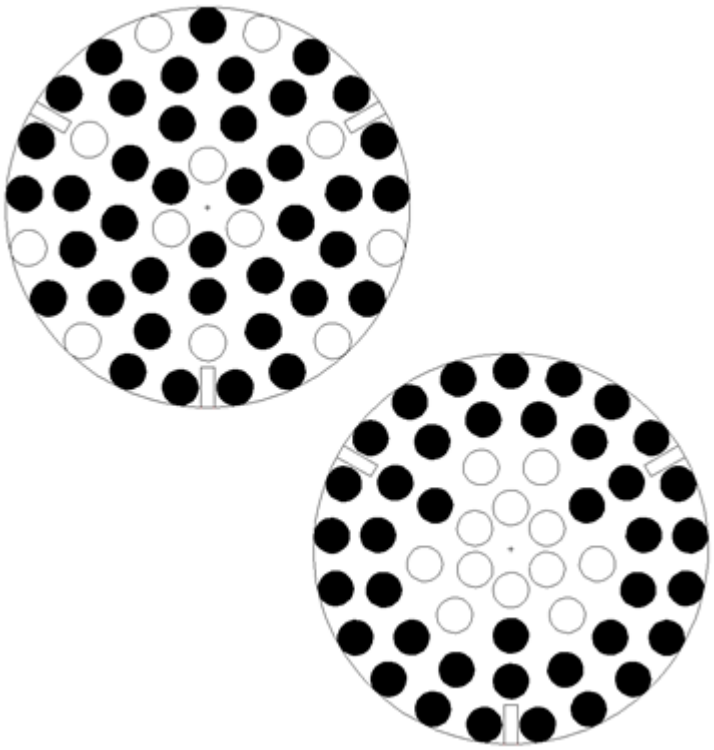

Figure 2.20. Assembly configurations for evenly spaced 2.49% distribution and unevenly spaced 2.49% distribution used in penetration measurements.

2.5.2 Fresh Fuel Measurement Results

Source scans were performed in many of the measurement configurations. In these scans, the source was moved axially in 2” increments from 4” above the top of the detector

to 4” below the bottom of the detector. The results from each set of fission chambers for the scan of assembly 1 at full LEU pins (3.2%) are shown below in Figure 2.21.

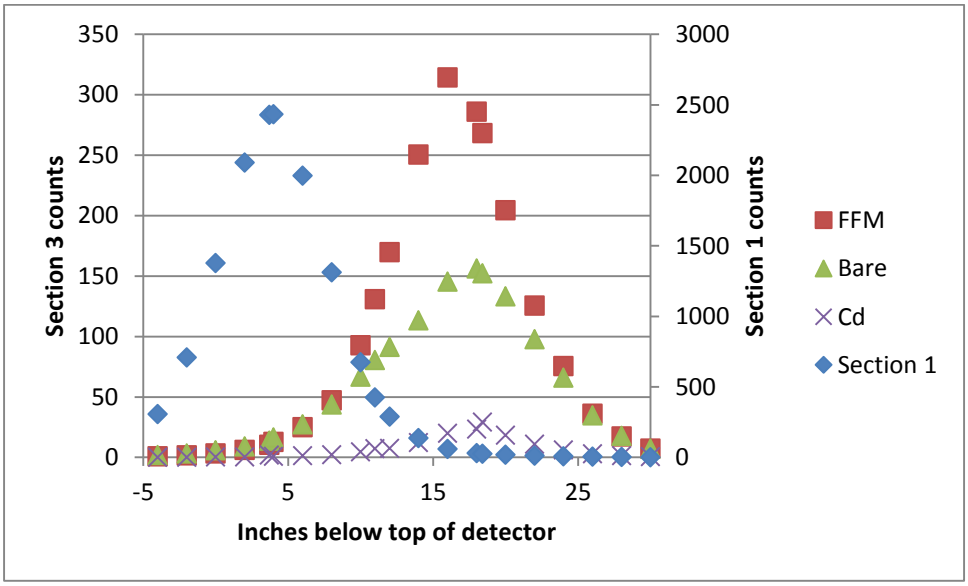

Figure 2.21 Source Scan for 3.2% configuration of fresh fuel assembly 1.

This shows that the fuel above and below the detector are negligibly affecting the total count rates. It shows that the curves for each detector response are not skewed, and they all have relative standard deviations between 0.9 and 1.2, which makes the midpoint of each detector a reasonable location for fresh fuel measurements.

This does show that the measurement center for the FFM detectors is slightly higher than the measurement center of the bare and Cd covered detectors. This is because while the center of all three fission chambers is the same, the polyethylene and cadmium around the FFMs is actually centered slightly higher, which affects the neutrons creating fissions in those fission chambers. This is a slight design factor that could be modified in

the future, but it is simply a calibration issue for point source measurements and not an issue in continuous source measurements as long as the fuel is relatively constant over a couple inches, as is typical for commercial SNF.

As mentioned in section 2.2.3.3, the PNAR ratio in this detector can be calculated as a ratio of the high multiplying region to any of several combinations of the low multiplying region detector sets. In the spent fuel measurements, the difference between the bare and cadmium tubes was used as the low multiplying region measurement, which highlights effects due to epithermal neutrons. This ratio was used again for the fresh fuel measurements for consistency, but since all fission chambers were assessed and fixed upon return to LANL, the sum of all detectors of each type was used rather than a single tube As such, the PNAR ratio used for fresh fuel measurements is:

$$PNAR = \frac{\text{Section 1}}{\text{Bare-Cd}}. \tag{2.2}$$

The PNAR ratios for assembly 1 and assembly 2 are shown in Figure 2.22 and Figure 2.23, respectively. Count rate errors for these plots are less than 1% and too small to be visible.

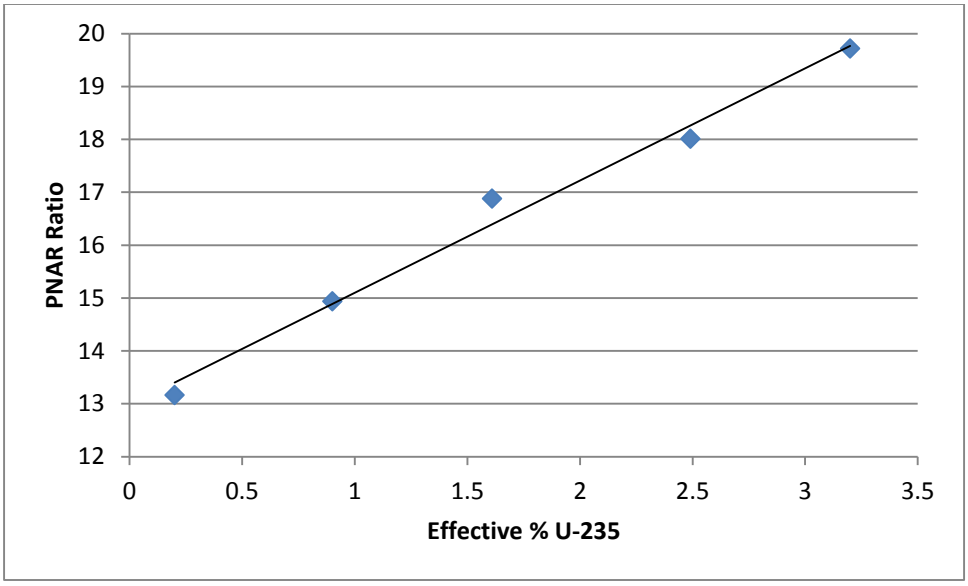

Figure 2.22. PNAR ratios for fresh fuel measurements of assembly 1 at different effective enrichments.

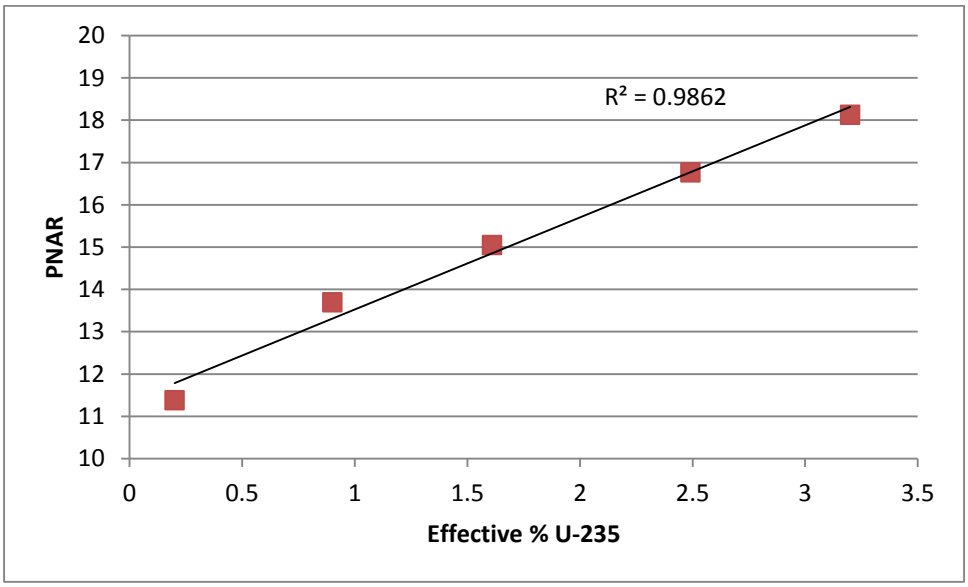

Figure 2.23. PNAR ratios for fresh fuel measurements of assembly 2 at different effective enrichments.

These measurements show that the PNAR Ratio trends quite linearly with enrichment of the assemblies. The total change in signal for assembly 1 and assembly 2 designs are 40% and 45%, respectively. The standard deviation of the best fit lines results in a standard deviation of 0.12% ^{235}U in estimating the effective enrichment, or 7% of the average effective enrichment.

Another series of fresh fuel measurements was to determine the effect of position of the assembly within the detector on the PNAR ratio. The racks for each fresh fuel assembly have three set screws on each grid plate which were used to specify the location of the assembly within the detector. To assess the worst case scenarios given the 120° symmetry of the detector, two measurement locations were selected for the full LEU configuration of each measurement design. These were shown in Figure 2.19. The results from the measurements are shown in Table 2.5

Table 2.5. Fresh fuel assembly positioning measurement results.

	% Difference in PNAR ratio from measurement with centered assembly	
Measurement location	**Assembly 1 (Fugen type)**	**Assembly 2 (PWR type)**
assembly away from cable port	-3.0	-2.9
assembly near cable port	-7.7	-2.5

In most cases, the change in PNAR ratio was under 3%, which corresponds to change in initial enrichment of about 0.25% ^{235}U. The one case with a change in PNAR ratio of almost 8% was with the wider water gap. The assembly with a water gap of only ¼" was under 3% for both cases.

Another detector response tested in these measurements was the penetration of the PNAR signal. The same number of DU and LEU pins used in the evenly distributed 2.49% ^{235}U configuration were unevenly distributed such that the LEU pins were all on the outside and the DU pins were all on the inside. These two configurations were shown in Figure 2.20. The PNAR ratios for the evenly and unevenly distributed configurations were 14.45 and 14.47, relatively, for a change in signal of 0.1%, which is better than the errors in the measurements. This indicates that the distribution of LEU and DU pins in the assembly are of little importance to the PNAR signal, at least in an assembly the size of the Fugen assemblies. This is a good sign for partial defect measurements.

2.5.3 Fresh Fuel Measurement Simulations

Simulations were performed of many of the measurement configurations for benchmarking purposes. A comparison of the simulations to experiments for each set of fission chambers for each effective enrichment configuration of assembly 1 is shown in Figure 2.24.

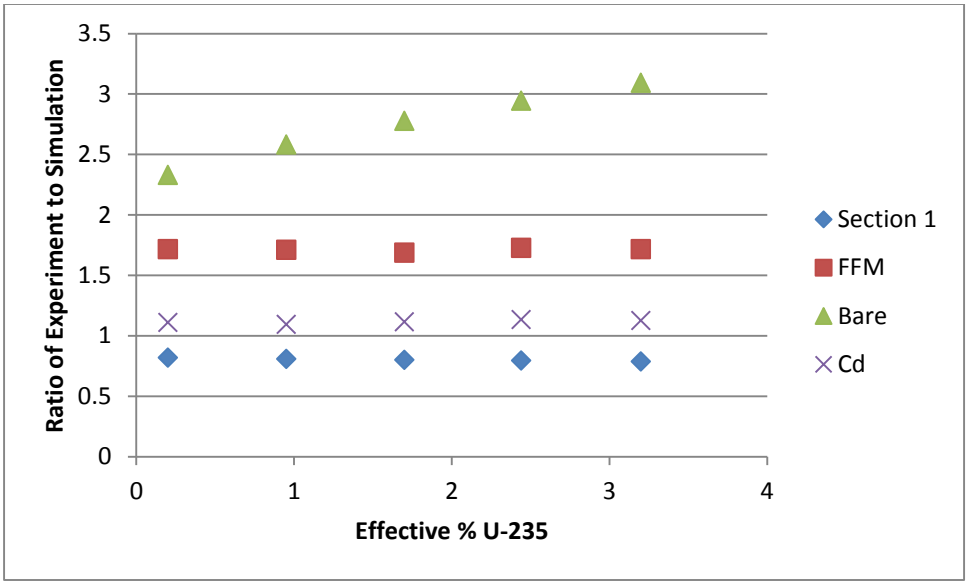

Figure 2.24. Comparison of experiment to simulation for each set of fission chambers

Figure 2.24 shows that the section 1, FFM, and Cd covered tubes have flat lines for experiment to simulation ratios. This indicates that simulations are accurately predicting trends in measurements. The vertical distance between these lines is likely due to difference in absolute calibration of the fission chambers. The slope of the bare fission chamber comparison is due to the fact that simulations show a trend of about 30% of the total signal, while experiments had almost the same count rate for each configuration. This is the case for both assembly 1 and assembly 2 configurations. The cause for this is still unknown, but one possibility is that these bare fission chambers are the most sensitive to changes in multiplication in the fuel, and are being affected by the moderating material surrounding the measurement set-up more than the other fission chambers. This is a concern for future simulations of the PNAR detector, but the trend in experimental PNAR

ratio for both sets of measurements still shows that the PNAR ratio is an effective measurement of multiplication.

2.6. Conclusions from PNAR Application to SNF Safeguards

Through experiment and simulation it has been shown that PNAR is applicable for safeguarding SNF. When supplied with appropriate SNF parameters, it is expected that PNAR can measure SNF plutonium content to within 4.2% (or 54 g $^{239}Pu_{eff}$) and detect the diversion of at least 25% of the pins from an assembly. The technique also has application to fresh fuel measurements and can accurately measure ^{235}U in LEU fresh fuel assemblies.

3. PHOTON MEASUREMENTS

In the previous section, we assessed the capability of PNAR to determine $^{239}Pu_{eff}$ in SNF. PNAR could measure this with a high degree of accuracy when supplied with sufficient information about the fuel assembly to allow a model of the assembly that links multiplication to $^{239}Pu_{eff}$ (specifically initial enrichment, burnup, and cooling time). This information could be declared by the operator; however, in safeguards it would be preferred to have an independent measure of any operator-supplied information. In this chapter, we will show that this fuel assembly information can be acquired from photon measurements of the assembly. Several measurement campaigns of solid SNF pins were conducted at ORNL, covering a range of burnups, cooling times, and fuel types to demonstrate this capability using commercially available detector systems.

This research started by determining what signals were identifiable with commercially available broad-energy coaxial and low-energy planar HPGe detectors. Next, simulations were performed to investigate how each of these signatures responded to changes in a set of fuel parameters. Then, a sensitivity characterization was performed by changing individual fuel parameters in simulations. These simulations were performed to determine which signatures were the best indicators for individual fuel parameters. While some of the signatures are more useful than others, and some signatures are only applicable to a subset of SNF (such as with low cooling times due to a short half-life), the goal of this research was to determine what is possible.

This research focuses on photon measurements of solid pressurized water reactor (PWR) fuel pins in air due to the availability of this fuel. In a safeguards application, these

measurements would likely be made with the assembly in water but using an air filled collimator. Thus, we expect these measurements to well approximate the application configuration. It may be useful for future measurements to be conducted on entire assemblies to verify the accuracy of this technique for entire assemblies as opposed to individual pins[14].

In this research we concentrated on the usage of ratios of signals to provide more robust analyses. Since photon signals can depend on many factors (including geometry, detector calibrations, and material properties), taking the ratio of two signals can often decrease the effect that lack of knowledge of these factors can have.

3.1 ORNL ADEPT Facility Measurement Setup

The spent fuel pin measurements were performed in hot cells at the Irradiated Fuels Examination Laboratory (IFEL) at ORNL. The IFEL hot cells have a precision positioning system called the Advanced Diagnostics Evaluation PlaTform (ADEPT) which was used for all the spent fuel pin measurements used in this study. The ADEPT system is shown in Figure 3.1 with a fuel pin in the hot cell during the October 2011 measurements. The yellow tint of the photographs inside the hot cell is due to the leaded glass used in the hot cell windows.

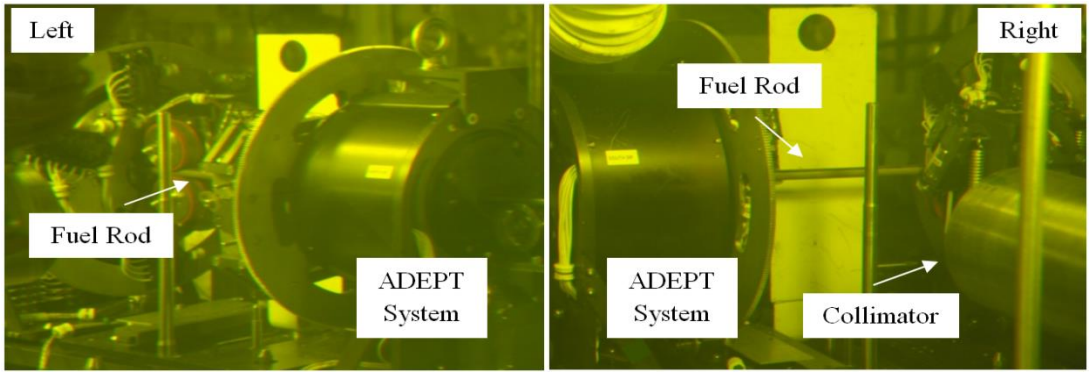

Figure 3.1. ADEPT system with a fuel pin placed directly in front of the collimator.

The ADEPT system uses a digital control system to measure the length of each fuel pin and adjust its position inside the hot cell so that various axial positions along the fuel pin can be measured through the beam port. There are manipulators inside the hot cell which are controlled manually from outside the hot cell. These manipulators are used to move fuel to and from the ADEPT system. For some measurements, they were also used to remove fuel from the shipping tubes the fuel had been transported in, as shown in Figure 3.2.

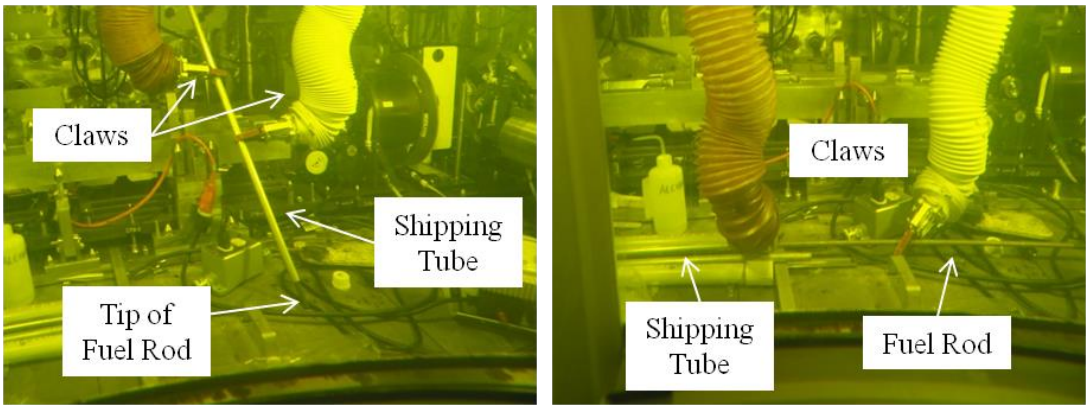

Figure 3.2. The ORNL technicians removing the Three Mile Island SNF from its shipping tube using the claws inside of the hot cell

The ADEPT system is situated so that the fuel is directly in front of one of the beam ports to the outside of the hot cell. The outside of the beam port is about 218 cm from the center of the fuel pin. The beam port is a rectangular slit which can be adjusted in thickness with a movable plate inside the collimator. The collimator can be seen on the inside of the hot cell in Figure 3.1.

Figure 3.3 shows a detector, dewar and the outside of the beam port during the October 2011 measurements.

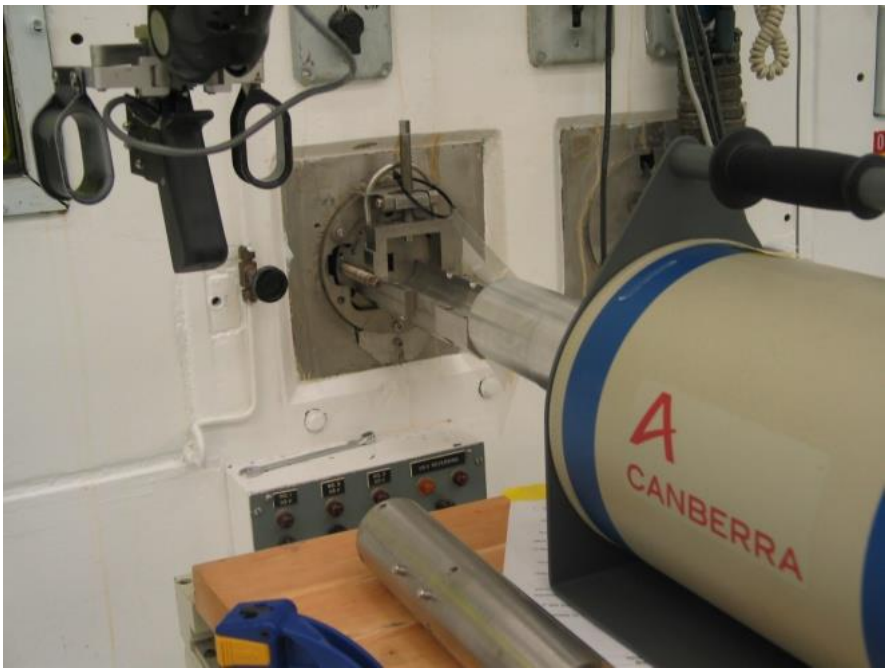

Figure 3.3. HPGe detector SNF photon measurement through the hot cell wall using the stainless steel collimator

Two sets of measurements were performed for each fuel pin. Measurements with a coaxial HPGe ORTEC PopTop detector using ORTEC Maestro software were used to acquire a broad-energy spectrum. This detector was usually set to collect data between 30

keV and 2040 keV, but cannot sufficiently resolve many peaks in SNF below 120 keV. A second set of measurements were taken with a Canberra Low Energy Germanium (LEGe) planar detector designed to measure energies between 30 keV and 300keV. The planar detector measured a low-energy spectrum which was usually set to collect data between 30 keV and 300 keV. For these measurements, long planar detector count times were used to provide good resolution of the 103.7 keV Pu X-ray peak while using a very long and thin collimator (resulting in a microscopic beam spot). This detector setup is likely not practical for field use and could possibly be replaced with a commercially available segmented HPGe planar detector (using up to 800 miniature HPGe crystal segments in one detector) with a specialized small collimator array. More information about the detector setup and measurements can be found in References [58] and [61].

Because the flux profile in a nuclear reactor is not homogeneous, not all fuel in the reactor reaches the same burnup. Of particular interest to measurements of single pins is the axial flux variation. Because the axial flux is largest in the center of the reactor, the ends of the fuel pin are at a lower burnup than the center. This was exploited for these measurements to collect data from several points along each pin at different burnup values. This allowed some investigation of how photon signatures changed with burnup when all other parameters were held constant.

3.2 Description of Measured Fuels

Fuel rods from North Anna, Three Mile Island, Catawba, and Calvert Cliffs were measured at the ORNL ADEPT facility. The first measurements investigated in this paper

were performed on North Anna fuel in July 2008. This fuel pin had an initial enrichment of 4.199 wt.% ^{235}U, cooling time of 4.2 years, and burnup values along a single fuel pin from 35 to 67 GWd/MTU. In January 2009, another measurement campaign looked at a fuel pin from the Three Mile Island unit 1 reactor. This fuel pin had an initial enrichment of 4.0 wt.% ^{235}U, cooling time of 13.3 years, and a burnup range of 27 to 59 GWd/MTU. In September 2009, a fuel pin from Catawba with MOX fuel was measured. This fuel had been produced with weapons-derived Pu. The original fuel was 4.4% Pu (5.25% of the heavy metal was Pu) and depleted U with 0.27% wt ^{235}U. The Catawba MOX fuel had a cooling time of 9 months and burnups from 18 to 52 GWd/MTU. In October 2009, measurements were taken on a fuel pin from Calvert Cliffs. This pin had an initial enrichment of 3.038 wt.% ^{235}U, a cooling time of 27.5 years and an estimated burnup of 37 GWd/MTU. In October 2011, more measurements were performed on the same Three Mile Island fuel pin, and at the time of this measurement the fuel had a cooling time of 16.1 years. Altogether, these measurements cover cooling times from 9 months to 27.5 years, burnups of 18 to 67 GWd/MTU, and both uranium dioxide and mixed oxide fuel. Fuel parameters for the measured fuels are shown in Table 3.1. More information about the histories of these fuels and specific measurement set-up information can be found in References [58] and [61].

Table 3.1. Parameters of SNF Measured at ORNL.

Fuel	Burnup [GWd/MTHM]	Initial Enrichment	Cooling Time [years]
North Anna	35-67	4.19% U^{235}	4.2
Three Mile Island	27-59	4.0% U^{235}	13.3, 16.1
Calvert Cliffs	41	3.038% U^{235}	27.5
Catawba (MOX fuel)	18-52	4.4% Pu with DU	0.75

3.3 Spectral Analysis of Fuel Measurements

The collected spectra were analyzed using GENIE 2000 software to determine photopeak energies and net peak areas, identify isotopes present in the fuel, and determine the relative isotope activities.

3.3.1 Spectrum Analysis Software

The Canberra spectrum analysis program, GENIE 2000, was used to analyze the spectra collected from the various measurement campaigns. In order to ensure that GENIE calculated peak areas correctly and consistently for each spectrum, an interactive peak fit tool was utilized to visually identify how well GENIE's automated analysis fit the measured data. This involved ensuring that the background was fit accurately and looking for overlapping peaks which were incorrectly being measured as one peak by GENIE's automated peak fitting process. Two screenshots from this interactive peak fit program are shown in Figure 3.4a and Figure 3.4b. They show the impact of the interactive peak fit software for a small portion of a complicated spectra. Each figure displays several

features. The green squares in the top half of each image are individual data points with counting uncertainties (the black lines above and below each point) for each channel. The calculated peak fit is shown as the black curve and associated red striped area. The calculated background is shown as the solid pink area below each peak. The residuals (or difference between the measurement and GENIE's fit for that point) for each channel are shown as the green squares in the lower half of each image. The red horizontal lines in the lower half of each image are at the same value in each image, and mark the area within which the residuals should fall if the region is fit correctly. Ideally, the residuals would be within these red lines and randomly scattered, as in Figure 3.4b. The definite curve visible in the residuals of Figure 3.4a indicates that a second peak is present in the measurement but not accounted for in GENIE's automated fit. This peak has been manually added in Figure 3.4b. GENIE 200 fits most gamma-ray peaks, which have a natural Gaussian shape, very well. However, GENIE 2000 does not fit the natural Lorentzian shape of x-ray peaks well. Since ratios are being used in this work instead of direct measurements, trends and relative changes are more important than absolute values. Therefore, it is more important that the peaks are fit in the same manner for each spectrum than that the actual value of each peak area is accurate. For this reason all x-ray fits were manually adjusted using the interactive peak fit program. To calculate peak areas for U x-rays, manual measurement regions were placed around the U 98 keV x-ray peak – which was well isolated – to compute the net peak area. The Pu 103 keV x-ray peak was too close to the ^{155}Eu 105 keV peak to fit in this method. The multi-peak region including these two peaks was manually fit in each spectrum, keeping as many features constant as possible, and it was assumed

that GENIE 2000 fit both these peaks in the same manner within the interactive fit program for each spectrum.

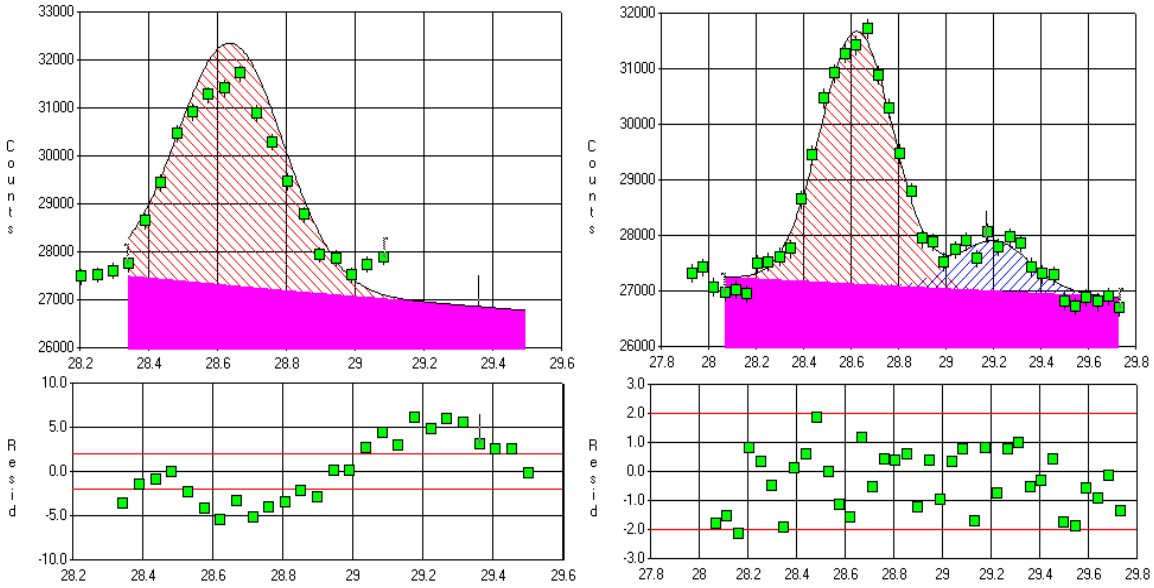

Figure 3.4. Interactive peak fit showing (a) fit directly from GENIE 2000 automated fit and (b) fit after manual correction by adding an additional peak in the interactive peak fit program. In (a) and (b), the upper half shows the spectra and the lower half shows the residuals.

3.3.2 Visible Nuclides

The nuclides visible for each group of measurements were identified. Isotopes with a half-life greater than ten days, along with decay products of these isotopes, were added to a library of fission products for use with the GENIE software. This half-life criterion was chosen because the youngest fuels dealt with in this analysis, and in most practical applications, are at least six months old. By this point, isotopes with half-lives less than

ten days are unlikely to be visible. This library was used with the peak identify feature in GENIE to identify the nuclides visible in each spectra.

Table 3.2 Measurable Nuclide Presence in the Four Fuels Measured.

Nuclide	NA	TMI	CC	MOX
^{137}Cs	All Coax	All Coax	All Coax	All Coax
^{134}Cs	All Coax	All Coax	All Coax	All
^{154}Eu	All	All	All Coax	All
^{144}Ce*	High BU Coax	None	None	All
^{125}Sb	High BU coax	All Coax	None	All
^{110m}Ag	High BU Coax	None	None	All Coax
^{106}Ru	All Coax	None	None	All Coax
^{60}Co	All Coax	All Coax	All Coax	All Coax
^{214}Bi	All Coax	All Coax	All Coax	All Coax
U x-ray	All	All	All Coax	All
Pu x-ray	All Planar	All Planar	All Planar	All
^{155}Eu	All Planar	All Planar	All Planar	All Planar
^{241}Am	None	All Planar	All	Low BU Planar

*While ^{144}Ce is one of the commonly used isotopes for measuring cooling time, this usually takes advantage of the low background around ^{144}Ce's 2185 keV peak. None of these measurements extended to this high of an energy.

Table 3.2 lists the presence of each isotope identified in the measured fuels. In this table, the entries list the measurements in which each signal was visible. For example, ^{106}Ru was seen in all coax measurements for the North Anna and Catawba MOX fuel (mostly due to the relatively short cooling times), but not in the coaxial spectra for Three Mile Island or Calvert Cliffs, or in any of the planar spectra. Figure 3.5 - Figure 3.7show some examples of the measured spectra.

Figure 3.5 shows a close up of the x-ray region for one of the low burnup Catawba MOX measurements (with a 10 hour count time).

Figure 3.6 shows the extent to which ^{134}Cs is still visible in the Calvert Cliffs fuel after almost 30 years cooling time. The strongest ^{134}Cs 604 keV peak is almost completely obscured by Compton background from the ^{137}Cs 662 keV peak. However, the ^{134}Cs 795 keV peak is still clearly visible, with a net peak area uncertainty of 2.9% after a 4.2 hour (live time) count.

Figure 3.7 displays the visibility of short-lived isotopes ^{110m}Ag and ^{106}Ru in relation to the strongest ^{137}Cs and ^{134}Cs peaks in the Catawba MOX fuel. This measurement was the highest burnup along the rod, at 52.5 GWd/MTHM, but the peaks are clearly visible at lower burnups as well.

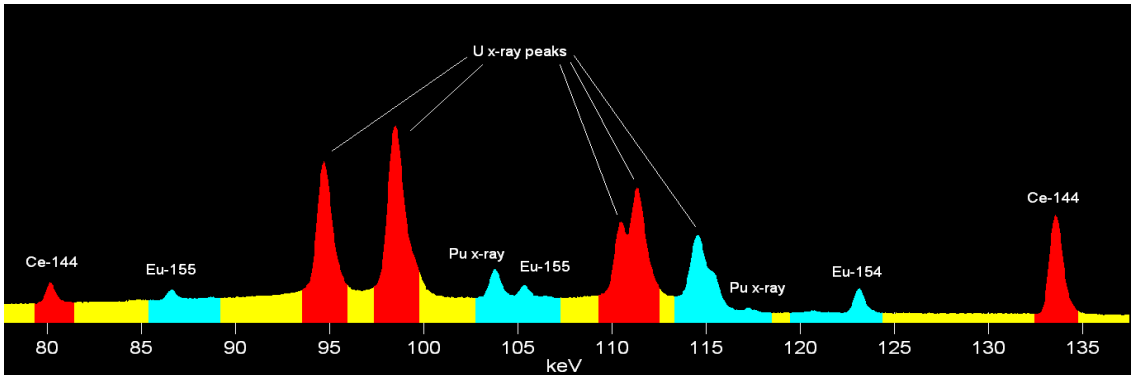

Figure 3.5. X-ray region of Catawba MOX fuel at position 1965.

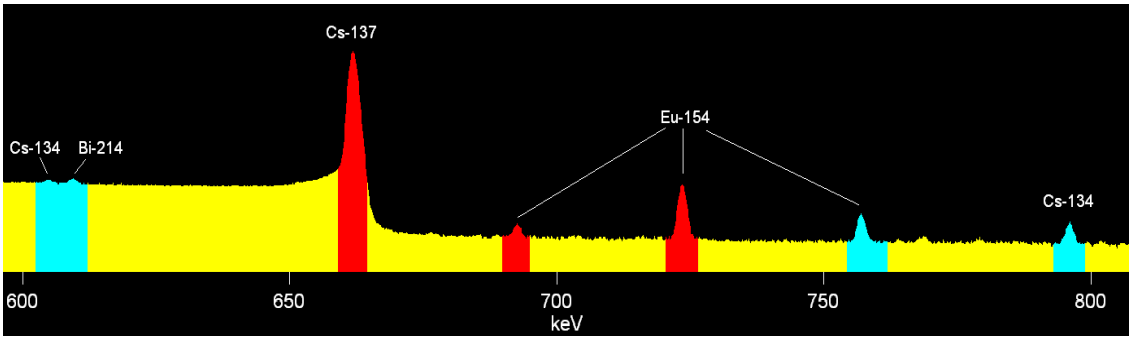

Figure 3.6. 600 keV to 800 keV region from Calvert Cliffs coax measurement.

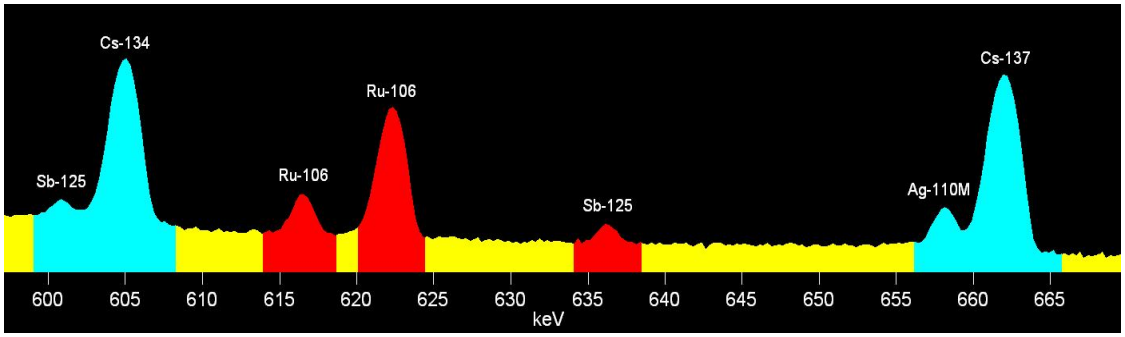

Figure 3.7. 600 keV to 670 keV region from Catawba MOX fuel at position 1865.

3.3.3 Determining Relative Isotope Activity Ratios

The net peak areas from GENIE 2000 were used to determine the isotope activities in each fuel. However, even in measurements of a single nuclide with multiple photon peaks, the known ratios of intensities of the peaks do not directly correspond to the peak heights in the spectra. This is because detector efficiencies and escape probabilities from the fuel (i.e., the probability that a photon born in the fuel rod escapes from the fuel rod and cladding) are both functions of energy. Detector efficiency calibration curves can be obtained by measuring a source with several photon peaks with known intensity ratios (such as ^{152}Eu) in a wide range of energies. Once generated for a detector, this calibration curve can be applied to ratios as a correction. Escape probabilities can be calculated in MCNP if the fuel composition and geometric specifications are well known. These calculations depend on geometric specifications, densities, and mean free paths in materials. These factors will not significantly change over the life time of SNF and should be the same for all fuel of a certain design. If several measurements are being taken on fuel with the same fuel composition and geometric specifications, as is often the case in

safeguards measurements, this information can be calculated once and can be used to correct ratios of future measurements.

$^{134}Cs/^{137}Cs$ ratios were used to determine the burnup for each set of measurements. ORIGEN simulations were run for each fuel over the known power history and cooling times, but with varying power levels to simulate the axial power distribution the fuel rod experiences in the reactor. The calculated ^{134}Cs and ^{137}Cs atom densities were compared to measured $^{134}Cs/^{137}Cs$ ratios to determine burnup. To account for differences in the energies of peaks used, detector efficiency curves were obtained with a ^{152}Eu source and escape ratios were calculated through MCNP simulations. Differences in peak intensities were also taken into account in the ratios. For more information on the process of calculating burnup base on photon measurements in a fuel with known geometric specifications, cooling time, power history, and initial enrichment, see Section 3.1 of Reference [58].

3.4 Fuel Measurement Results

Using the planar detector provided the unique opportunity to measure several U x-rays, as well as the main Pu x-ray, in spent fuel and to use these as a monitor of burnup without the need for *a priori* knowledge of the fuel history and dimensions. The fact that the half-lives of most U and Pu isotopes are much longer than the age of any SNF means that this ratio is relatively independent of cooling time, unlike the $^{134}Cs/^{137}Cs$ ratio often used to calculate the burnup of SNF measurements. Since the energies of the U and Pu x-ray peaks differ by only ~5 keV, the detector efficiency and escape ratios are not needed

in order to draw meaningful conclusions. Simulations later in this section show that both bulk U and bulk Pu are insensitive to initial enrichment. This adds to the convenience of using this ratio as a potential burnup monitor in the field if little information is known about the fuel being measured. In addition, UO_2 fuel is known to have zero Pu content before irradiation which adds an anchor point to correlations. The Three Mile Island and Catawba MOX measurements indicate that Pu x-ray/U x-ray ratios scale very well with burnup. Figure 3.8 shows the Pu/U x-ray ratio for the Three Mile Island fuel measurements.

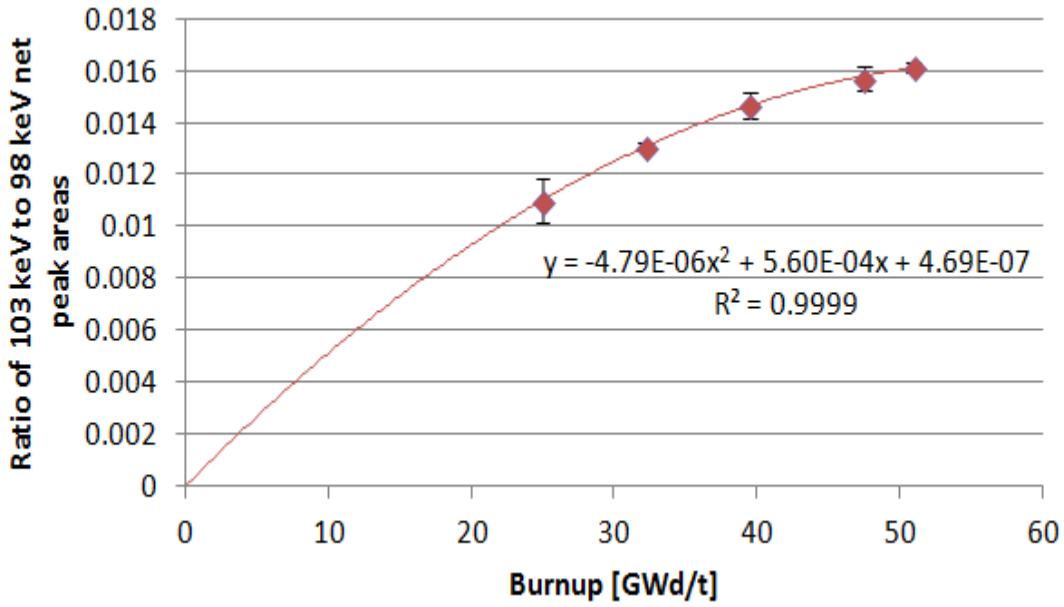

Figure 3.8. Ratio of Pu 103 keV x-ray to U 98 keV x-ray vs. burnup for Three Mile Island fuel.

As expected from normal LWR fuel, this indicates that the Pu content grows with burnup, but levels off as the Pu builds up enough to become a decent source of fissions.

This plot was fit with a second degree polynomial, but was not manually anchored at the origin, so it is promising that the y-intercept is almost zero, which is expected as described above.

Figure 3.9 shows the Pu/U x-ray ratio for the Catawba MOX fuel as a function of burnup. Count rate errors on these ratios are below 1% and are too small to be seen. This shows the expected downward trend in Pu content in Catawba MOX fuel as the Pu in the original fuel is burned off even though Pu is also building up from ^{238}U neutron absorptions. The y-intercept suggests that the initial Pu content was 5.35% of the total heavy metal content of the fuel, which has a relative error of only 2% from the actual value of 5.25%.

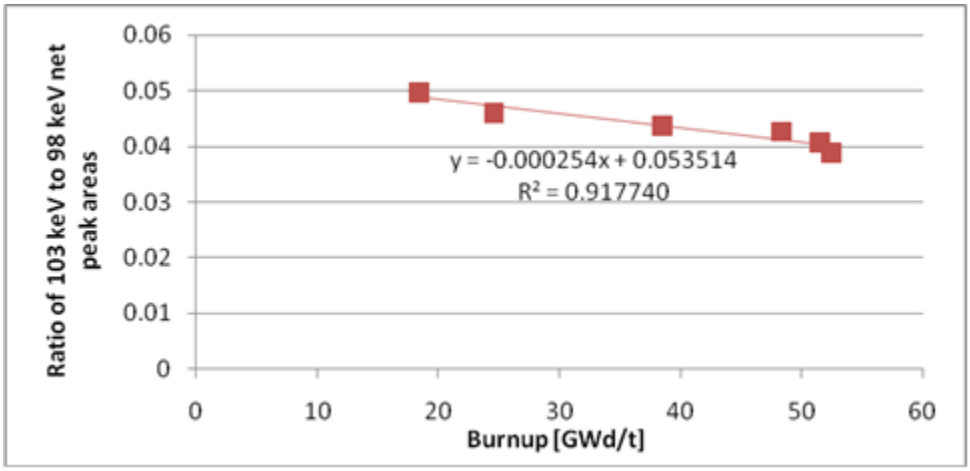

Figure 3.9. Ratio of Pu 103 keV x-ray to U 98 keV x-ray vs. burnup for Catawba MOX fuel.

The ratio of the ^{155}Eu 105 keV peak to the 98 keV U x-ray peak (shown in Figure 3.10) is another promising burnup indicator measurable with planar detectors but not

typical coaxial detectors. The ratio of any fission product to a U x-ray peak should have a value of zero when extrapolated to the fresh fuel case. This plot has a y-intercept of 0.0015, which is very close to zero even for the low magnitude of the ratio measurements.

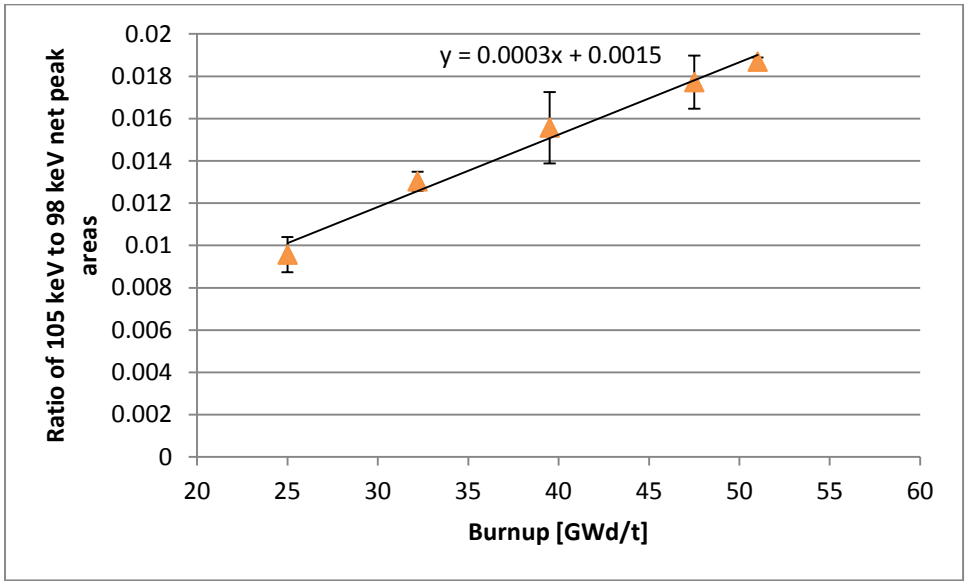

Figure 3.10. Ratio of ^{155}Eu 105 keV peak to 98 keV U x-ray peak vs. burnup for Three Mile Island fuel.

3.5. Sensitivity Analysis

In order to determine how much knowledge about the history of SNF can be obtained from photon measurements, it is necessary to determine how each signal depends on different fuel history parameters. There are many parameters which could change isotopic composition of the fuel. These parameters include burnup, cooling time, power level of the last burn cycle, total days of shutdown before the last burn cycle, initial

enrichment, moderator temperature and density, cladding composition and thickness, fuel assembly pitch, and burnable poisons.

This section discusses a series of sensitivity simulations performed with MONTEBURNS to investigate how each of the signals found in the SNF measurements at ORNL depends on several of these parameters. The parameters investigated here are initial enrichment, moderator density, soluble boron concentration in the pool water, power level, and power cycle. A range was selected for each of these parameters based on the range seen in the fuels measured at ORNL. Each time a parameter was perturbed for the sensitivity analysis, it was randomly sampled in this range. Burnup was not considered an input parameter because it is really a result of combinations of power level and power cycle. Burnup is a main factor in many isotopes' concentrations, though, and it is considered in the power level and power cycle analysis.

Each photon signature's dependence on each individual fuel parameter was tested as well as its dependence on combinations of changes in multiple parameters. First, a reference fuel was chosen in order to be more representative of fuels typically measured in safeguards scenarios. This was considered the 'base case,' and every other simulation was compared to it. Using relative changes rather than absolute values makes this study more widely applicable and mitigates possible errors in the inputs or fuel simulation in the same manner as taking ratios of photon peaks rather than trying to use absolute activities.

Since MONTEBURNS does not provide statistical errors, the base case was run ten times with different starting seed values to obtain statistical errors for each signature

at each cooling time. It was assumed that these percentage errors could be applied to all other simulations at the same cooling times.

To investigate effects of changing each parameter on each fuel signature, and thus how well that fuel signature is an indication of that fuel parameter, each parameter was changed up and down from the base case.

3.5.1 Reference Fuel Model

The reference fuel pin used in these simulations was chosen with the intention of being representative of typical fuel measured in safeguards applications. A 17x17 PWR fuel pin was used with initial enrichment of 4%, 45 GWd/MTU burnup, 5 years cooling time, and a power history of three cycles of 455 days at 33 W/g with shutdowns of 20 days between each cycle and sitting out of the reactor for one cycle after the first two. This case also had 0.715 g/cc moderator density and 500 ppm of natural boron in the water. This reference fuel pin became the 'base case' with which all other simulations were compared.

Many factors of the MONTEBURNS spent fuel sensitivity simulations are the same for all simulations. The fuel pin geometry, MCNP cross-section libraries used, fission Q-value, number of outer, inner, and predictor steps to run from MONTEBURNS, ORIGEN library used, and automatic tallying in MONTEBURNS, and cooling time values used were held constant for all the simulations. The only things that changed were initial enrichment, moderator density, boron concentration, power level, and power cycle, and at most two of these deviated from the base case in any one simulation.

The fuel pin geometry is based off of a standard 17x17 PWR assembly with fuel outer diameter of 0.4096 cm, cladding inner diameter of 0.418 cm, and cladding outer

diameter of 0.475 cm. The fuel was expanded to fill the fuel-cladding gap and the density was reduced accordingly to a density of 10.02 g/cc. The fuel-to-moderator ratio was calculated taking into account water holes in the assembly, and this was used to calculate the pin pitch for the simulation. A square was created, centered around the round fuel pin, with infinitely reflecting sides that were each 1.3236 cm for the water moderator. A 10 cm tall piece of fuel pin was simulated with infinitely reflecting upper and lower boundaries. The fuel was split into five exponential radial regions. The radii for each region were calculated with Eq. 3.1, where r_i is the radius of region i, $R_{f,O}$ is the outer radius of the fuel, Σ_a is the absorption cross section, and N_r is the number of regions. Σ_a was calculated to be 0.6942 cm^{-1} for 4% i.e. UO_2 fuel, which resulted in fuel region radii being located at 0.2159 cm, 0.3238 cm, 0.3777 cm, and 0.4046 cm, and 0.418 cm.

$$r_i = R_{f,O}\left[\frac{1-e^{(-\Sigma_a i)}}{1-e^{(-\Sigma_a N_r)}}\right] \tag{3.1}$$

The MCNP input deck for each simulation included a kcode criticality simulation card with 1000 source histories per cycle, 1.0 as an initial guess for k_{eff}, with the first 30 of 400 cycles skipped. Source particles were started at the center of the simulated fuel pin. This MCNP deck was run on its own for the base case to make sure that this kcode simulation converged.

In the MONTEBURNS input file, the Q-value for fission was set to -200. Number of outer burn, inner burn, and predictor steps were set to 55, 10, and 1, respectively. The

fractional importance limit was set to 0.005, and 34 specified nuclides were listed for automatic tally in each material.

The Monteburns feed file was used to define the power history of each simulation. For the base case, the fuel was in the reactor for two cycles, out for one cycle, then in for a third cycle. Each power cycle was 455 days with 20 days of shutdown in between each cycle. In the MONTEBURNS feed file, the beginning of each burn cycle started with two 15 day burn steps followed by a third burn step to the end of that cycle. Shutdowns between reactor power cycles were each one step. The cooling time steps were arranged in order to provide the output cooling times desired, with no single step being longer than 1000 days.

The MCNP and MONTEBURNS input decks and the MONTEBURNS feed file for the base case can be found in Appendix B.

3.5.2 Fuel Parameters Tested

In the MONTEBURNS simulations, the examined parameters were initial enrichment, moderator density, boron concentration, power level, and power cycle. For each perturbation in the MONTEBURNS simulations, the value of each parameter changed was chosen randomly in a designated range. The specific range for each parameter was chosen by reviewing the range of parameters visible in the detailed fuel histories of the spent fuel pins measured at ORNL.

First, each parameter was individually perturbed up and down from the base case randomly within the ranges chosen in order to determine how each parameter individually affects the different photon signatures in the fuel. Next, each two parameters were

perturbed up and then down for each combination of two parameters examined in the MONTEBURNS simulations.

3.5.2.1 Initial Enrichment

The main effect from a change in initial enrichment is a change in the ratio of fissions in U to Pu. For fuels with lower initial enrichments, there is less ^{235}U available for fissioning and more Pu produced from ^{238}U, which both lead to more Pu fissions than there would be in fuel of the same burnup with a higher initial enrichment. Since some fission products have higher fission yields from U than from Pu, they will have different concentrations in fuel at the same burnup based on how many of the fissions were in U vs. Pu. Table 3.3 shows the thermal neutron fission yields of many of the fission products and activation products in SNF[51].

While the Pu/U fission yield ratio for ^{154}Eu and ^{134}Cs are both very high, the magnitudes of the U and Pu fission yields for these isotopes are quite small. They are still produced in high quantities in SNF, but are produced more by neutron absorption than by direct fission yield. This is why the yield information for ^{153}Eu and ^{133}Cs are also shown, even though they are not visible in photon measurements of SNF. Similarly, ^{110m}Ag is not directly produced in meaningful concentrations by Pu fission, but more ^{110m}Ag is produced by neutron absorption from ^{109}Ag than is produced directly from fission, so the Pu/U fission yield ratio data for ^{109}Ag is more relevant to initial enrichment effects on ^{110m}Ag production. Based on these caveats, the isotopes with the strongest expected visible dependence on initial enrichment are ^{155}Eu, ^{125}Sb, ^{106}Ru, and ^{110m}Ag.

Table 3.3. Cumulative fission yields and half-lives.

Nuclide	^{235}U fission yield	^{239}Pu fission yield	^{239}Pu/^{235}U yield ratio	Half-life
Cs-137	6.19E-2	6.61E-2	1.07	30.04 y
Cs-134*	3.85E-8	3.35E-6	86.9	2.06 y
Cs-133	6.7E-2	7.02E-2	1.05	Stable
Eu-154*	9.7E-10	1.4E-7	144	8.59 y
Eu-153	1.58E-3	3.61E-3	2.28	Stable
Eu-155	3.21E-4	1.66E-3	5.15	4.76 y
Co-60	0	0	n/a	5.27 y
Bi-214	0	0	n/a	19.9 m
Sb-125	3.40E-4	1.12E-3	3.28	2.76 y
Ru-106	4.02E-3	4.35E-2	10.83	373 d
Ce-144	5.5E-2	3.74E-2	.68	284 d
Ag-110m*	2.28E-14	0	n/a	249 d
Ag-109	3.12E-4	1.48E-2	47.34	Stable
Am-241	0	0	n/a	432.2 y

*This nuclide is shielded by a stable isotope, thus individual fission yields are shown rather than cumulative.

For the sensitivity simulations, a range of initial enrichments between 2% and 5% ^{235}U was chosen based on values present in the fuels measured at the ORNL ADEPT facility. For values lower than the base value of 4%, an initial enrichment was randomly chosen between 2% and 3.8%. For values higher than the base value, an initial enrichment was randomly chosen between 4.2% and 5%.

3.5.2.2 Moderator Density

The main result of a change in moderator density is a change in the neutron spectrum. As the water temperature in a LWR reactor increases, the density of the moderator decreases. When this occurs, there is less moderation between fuel pins in the reactor. This results in a harder neutron spectrum. The effects of changes in moderator

density are especially visible in BWR reactors where there is a large moderator density gradient across the length of the fuel.

Since current safe LWR designs are over-moderated, this results in an increase in resonance energy neutrons (around $1x10^{-6}$ MeV to $1x10^{-1}$ MeV) entering the fuel as well as a decrease in thermal neutrons (around $1x10^{-8}$ MeV) and an increase in fast neutrons (around 1 MeV) entering the fuel. Since neutron cross sections are energy dependent, this affects the way certain nuclides are produced in SNF. Neutron cross sections for ^{235}U fission, ^{238}U fission, ^{238}U radiative capture, and ^{239}Pu fission are shown in

Figure. 3.11.

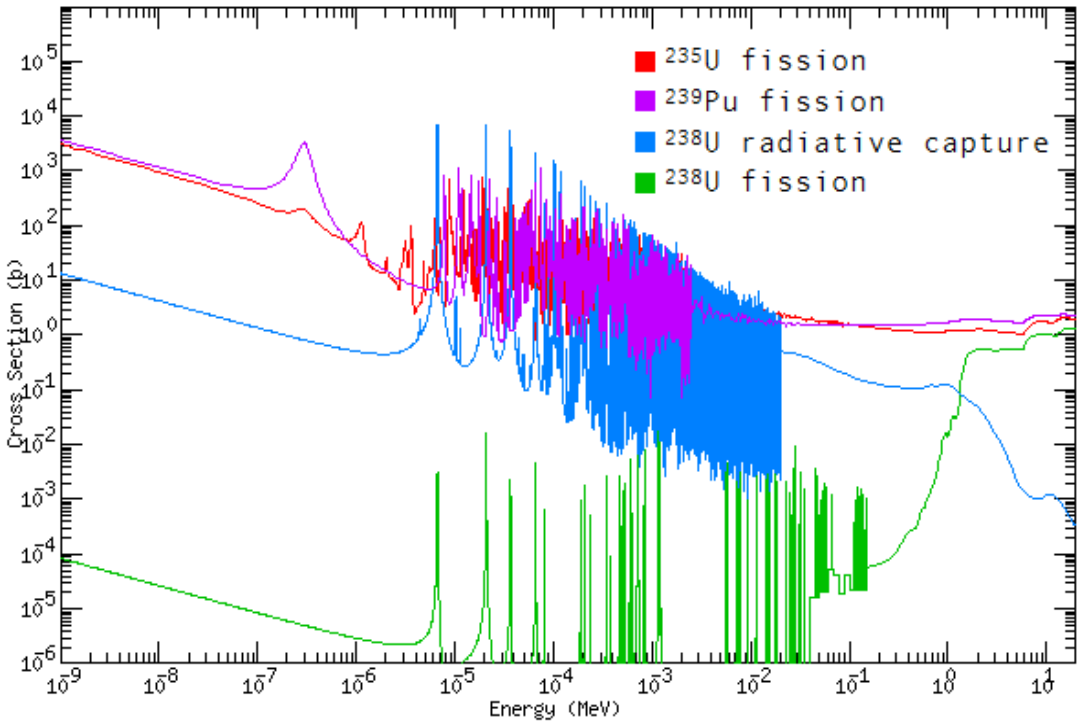

Figure. 3.11. Neutron cross sections for ^{235}U fission, ^{238}U fission, ^{238}U radiative capture, and ^{239}Pu fission[50].

The increase in resonance energy neutrons results in more radiative capture in ^{238}U, which in turn results in more Pu production as described in section 1.4.8. This increase in Pu results in a larger macroscopic Pu fission cross section and more fissions from Pu to reach the same burnup. This higher portion of fissions from Pu will affect the fission product distribution and lead to an increase in the concentration of the isotopes created more by Pu fissions (^{110m}Ag, ^{106}Ru, and ^{125}Sb) for the same burnup.

Moderator density was simulated over a range from 0.6 g/cc and 0.8 g/cc based on values listed in fuel histories for the fuels measured at ORNL as well as expert advice. It was chosen as a random value between 0.6 g/cc and 0.705 g/cc for perturbations below the base value of 0.715 g/cc and between 0.725 g/cc and 0.8 g/cc for perturbations above the base value.

3.5.2.3 Boron Concentration

A change in boron density also changes the neutron spectrum, with results similar, but opposite, to changes in moderator density. Adding boron to the water in a reactor is one way by which reactor operators maintain or change the operating power level of a reactor. There are other ways that reactor operators change power level, including control rods and burnable poisons incorporated into fresh fuel, but these all change power level when inserted by absorbing thermal neutrons which reduces the neutron population in a reactor. Absorbing thermal neutrons, however, not only decreases the neutron population but hardens the spectrum as mostly the thermal neutrons are absorbed. The radiative capture cross section of ^{10}B is shown in Figure. 3.12.

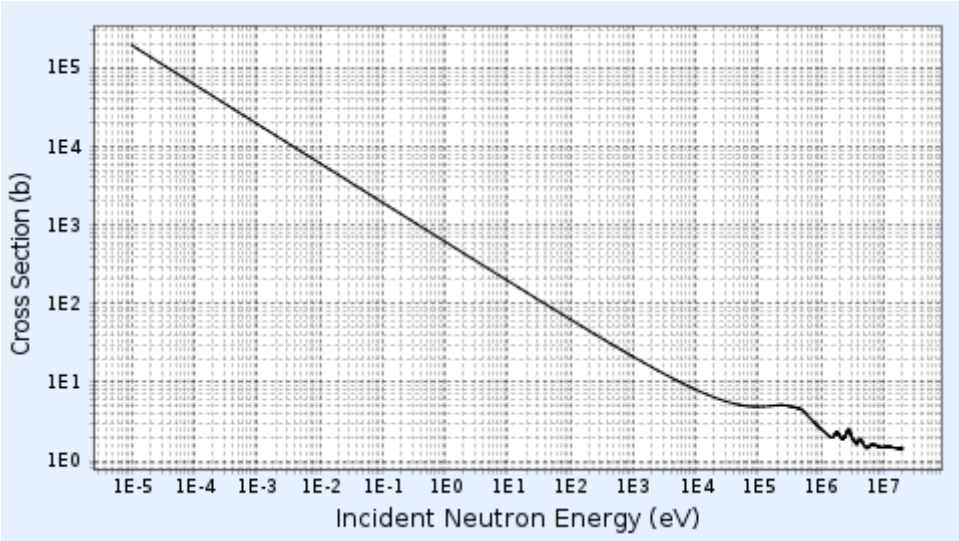

Figure. 3.12. ^{10}B (n,α) capture cross section[50].

A range of 0 to 400 ppm natural boron was randomly sampled for decreases from the base case and a range of 600 to 1000 ppm natural boron was randomly sampled for increases in boron concentration from the base case. In real reactors, boron concentration is not constant and follows what is called a 'let down curve' over each cycle. More detailed simulations could be performed taking this into account or varying the shape of the let-down curve.

3.5.2.4 Burnup, Power Level, and Power Cycle

Burnup is one of the most frequently used and discussed fuel history parameters. Burnup is a measurement of the amount of energy produced by the fuel per mass of fuel, often provided in units of MWd/MTU. Since many of the visible photon signatures are from fission products, higher burnup fuel will generally have stronger photon signatures. Burnup is a function of both power level and power cycle, as shown in Eq. 3.2, where

BU is burnup in Wd/MTU, p is the specific power in W/g, and d is the number of days in the reactor. If there are multiple cycles at different specific power levels, the burnup of each burn cycle can be calculated with Eq. 3.2 and then added together.

$$BU = p \cdot d \tag{3.2}$$

This means that unlike the other fuel parameters, burnup is not a quantity that can be changed on its own. In order to obtain a different burnup, fuel needs to be exposed to a different power level, a different power cycle, or both for given fissile content enrichment. There are also multiple combinations of power level and power cycle that will lead to the same burnup.

For these simulations, burnup was considered a function of power level and fuel history. Burnup was not a parameter that was tweaked on its own; rather power level and power history were perturbed independently as two separate parameters.

Power level is directly proportional to neutron flux in a reactor. A higher power level, or neutron flux, will cause nuclides to build up and decay faster because fissions are occurring more rapidly. In some cases, such as fission, these results will only show up as a change in burnup: two cases with the same burnup but different power levels will have negligible difference in number of fissions. Only some neutron interactions, such as radiative capture, are dependent on neutron flux aside from burnup effects. Nuclides with production paths that include these interactions can be affected by power level changes even if burned to the same burnup. In some nuclides, such as ^{154}Eu, changes in power level

will change the relative importance of different production and decay mechanisms. Some nuclides reach an equilibrium based on production through one mechanism and decay through another, often fission and radiative capture, respectively. If one of these mechanisms (i.e. radiative capture) is dependent on the neutron flux, a change in power level will affect the equilibrium level this nuclide reaches in the core. For these nuclides, such as ^{144}Ce, if it can be assumed that the last burn cycle was long enough to reach equilibrium and the cooling time is known, the power of the last cycle could be determined. Many nuclides, such as ^{137}Cs, should have no change in concentration based on power level because they are neither produced nor removed through any mechanisms depending on neutron flux.

Specific power level was randomly chosen in the range of 15 to 30 W/g for decreases in specific power level from the base case and in the range of 36 to 45 W/g for increases in specific power level from the base case. In order to separate effects due to changes in specific power level from effects due to changes in burnup, two more cases were run with a specific power level of 33 W/g but with shorter or longer burn cycles to reach the burnups of the two previous cases.

The other main cause of changes in power history is the operation cycle – the combination and arrangement of days during which the reactor is at full power and shut down. Total days of shutdown was used as the second metric for this case. In addition to the base case of three cycles with 20 days shutdown between each cycle, another common case was chosen in which the assembly is in the reactor for two cycles, out for one cycle, and then in for a third burnup cycle. The third chose case also had the assembly out of the

reactor for one cycle between the second and third operating cycles, but had shutdown periods of 70 days rather than 20 days between cycles. These three cases had 40, 505, and 655 total days shutdown.

3.5.2.5 Cooling Time

Cooling time is the amount of time between the fuel being discharged from the reactor and a measurement being taken. Cooling time often has a very predictable effect on isotopic concentrations. Since unstable isotopes decay with a constant half-life, one simple equation can be used to calculate how quickly any given unstable isotope will decay. This equation is shown in Eq. 3.3, where N_0 is the initial quantity of a given isotope at the time of discharge from the reactor, N is the quantity of that isotope at cooling time t, and λ is the decay constant of that isotope. This equation works very well for calculating how some isotopes will depend on cooling time, including ^{137}Cs, ^{134}Cs, ^{154}Eu, ^{155}Eu, ^{106}Ru, ^{125}Sb, ^{110m}Ag, and ^{144}Ce.

$$N = N_0 \cdot e^{-\lambda t} \tag{3.3}$$

The U and Pu x-rays are a slightly different case because they provide a photon signature even though they mostly have half-lives that are long enough to be considered stable even for the longest cooling times considered here. ^{241}Pu is the one exception to this with a half-life of 14.4 years. This means that while the U x-ray will be effectively

independent of cooling time, the Pu x-ray signal will have a slight dependence on cooling time, but it will depend on the isotopic abundance of ^{241}Pu.

Some isotopes are built up in fuel after discharge from the reactor instead of decaying if they are a daughter product of another fission product. This is the case for both ^{241}Am and ^{155}Gd. They are produced according to Eq. 3.4, where in addition to the variables from Eq. 3.3, N_0^P is the initial quantity of the parent isotope at the time of discharge from the reactor and λ^P is the half-life of the parent isotope.

$$N = N_0 \cdot e^{-\lambda t} + N_0^P \cdot \left(1 - e^{-\lambda^P t}\right) \tag{3.4}$$

The half-lives of the isotopes investigated in these simulations are provided in Table 3.3. Each simulation case was burned to the final burnup and then several cooling time steps were performed so that every case has isotopic concentrations for several cooling times. The cooling time values simulated were 1, 2, 5, 10, 20, 50, 80, and 100 years. The cooling time values of 1, 5, 20, and 80 years were specifically chosen for comparison with the NGSI Spent Fuel Library.

3.6 MONTEBURNS Sensitivity Simulation Results

First, the base case was run ten times with different seeds – or starting random number values. These results were used to compile estimated statistical uncertainties from the MONTEBURNS code, since MONTEBURNS provides no statistical error results.

Next, each input parameter chosen for analysis with MONTEBURNS was perturbed individually, once above and once below the base case value. For these simulations, the changed input parameter was the only difference between each simulation and the base case – all other values were held constant. These results were compiled into tables for each input parameter, as shown in Table 3.5 for initial enrichment, Table 3.6 for moderator density, Table 3.7 for boron concentration, and Table 3.9 for specific power level. A larger value for one of these sensitivity coefficients means that the concentration of that isotope changes more drastically in the range of the parameter specified. Comparisons between different parameters are not necessarily meaningful, since the ranges of each parameter are not comparable.

3.6.1 MONTEBURNS Statistical Error Analysis

Since no statistical errors are provided in the code output, a statistical test was performed along with the MONTEBURNS simulations. In order to analyze the statistical uncertainty, the base case was run ten times with different seed values. The one sigma standard deviations for the concentrations of each isotope are provided in Table 3.4.

As expected, some of the isotopes had higher variations than others. This variation is largely a result of both the simplicity of each signature's build up and decay and the quantity of each signature in the fuel. These percentage standard deviations are used for statistical analysis for all following MONTEBURNS results.

Table 3.4. MONTEBURNS statistical variations

signature	σ (%)
U	1.65E-14
Pu	0.15
^{134}Cs	0.65
^{137}Cs	0.07
^{154}Eu	0.44
^{155}Eu	0.47
^{106}Ru	0.22
^{125}Sb	0.13
^{144}Ce	0.16

There are several sources of potential error in these simulations. They include the statistical error inherent in a Monte Carlo calculation as well as model uncertainty, cross section and other input data uncertainty, and measurement uncertainty. This study is looking only at relative changes, not absolute quantities of material. This makes most uncertainties other than statistical error less important, since they would likely affect all simulations equally.

3.6.2 Sensitivity Analysis

Each of the first four fuel parameters (initial enrichment, moderator density, boron concentration, and power level) was perturbed up and down from the base case randomly within the selected ranges.

For sensitivity to initial enrichment, 2.7% and 4.3% initial enrichments were selected for comparison to the base case which had 4% initial enrichment. These

simulations all had the same power level and power history, and so also had the same burnup. The results of these simulations are shown in Table 3.5. The errors shown in Table 3.5 and the following similar tables are the product of the grams of material and the computational standard deviation from MONTEBURNS listed in Table 3.4. The percent change listed in Table 3.5 is calculated as the change in grams of material between the cases where initial enrichment was perturbed up and down divided by the grams of material present in the base case, as shown in Eq. 3.5, where c_i^x is the concentration of signature i at initial enrichment value x wt.% ^{235}U. A positive percent change means that the element or nuclide concentration increases with an increase in initial enrichment, while a negative percent change means the opposite.

$$\frac{c_i^{4.3} - c_i^{2.7}}{c_i^{4.0}} \tag{3.5}$$

Table 3.5. Initial Enrichment Sensitivity Simulation Results

Signature	4.3% i.e.		4% i.e.		2.7% i.e.		% change
	Grams	σ	Grams	σ	Grams	σ	
U	4.56E+01	7.53E-15	4.56E+01	7.53E-15	4.56E+01	7.53E-15	0.01
Pu	5.06E-01	7.72E-04	5.08E-01	7.75E-04	5.10E-01	7.77E-04	-0.71
^{134}Cs	1.54E-03	9.96E-06	1.59E-03	1.03E-05	1.82E-03	1.18E-05	-17.68
^{137}Cs	6.84E-02	5.04E-05	6.85E-02	5.04E-05	6.90E-02	5.08E-05	-0.81
^{154}Eu	1.29E-03	5.65E-06	1.30E-03	5.68E-06	1.34E-03	5.88E-06	-4.03
^{155}Eu	2.91E-04	1.38E-06	2.98E-04	1.41E-06	3.36E-04	1.59E-06	-15.30
^{155}Gd	2.99E-04	1.45E-06	3.07E-04	1.48E-06	3.44E-04	1.66E-06	-14.56
^{106}Ru	2.34E-04	5.11E-07	2.46E-04	5.37E-07	3.10E-04	6.76E-07	-30.66
^{125}Sb	2.03E-04	2.71E-07	2.08E-04	2.78E-07	2.36E-04	3.15E-07	-15.93
^{144}Ce	1.63E-04	2.68E-07	1.61E-04	2.65E-07	1.53E-04	2.52E-07	6.07

As expected from the fission yield data in Table 3.3 and associated description of isotope production following that table, ^{155}Eu, ^{125}Sb, and ^{106}Ru are some of the signatures with the highest percentage change due to initial enrichment. ^{110m}Ag is not capable of being tracked in MONTEBURNS, so there are no results for this signature available. One of ^{155}Eu's main production paths is through fission, and it has a cumulative fission yield from ^{239}Pu that is 5 times the cumulative fission yield from ^{235}U. Since ^{155}Gd in the measured fuel is mostly created as a daughter product from ^{155}Eu, it makes sense that the percent change of those two signatures would be similar. Even though the change in these isotopes is mainly due to a difference in U/Pu fissions, the Pu concentration has less than

a 1% change. This is because of competing effects between more Pu being produced because there was more ^{238}U and more Pu being removed by fission because there was less ^{235}U.

Also as expected, U and ^{137}Cs have very little dependence on initial enrichment. There is so much ^{238}U that the minor change in ^{235}U is roughly negligible, even aside from the fact that some of the extra ^{235}U in the higher enriched fuel will be burned out. ^{137}Cs is expected to be only a function of burnup, which is constant in all three of these simulations.

Every signature with a meaningful change other than ^{144}Ce had a negative percent change, which means that these signatures all increased when initial enrichment decreased. This makes sense for ^{155}Eu, ^{155}Gd, ^{125}Sb, and ^{106}Ru because their dependence on initial enrichment stems from having a higher production yield from Pu fissions, and there will be more Pu fissions in fuel with equal burnup but a lower initial enrichment.

For changes in moderator density, the two moderator density values selected were 0.785 g/cc and 0.672 g/cc, in comparison to the base case which had 0.715 g/cc water. The results of these simulations are shown in Table 3.6. These simulations all had the same power level and power history because these are separate inputs into the MONTEBURNS input decks, and so also had the same burnup. In reality, changing the moderator density drastically would have an effect on power level. The percent change listed in Table 3.6 is calculated as the change in grams of material between the cases where moderator density was perturbed up and down divided by the grams of material present in the base case, as shown in Eq. 3.6, where c_i^x is the concentration of signature i at moderator density value

x g/cc. A positive percent change means that the element or nuclide concentration increases with an increase in moderator density, while a negative percent change means the opposite.

$$\frac{c_i^{0.785} - c_i^{0.618}}{c_i^{0.715}} \tag{3.6}$$

Table 3.6. Moderator Density Sensitivity Simulation Results

Signature	0.785 g/cc		0.715 g/cc		0.618 g/cc		% change
	Grams	σ	Grams	σ	Grams	σ	
U	4.57E+01	7.53E-15	4.56E+01	7.53E-15	4.56E+01	7.52E-15	0.21
Pu	4.79E-01	7.30E-04	5.08E-01	7.75E-04	5.61E-01	8.55E-04	-16.19
^{134}Cs	1.55E-03	1.00E-05	1.59E-03	1.03E-05	1.67E-03	1.08E-05	-7.44
^{137}Cs	6.85E-02	5.04E-05	6.85E-02	5.04E-05	6.87E-02	5.06E-05	-0.33
^{154}Eu	1.21E-03	5.29E-06	1.30E-03	5.68E-06	1.48E-03	6.50E-06	-21.30
^{155}Eu	2.91E-04	1.38E-06	2.98E-04	1.41E-06	3.12E-04	1.48E-06	-7.04
^{155}Gd	2.99E-04	1.44E-06	3.07E-04	1.48E-06	3.23E-04	1.56E-06	-7.69
^{106}Ru	2.44E-04	5.31E-07	2.46E-04	5.37E-07	2.52E-04	5.50E-07	-3.42
^{125}Sb	2.03E-04	2.71E-07	2.08E-04	2.78E-07	2.17E-04	2.90E-07	-6.67
^{144}Ce	1.62E-04	2.66E-07	1.61E-04	2.65E-07	1.61E-04	2.66E-07	0.04

As explained in section 4.2.2, a decrease in moderator density causes an increase in resonance and fast energy neutrons and a decrease in thermal neutrons entering the fuel. This increase in higher energy neutrons results in more Pu creation, which is why Pu mass

increases with a decrease in moderator density. Some of the additional Pu formed leads to additional fissions from Pu. This is why the isotopes created mainly by Pu fission, ^{110m}Ag, ^{106}Ru, and ^{125}Sb, show an increase in mass, on a smaller scale than the change in Pu, for a decrease in moderator density as well.

An increase in moderation in an already over moderated system reduces the number of resonance integral neutrons in the system. Since most ^{134}Cs is created by absorptions of resonance integral neutrons in ^{133}Cs, an increase in moderation, and therefore reduction in density of resonance energy neutrons, reduces the amount of ^{134}Cs produced.

It is interesting to note that ^{154}Eu has the strongest dependence on moderator density of all the signatures investigated here. This suggests that one or more of ^{154}Eu's production paths in this occurs more often due to an increase in resonance or fast neutrons. The resonance radiative capture cross-section in ^{153}Eu is about 5 times higher than the thermal radiative capture cross section (1500 and 350, respectively)[52]. ^{153}Eu is also produced twice as often in ^{239}Pu fissions as in ^{235}U fissions. Regardless of the weights of each of these causes, ^{154}Eu's strong dependence on moderator density makes it a good indicator for moderator density in photon measurements.

For changes in boron concentration, the two boron concentration values selected were 868 ppm and 136ppm natural boron, in comparison to the base case which had 500 ppm natural boron. The results of these simulations are shown in Table 3.7. These simulations all had the same power level and power history, and so also had the same burnup. In reality, changing the boron concentration drastically would have an effect on

power level, which could have an effect on burnup. The percent change listed in Table 3.6 is calculated as the change in grams of material between the cases where boron concentration was perturbed up and down divided by the grams of material present in the base case, as shown in Eq. 3.7, where c_i^x is the concentration of signature i at boron concentration value x ppm natural boron. A positive percent change means that the element or nuclide concentration increases with an increase in boron concentration, while a negative percent change means the opposite.

$$\frac{c_i^{868} - c_i^{136}}{c_i^{500}} \tag{3.7}$$

Since boron concentration and moderator density both change the hardness of the neutron spectrum in the reactor, it is not surprising that they have similar effects on almost all of the signatures. Table 3.8 shows the percent change of each signature with a significant percent change over one percent in the moderator density and boron concentration simulations, sorted based on moderator density percent change.

Table 3.7. Boron Concentration Sensitivity Simulation Results

Signature	868 ppm		500 ppm		136 ppm		% change
	Grams	σ	Grams	σ	Grams	σ	
U	4.56E+01	7.52E-15	4.56E+01	7.53E-15	4.57E+01	7.53E-15	-0.13
Pu	5.29E-01	8.06E-04	5.08E-01	7.75E-04	4.84E-01	7.38E-04	8.88
^{134}Cs	1.62E-03	1.05E-05	1.59E-03	1.03E-05	1.55E-03	1.00E-05	4.77
^{137}Cs	6.86E-02	5.05E-05	6.85E-02	5.04E-05	6.84E-02	5.04E-05	0.30
^{154}Eu	1.38E-03	6.05E-06	1.30E-03	5.68E-06	1.22E-03	5.36E-06	11.98
^{155}Eu	3.04E-04	1.44E-06	2.98E-04	1.41E-06	2.93E-04	1.39E-06	3.81
^{155}Gd	3.14E-04	1.51E-06	3.07E-04	1.48E-06	3.01E-04	1.45E-06	4.18
^{106}Ru	2.50E-04	5.45E-07	2.46E-04	5.37E-07	2.43E-04	5.30E-07	2.80
^{125}Sb	2.13E-04	2.84E-07	2.08E-04	2.78E-07	2.03E-04	2.71E-07	4.48
^{144}Ce	1.62E-04	2.66E-07	1.61E-04	2.65E-07	1.61E-04	2.65E-07	0.41

Table 3.8. Comparison of Moderator Density and Boron Sensitivity Results

Signature	Moderator Density % Change	Boron Concentration % Change	Ratio
Eu154	-21.30	11.98	-1.78
Pu	-16.19	8.88	-1.82
Gd155	-7.69	4.18	-1.84
Cs134	-7.44	4.77	-1.56
Eu155	-7.04	3.81	-1.85
Sb125	-6.67	4.48	-1.49
Ru106	-3.42	2.80	-1.22

Comparing magnitudes between moderator density and boron concentration percent changes is difficult because the ranges are not directly comparable. Trends over both lists and the ratio of the two values, however, are valuable because they show relative dependencies. The rankings of these signatures are quite similar for moderator density and boron concentration changes. The ratio of the two percent changes is also fairly constant through all signatures. This implies that changes in moderator density and boron concentration affect spent fuel in roughly the same way through changing the energy spectrum of neutrons in the reactor. This means that unfolding the contributions between moderator density and boron concentration (and likely any other types of power level control such as control rods) will probably not be possible with photon measurements. A combination of these factors could still be used to verify a more extensive fuel history than is currently analyzed be the IAEA for safeguards or rule out possible fuel sources in a forensics situation. It should also be noted that an increase in moderator density has the same type of results as a decrease in boron concentration. This makes sense because both increasing moderator density in an already over-moderated reactor system and decreasing boron concentration soften the neutron spectrum.

For changes in power level, the two power level values selected were 24 W/g and 44.5 W/g, in comparison to the base case which was run at 33 W/g. The results of these simulations are shown in Table 3.9. Since these simulations involved changing power level but keeping the power cycle constant, the main change should be due to the resulting change in burnup. In order to also investigate the specific effect of power level on each of the signatures being considered, two more simulations were run which will be explained

later. The percent change listed in Table 3.9 is calculated as the change in grams of material between the cases where power level (and therefore burnup) was perturbed up and down divided by the grams of material present in the base case, as shown in Eq. 3.8, where c_i^x is the concentration of signature i at power level x W/g. A positive percent change means that the element or nuclide concentration increases with an increase in power level, while a negative percent change means the opposite.

$$\frac{c_i^{44.5} - c_i^{24}}{c_i^{33}} \tag{3.8}$$

Burnup is the only parameter for which every signature changes noticeably. Even bulk U changes by 3% due mainly to the loss of ^{235}U through fission. Every other signature increases with an increase in burnup, which is expected since they are all nonexistent in fresh fuel but are being created while the fuel is in the reactor.

Table 3.9. Power Level Sensitivity Simulation Results

Signature	44.5 W/g		33 W/g		24 W/g		% change
	Grams	σ	Grams	σ	Grams	σ	
U	4.48E+01	7.39E-15	4.56E+01	7.53E-15	4.63E+01	7.64E-15	-3.44
Pu	5.73E-01	8.74E-04	5.08E-01	7.75E-04	4.34E-01	6.62E-04	27.35
^{134}Cs	2.78E-03	1.80E-05	1.59E-03	1.03E-05	8.53E-04	5.53E-06	121.16
^{137}Cs	9.24E-02	6.80E-05	6.85E-02	5.04E-05	5.00E-02	3.68E-05	61.94
^{154}Eu	1.94E-03	8.51E-06	1.30E-03	5.68E-06	7.67E-04	3.37E-06	90.56
^{155}Eu	4.58E-04	2.17E-06	2.98E-04	1.41E-06	1.77E-04	8.40E-07	94.08
^{155}Gd	4.68E-04	2.26E-06	3.07E-04	1.48E-06	1.83E-04	8.85E-07	92.94
^{106}Ru	3.93E-04	8.57E-07	2.46E-04	5.37E-07	1.50E-04	3.27E-07	98.61
^{125}Sb	2.99E-04	3.99E-07	2.08E-04	2.78E-07	1.42E-04	1.90E-07	75.11
^{144}Ce	2.07E-04	3.41E-07	1.61E-04	2.65E-07	1.23E-04	2.03E-07	51.97

In order to separate burnup effects from specific power level effects, two more cases were run in which the specific power level was set back to the base value of 33 W/g, but the lengths of each burn cycle were changed with Eq. 3.2 so that the burnups matched those of the cases in Table 3.9 where specific power level was changed to 44.5 W/g and 24 W/g. The burnups for the previous cases with specific power levels at 44.5 W/g and 24 W/g were 60.7 GWd/MTU and 32.8 GWd/MTU, respectively. To reach these burnups at 33 W/g, the burn cycle lengths were changed from the base case value of 455 days each

(45 GWd/MTU) to 601 days each (60.7 GWd/MTU) and 331 days each (32.8 GWd/MTU). These results are shown in Table 3.10 and Table 3.11.

Table 3.10. First Specific Power Level and Burnup Comparison

Power Level (W/g)	24	33	Ratio
Burnup (GWd/MTU)	32.760	32.769	
U	4.48E+01	4.48E+01	1.00
Pu	5.73E-01	5.72E-01	1.00
^{134}Cs	2.78E-03	2.56E-03	1.08
^{137}Cs	9.24E-02	9.10E-02	1.02
^{154}Eu	1.94E-03	1.90E-03	1.02
^{155}Eu	4.58E-04	4.47E-04	1.02
^{155}Gd	4.68E-04	4.60E-04	1.02
^{106}Ru	3.93E-04	3.33E-04	1.18
^{125}Sb	2.99E-04	2.68E-04	1.11
^{144}Ce	2.07E-04	1.68E-04	1.23

Table 3.11**.** Second Specific Power Level and Burnup Comparison

Power Level (W/g)	44.5	33	Ratio
Burnup (GWd/MTU)	60.74	60.79	
U	4.63E+01	4.63E+01	1.00
Pu	4.34E-01	4.34E-01	1.00
^{134}Cs	8.53E-04	9.24E-04	0.92
^{137}Cs	5.00E-02	5.05E-02	0.99
^{154}Eu	7.67E-04	7.75E-04	0.99
^{155}Eu	1.77E-04	1.80E-04	0.98
^{155}Gd	1.83E-04	1.86E-04	0.99
^{106}Ru	1.50E-04	1.73E-04	0.87
^{125}Sb	1.42E-04	1.56E-04	0.91
^{144}Ce	1.23E-04	1.48E-04	0.83

These simulations show that power level only makes a significant difference to a few isotopes. U, Pu, ^{137}Cs, ^{154}Eu, ^{155}Eu, and ^{155}Gd are unaffected by changes in power level if burnup is held constant. ^{144}Ce is the signature with the strongest dependence on power level, but it is not a linear dependence.

For changes in cooling time, every simulation was aged to cooling times of 0, 1, 2, 5, 10, 20, 50, 80, and 100 years. The fission product results for most of these cooling times (a few were left out for the sake of space) for the base case are shown in Table 3.12. The bulk U and Pu results are shown in Table 3.13. For each isotope, the simulated mass at zero years cooling time was decayed with Eq. 3.3 or 3.4 to obtain the calculated expected mass at each cooling time. The cooling times used for each of these isotopes can be found in Table 3.3. This is what is shown in the 'Calculated' row for each fission product. The 'Calculated/Simulation' row for each isotope shows the ratio of this

calculated value to the simulation results for each cooling time. ^{155}Gd is a special case for cooling time because it stable and is being created by ^{155}Eu rather than decaying away itself. The calculated values for ^{155}Gd were obtained by summing up the ^{155}Eu that had decayed since discharge from the reactor.

Table 3.12. Fission Product Cooling Time Data

Cooling Time [yrs]		0	1	5	10	50	100
^{134}Cs	Calculated [g]	8.51E-03	6.08E-03	1.59E-03	2.96E-04	4.37E-10	2.24E-17
	Calc/Sim	1.00	1.00	1.00	1.00	1.01	1.02
^{137}Cs	Calculated [g]	7.69E-02	7.51E-02	6.85E-02	6.11E-02	2.43E-02	7.67E-03
	Calc/Sim	1.00	1.00	1.00	1.00	1.00	1.00
^{154}Eu	Calculated [g]	1.94E-03	1.79E-03	1.29E-03	8.65E-04	3.43E-05	6.08E-07
	Calc/Sim	1.00	1.00	1.00	1.00	0.99	0.99
^{155}Eu	Calculated [g]	5.99E-04	5.18E-04	2.89E-04	1.40E-04	4.13E-07	2.85E-10
	Calc/Sim	1.00	0.99	0.97	0.94	0.74	0.55
^{155}Gd	Calculated [g]	0.00E+00	8.12E-05	3.10E-04	4.60E-04	5.99E-04	5.99E-04
	Calc/Sim	0.00	0.97	1.01	1.01	0.99	0.99
^{106}Ru	Calculated [g]	7.65E-03	3.88E-03	2.56E-04	8.56E-06	1.34E-17	2.35E-32
	Calc/Sim	1.00	1.01	1.04	1.08	1.46	0.00
^{125}Sb	Calculated [g]	7.21E-04	5.61E-04	2.05E-04	5.84E-05	2.51E-09	8.77E-15
	Calc/Sim	1.00	0.99	0.99	0.98	0.93	0.88
^{144}Ce	Calculated [g]	1.38E-02	5.67E-03	1.62E-04	1.90E-06	6.86E-22	3.41E-41
	Calc/Sim	1.00	1.00	1.01	1.01	0.81	0.00

Cooling time dependence for most fission products is straight forward, and the simple equation used to generate these calculated numbers compared very well to simulation results for ^{134}Cs, ^{137}Cs, ^{154}Eu, and ^{155}Gd. It also did well for ^{106}Ru, ^{125}Sb, and ^{144}Ce out to about 10 years, which is as long as these signatures are likely to be useful.

After this time, they had reached a small enough concentration in the fuel that MONTEBURNS no longer tracked them. The one strange feature in Table 3.12 is the combination of ^{155}Eu and ^{155}Gd data. Even though ^{155}Gd is only calculated as the amount of ^{155}Eu that has decayed since discharge from the reactor, this calculation is very close to the simulated value of ^{155}Gd while the calculated value of ^{155}Eu itself does not match well with the simulated value of ^{155}Eu. ^{155}Gd is generally of more interest to reactor physics codes benchmarks due to its large neutron absorption cross section. If MONTEBURNS has been tested more for ^{155}Gd than ^{155}Eu, then that could explain this anomaly.

Table 3.13. Bulk Uranium and Plutonium Cooling Time Data

Cooling Time [years]	U [g]	Pu [g]	Pu/Pu_0
0	4.56E+01	5.19E-01	1.00
1	4.56E+01	5.21E-01	1.00
2	4.56E+01	5.18E-01	1.00
5	4.56E+01	5.08E-01	0.98
10	4.56E+01	4.95E-01	0.95
20	4.56E+01	4.76E-01	0.92
50	4.56E+01	4.52E-01	0.87
80	4.56E+01	4.44E-01	0.85
100	4.56E+01	4.41E-01	0.85

Table 3.13 shows bulk U and Pu masses as a function of cooling time for the base case simulation. The third column, Pu/Pu_0, shows the ratio of the bulk Pu for that cooling time to the bulk Pu at zero years cooling time. Bulk U does not change to the third

significant digit even to 100 years cooling time, because of the four main U isotopes (234, 235, 236, and 238), the shortest half-life is 245,500 years. Bulk Pu decays slightly, but not with a constant half-life like the fission products in Table 3.12. Only one of the plutonium isotopes, ^{241}Pu, has a half-life of less than 6,500 years. ^{241}Pu has a half-life of 14.4 years, but its percentage of the plutonium vector will change with burnup and power level. This uncertainty in the plutonium vector makes Pu's dependence on cooling time difficult to estimate. One option is to assume a standard Pu vector at discharge from the reactor and use this to calculate plutonium dependence on burnup. In this base case, 15% of the Pu is ^{241}Pu at zero years cooling time. The results of this assumption are shown for the base case in Table 3.14, where the calculated values are obtained using Eq. 3.9. Again, the calculated/simulated values are ratios of the calculated values using Eq. 3.10 to the simulated value in MONTEBURNS. In Eq. 3.10, $Pu(CT)$ is bulk Pu mass as a function of cooling time in years, x is the assumed percentage of ^{241}Pu in bulk Pu (0.15 in this case), Pu_0 is plutonium mass at zero years cooling time, and $\lambda^{^{241}Pu}$ is the decay constant of ^{241}Pu, which is 0.048 yr^{-1}. As future work, this could be refined by coming up with a correlation of the Pu vector with burnup and/or specific power level.

$$Pu(CT) = (1-x)\cdot Pu_0 + x\cdot e^{\left(-\lambda^{^{241}Pu}\cdot CT\right)} \tag{3.9}$$

Table 3.14. Bulk Plutonium Calculation for Base Case Assuming 15% ^{241}Pu.

Cooling Time [years]	Calculated Pu [g]	calc/sim
0	5.19E-01	1.00
1	5.16E-01	0.99
2	5.12E-01	0.99
5	5.03E-01	0.99
10	4.90E-01	0.99
20	4.71E-01	0.99
50	4.48E-01	0.99
80	4.43E-01	1.00
100	4.42E-01	1.00

One of the metrics used to look at power cycle was total days of shutdown. The base case and two cases used to test total days of shutdown are shown in Figure 3.13. The base case and two test cases had 505, 40, and 655 total days of shutdown, respectively.

Figure 3.13. Simulations with different total days shutdown (not to scale).

The results from these simulations are shown in Table 3.15. Since these simulations involved changing only number of days shutdown, they all have the same

burnup. The percent change listed in Table 3.15 is calculated as the change in grams of material between the cases where total days of shutdown was perturbed up and down divided by the grams of material present in the base case, as shown in Eq. 3.10, where c_i^x is the concentration of signature i at x total days shutdown. A positive percent change means that the element or nuclide concentration increases with an increase in total days shutdown, while a negative percent change means the opposite.

$$\frac{c_i^{655} - c_i^{40}}{c_i^{505}} \tag{3.10}$$

Table 3.15. Total Days Shutdown Sensitivity Simulation Results

Signature	40 days shutdown		505 days shutdown		655 days shutdown		% change
	Grams	σ	Grams	σ	Grams	σ	
U	4.56E+01	7.53E-15	4.56E+01	7.53E-15	4.56E+01	7.53E-15	0.00
Pu	5.07E-01	7.72E-04	5.08E-01	7.75E-04	5.08E-01	7.75E-04	-0.32
^{134}Cs	1.76E-03	1.14E-05	1.59E-03	1.03E-05	1.55E-03	1.01E-05	13.03
^{137}Cs	6.99E-02	5.15E-05	6.85E-02	5.04E-05	6.82E-02	5.02E-05	2.48
^{154}Eu	1.31E-03	5.76E-06	1.30E-03	5.68E-06	1.30E-03	5.70E-06	1.07
^{155}Eu	3.01E-04	1.43E-06	2.98E-04	1.41E-06	2.97E-04	1.41E-06	1.54
^{155}Gd	3.09E-04	1.49E-06	3.07E-04	1.48E-06	3.05E-04	1.47E-06	1.33
^{106}Ru	2.95E-04	6.44E-07	2.46E-04	5.37E-07	2.41E-04	5.25E-07	22.14
^{125}Sb	2.41E-04	3.22E-07	2.08E-04	2.78E-07	2.02E-04	2.69E-07	18.84
^{144}Ce	2.05E-04	3.37E-07	1.61E-04	2.65E-07	1.57E-04	2.58E-07	29.74

As expected, the isotopes with the shortest half-lives are the ones that change the most when additional shutdown days are added between cycles. This is because they decay more over an additional 600 days before discharge than isotopes with longer half-lives. Half-lives of each isotope can be found in Table 3.3. The ranking of the four shortest half-lives corresponds directly to the ranking of the four highest sensitivities to total days shut down.

4. CONCLUSIONS AND FUTURE WORK

PNAR and spectral photon measurements were investigated in order to improve the state-of-the-art of nuclear safeguards measurements performed by the IAEA. Spectral photon measurements are useful for determining the operating history of SNF, such as burnup and cooling time. Ratios between different isotopes can be used to reduce dependence on calibration factors. Passive photon measurements are limited by self-shielding to only being able to measure a small portion of a typical SNF assembly (typically from the outer fuel pins). They can provide these operating history parameters to other techniques, such as PNAR. PNAR measures the neutron multiplication of SNM and is sensitive to the bulk fissile content of the entire assembly. If similar fuels are being measured or operating parameters such as those obtained from spectral photon measurements are known, this multiplication can be used to calculate fissile content in the assembly and detect the diversion of a significant quantity of pins from the assembly.

The PNAR concept has been tested on fresh and spent fuel and shown to correlate with neutron multiplication and Pu_{eff} content. Measurements were performed on spent fuel from the Fugen reactor as well as fresh fuel at LANL to assess the capability of the PNAR ratio to predict multiplication and fissile content of SNM. The PNAR detector and these fuels were modeled in MONTEBURNS and MCNPX in order to determine the multiplication of the materials being measured and to benchmark simulations for further investigation of the PNAR technique.

Fugen fuel, a very difficult measurement scenario in comparison to typical PWR fuel measurements, showed a 73% change in signal from a range of 7.1 to 19.2

GWd/MTHM and suggested an ability to measure multiplication with a standard deviation of 1%. Fugen PNAR ratios trended well with Pu_{eff}, with a 77% change in signal and a standard deviation of 4% in plutonium content. It is important to note that these Pu_{eff} values could likely be improved if initial isotopics of the fuel were known rather than relying on calculating MOX isotopics by simulating typical LEU fuel history.

Fresh fuel measurements also showed a direct correlation between neutron multiplication and PNAR ratio. This change in signal was 40-45% from a range of initial enrichment from 0.2% to 3.2% ^{235}U. This change in initial enrichment is relevant because it results in a similar change in neutron multiplication from fresh to spent fuel. Fresh fuel measurements showed that the position of the assembly within the detector has a worst-case effect of 7% on the PNAR signal for ½" water gap and 3% for a ¼" water gap. Fresh fuel measurements also showed that for the 6 cm radius assemblies in these measurements, the distribution of pins has a negligible effect on the measured PNAR ratio, which indicates that PNAR would do well at detecting a diversion of pins. The C/E ratios for the section 1, cadmium covered, and FFM fission chambers were very flat, indicating that the physics of these detectors is being well simulated by the MCNPX simulations. The C/E ratio for the bare fission chambers in section 3 show a slight slope which needs to be investigated further. Future PNAR work includes further measurements to quantify the ability of PNAR to detect pin diversion, and investigate the slope in the C/E ratio for the section 3 bare fission chambers. Experiments should also be performed on typical spent fuel assemblies, such as 17x17 PWR assemblies.

Spectral photon measurements have been obtained from a wide variety of spent nuclear fuel pins using both broad-energy and low-energy HPGe detectors. The spectra obtained from these measurements were analyzed, and 13 isotopic and elemental signatures were identified. These signatures were then simulated in a sensitivity study in order to determine how each one is affected by fuel operating parameters including initial enrichment, power history (power level, days shutdown, burnup, and cooling time), moderator density, and boron concentration. Future work includes further simulations to aid in developing a methodology to use these sensitivities to gather information from spent fuel measurements.

REFERENCES

[1] NEI. *World Statistics*. [20 March 2015]; Available from: http://www.nei.org/Knowledge-Center/Nuclear-Statistics/World-Statistics.

[2] Agency, I.A.E., *Costing of Spent Nuclear Fuel Storage*, in *IAEA Nuclear Energy Series*2009.

[3] *IAEA Statute*, 1957. https://www.iaea.org/about/statute

[4] Chen, J.D., et. al. *Detection of partial defects using a digital cerenkov viewing device*. in *Preparing for future verification challenges: proceedings of an International Safeguards Symposium*. 2010. Vienna.

[5] Nicolaou, G., *Determination of the origin of unknown irradiated nuclear fuel.* Journal of Environmental Radioactivity. **86**(3): p. 313.

[6] Cousinou, P. and e. al., *Taking Burnup Credit into Account in Criticality Studies: the Situation as it is Now and the Prospect for the Future.* Nuclear Engineering and Design, 2001. **208**(2): p. 205-214.

[7] Veal, K.D., et al. *NGSI Program to Investigate Techniques for the Direct Measurement of Plutonium in Spent LWR Fuels by Non-destructive Assay*. in *INMM 51st Annual Conference Proceedings*. 2010. Baltimore, Maryland.

[8] Tobin, S.J., et al., *Technical Cross-cutting Issues for the Next Generation Safeguards Initiative's Spent Fuel Nondestructive Assay Project.* Journal of Nuclear Materials Management, 2012. **40**(3): p. 18-24.

[9] Tobin, S.J., et al., *Next Generation Safeguards Initiative research to determine the Pu mass in spent fuel assemblies: Purpose, approach, constraints, implementation, and calibration.* Nuclear Instruments and Methods in Physics Research Section A: Accelerators, Spectrometers, Detectors and Associated Equipment, October 2011. **652**(1): p. 73-75.

[10] Poston, D.L. and H.R. Trellue, *User's Manual, Version 2.0 for MONTEBURNS Version 2.0*, September 1999.

[11] Pelowitz, D.B., *MCNPX user's manual version 2.5. 0.* Los Alamos National Laboratory, 2005. **76**.

[12] Lebrun, A., et al., *SMOPY a new NDA tool for safeguards of LEU and MOX spent fuel*, 2003, International Atomic Energy Agency Report.

[13] Willman, C. and e. al., *Nondestructive Assay of Spent Nuclear Fuel with Gamma-ray Spectroscopy.* Annals of Nuclear Energy, 2006. **33**: p. 428-429.

[14] Phillips, J.R.e.a., *Application of Nondestructive Gamma-Ray and Neutron Techniques for the Safeguarding of Irradiated Fuel Materials*, May 1980, Los Alamos National Laboratory.

[15] Attas, E.M., J.D. Chen, and G.J. Young, *A Cherenkov Viewing Device for Used-Fuel Verification.* Nuclear Instruments and Methods in Physics Research Section A: Accelerators, Spectrometers, Detectors and Associated Equipment, 1990. **299**(1-3): p. 88-93.

[16] Chen, J.D., et al., *Long-Cooled Spent Fuel Verification Using a Digital Cerenkov Viewing Device,* 2007, International Atomic Energy Agency.

[17] Lebrun, A., et al., *SMOPY a new NDA tool for safeguards of LEU and MOX spent fue*, 2003, International Atomic Energy Agency.

[18] Menlove, H.O., T.D. Reilly, and R. Siebelist. *The Verification of Reactor Operating History Using the Fork Detector*. in *37th Annual INMM Meeting*. July 1996. Naples, Florida.

[19] Rinard, P.M. and G.E. Bosler, *Safeguarding LWR Spent Fuel with the Fork Detector*, in *United States Program for Technical Assistance to IAEA Safeguards*1988, Los Alamos National Laboratory.

[20] Hu, J., et al., *Performance assessment of self-interrogation neutron resonance densitometry for spent nuclear fuel assay.* Nuclear Instruments and Methods in Physics Research Section A: Accelerators, Spectrometers, Detectors and Associated Equipment, 2013. **729**: p. 247-253.

[21] LaFleur, A.M., et al., *Comparison of fresh fuel experimental measurements to MCNPX calculations using self-interrogation neutron resonance densitometry.* Nuclear Instruments and Methods in Physics Research Section A: Accelerators, Spectrometers, Detectors and Associated Equipment, 2012. **680**: p. 168-178.

[22] Menlove, H.O., S. Menlove, and S. Tobin, *Fissile and fertile nuclear material measurements using a new differential die-away self-interrogation technique.* Nuclear Instruments and Methods in Physics Research Section A: Accelerators, Spectrometers, Detectors and Associated Equipment, 2009. **602**(2): p. 588-593.

[23] Kaplan, A.C., et al., *Determination of spent nuclear fuel assembly multiplication with the differential die-away self-interrogation instrument.* Nuclear Instruments

and Methods in Physics Research Section A: Accelerators, Spectrometers, Detectors and Associated Equipment, 2014. **757**: p. 20-27.

[24] Goodsell, A.V., V. Henzl, and M.T. Swinhoe, *Differential Die-Away Instrument: Report on Initial Simulations of Spent Fuel Experiment*, 2014, Los Alamos National Laboratory.

[25] Hu, J., et al., *Developing the Californium Interrogation Prompt Neutron Technique to Measure Fissile Content and to Detect Diversion in Spent Nuclear Fuel Assemblies.* Journal of Nuclear Materials Management, 2012. **40**: p. 49-58.

[26] Richard, J., et al., *Determining the Pu Mass in Low Enriched Uranium Spent-Fuel Assemblies Using Assembly Interrogation Prompt Neutron (AIPN) Detection*, 2010, Los Alamos National Laboratory.

[27] Favalli, A., et al. *On Determination of Initial Enrichment, Burnup, Cooling Time of PWR Spent Fuel Assemblies by Analysis of Passive Gamma Spectra and Neutron Count Rate*. in *Institute of Nuclear Materials Management 53rd Annual Meeting*. 2012.

[28] Fensin, M.L., et al., *Determining the Pu Mass in LEU Spent Fuel Assemblies-Focus on Passive Gamma Detection.* Los Alamos National Laboratory: LA-UR-11-00511 (January 2011), 2010.

[29] Mozin, V., et al., *Delayed Gamma-Ray Spectroscopy for Spent Nuclear Fuel Assay*. Journal of Nuclear Materials Management, 2012. **40**(3): p. 78-87.

[30] Blanc, P., et al., *An Integrated Delayed-neutron Differential Die-away Instrument to Quantify Plutonium in Spent Nuclear Fuel.* JNMM-Journal of the Institute of Nuclear Materials Management, 2012. **40**(3): p. 70.

[31] Croft, S., et al. *Feasibility of classic multiplicity analysis applied to spent nuclear fuel assemblies*. in *52nd Annual Meeting of the Institute of Nuclear Materials Management (INMM), Palm Desert, California*. 2011.

[32] Kulisek, J., et al., *Lead Slowing-Down Spectrometry Time Spectral Analysis for Spent Fuel Assay: FY11 Status Report*. 2011: Pacific Northwest National Laboratory.

[33] Smith, L.E., et al., *Time-spectral analysis methods for spent fuel assay using lead slowing-down spectroscopy.* Nuclear Science, IEEE Transactions on, 2010. **57**(4): p. 2230-2238.

[34] Chichester, D.L. and J.W. Sterbentz, *Neutron resonance transmission analysis (NRTA): initial studies of a method for assaying plutonium in spent fuel*, 2011, Idaho National Laboratory (INL).

[35] Rudy, C., et al. *Determination of Pu in Spent Fuel Assemblies by X-Ray Fluorescence*. in *Institute of Nuclear Materials Managment 46th Annual Meeting*. July 2005. Phoenix, Arizona.

[36] Hoover, A.S., et al. *Measurement of Plutonium in Spent Nuclear Fuel by Self-Induced X-Ray Fluorescence*. in *Institute of Nuclear Materials Management 50th Annual Meeting*. 2009. Tucson, AZ.

[37] Freeman, C., et al. *Feasibility of X-Ray fluorescence for spent fuel safeguards*. in *Proceedings of the 2010 ANS annual meeting, San Diego, California*. 2010.

[38] Hayakawa, T., et al., *Nondestructive assay of plutonium and minor actinide in spent fuel using nuclear resonance fluorescence with laser Compton scattering γ-rays.* Nuclear Instruments and Methods in Physics Research Section A: Accelerators, Spectrometers, Detectors and Associated Equipment, 2010. **621**(1): p. 695-700.

[39] Quiter, B.J., et al., *Nuclear resonance fluorescence for materials assay.* Nuclear Science, IEEE Transactions on, 2011. **58**(2): p. 400-403.

[40] Galloway, J.D., et al., *Design and description of the NGSI spent fuel library with emphasis on the passive gamma signal.* JNMM-Journal of the Institute of Nuclear Materials Management, 2012. **40**(3): p. 25.

[41] Menlove, H.O. and D.H. Beddingfield, *Passive Neutron Reactivity Measurement Technique*, 1997, Los Alamos National Laboratory

[42] Evans, L., et al. *Non-destructive assay of spent nuclear fuel using passive neutron Albedo reactivity*. in *Institute of Nuclear Materials Management 51st Annual Meeting, Baltimore, MD (July 11-16, 2010)*. 2010.

[43] Conlin, J.L. and S. Tobin. *Determining Fissile Content in PWR Spent Fuel Assemblies Using a Passive Neutron Albedo Reactivity with Fission Chambers Technique*. in *INMM 51st Annual Conference Proceedings*. 2010. Baltimore, Maryland.

[44] Freeman, C., et al., *Passive neutron Albedo reactivity with fission chambers* 2011, Los Alamos National Laboratory.

[45] Gerhart, J.J., et al., *Passive Neutron Albedo Reactivity with Fission Chambers.* Journal of Nuclear Materials Management, 2012. **40**(3): p. 45-48.

[46] Conlin, J.L. and S.J. Tobin. *Predicting fissile content of spent nuclear fuel assemblies with the passive neutron Albedo reactivity technique and Monte Carlo code emulation*. in *International Conference on Mathematics and Computational Methods Applied to Nuclear Science and Engineering (M&C 2011), Rio de Janeiro, RJ, Brazil*. 2011.

[47] Hu, J., et al., *Determining Plutonium Mass in Spent Fuel Using 252Cf Interrogation with Prompt Neutron Detection.* 2010.

[48] Willman, C.e.a., *Nondestructive Assay of Spent Nuclear Fuel with Gamma-ray Spectroscopy.* Annals of Nuclear Energy, 2006. **33**: p. 428-429.

[49] Matsson, I., *Developments in gamma scanning irradiated nuclear fuel.* Applied Radiation and Isotopes, 1997. **48**(10-12): p. 1289-1298.

[50] *Korea Atomic Energy Research Institute Table of Nuclides*. 2000 [cited 2012 September 18]; Available from: http://atom.kaeri.re.kr/.

[51] Group, C.S.E.W., *Evaluated Nuclear Data File ENDF/B-VII.0*, B.N. Laboratory, Editor.

[52] Baum, E.M., et al., *Nuclides and isotopes*. 2002, [New York]: KAPL : Lockheed Martin.

[53] Lebrun, A. and G. Bignan, *Non Destructive Assay of Nuclear LEU Spent Fuels for Burnup Credit Application*, Commissariat a l'Energie Atomique CEA.

[54] Chesterman, A.S. and P.A. Clark. Spent Fuel and Residue Measurement Instrumentation at the Sellafield Nuclear Fuel Reprocessing Facility. in *Institute of Nuclear Materials Management 32nd Annual Meeting*. 1995.

[55] Tait, J.C., *Validation of the ORIGEN-S code for predicting radionuclide inventories in used CANDU fuel.* Journal of nuclear materials, 1995. **223**(2): p. 109.

[56] Dennis, M.L., *Feasibility of 106Ru peak measurement for MOX fuel burnup analysis.* Nuclear Engineering and Design, 2010. **240**(10): p. 3687.

[57] Hsue, S.T., et al., *Nondestructive assay methods for irradiated nuclear fuels*. Program for Technical Assistance to IAEA Safeguards. 1978, Los Alamos Scientific Laboratory.

[58] Stafford, A.S., *Spent Nuclear Fuel Self-Induced XRF to Predict Pu to U Content*, in *Nuclear Engineering*2010, Texas A&M University: Texas A&M University.

[59] W.S. Charlton, D.S., A. Stafford, S. Saavedra, A. Hoover, and C. Rudy *The Use of Self-Induced XRF to Quantify the Pu Content in PWR Spent Nuclear Fuel*. in *31st ESARDA Annual Meeting*. May 2009. Vilnius, Lithuania.

[60] *Fugen Advanced Thermal Reactor: R&D and Operational Performance Achievements*, J.N.C.D. Institute, Editor March 2003: Tsuruga, Japan.

[61] Goodsell, A.V., *Flat Quartz-Crystal X-Ray Spectrometer for Nuclear Forensics Applications*, in *Nuclear Engineering*2012, Texas A&M University.

APPENDIX A

MCNPX Input Deck for Fresh Fuel PNAR Measurement

```
PNAR ASSEMBLY 1 319 -- SINRD + PNAR Detector
c
c
*************************************************************
*******
c                              CELL CARDS
c
*************************************************************
*******
c
c
c ----------------- Begin Detector Cells ------------------
--
c Note: #'s <=502 define the FA and the FA region from Holly
Trellue
c       #'s 6XX refer to detectors in section 1
c       #'s 7XX refer to detectors in section 2
c       #'s 8XX refer to detectors in section 3
c       #'s 9XX refer to global detector housing
c
c ----- concentric cylinders around FA -----
c -- FA region ... void for now
c 502 0 -502 imp:n=1
c
c -- Water (or Air) gap between detector & FA
c replace mat 9920 with water (4) or air (3) from Holly's
Fugen FA
c 920 9920 -1.0 #343 -920   imp:n=1
c          710 #711 #712 740 #741 #742 780 #781 #782 imp:n=1
c fill taper (i.e., remove poly) with water
925 9920 -1.0 920 -905  imp:n=1
c
c -- Stainless Steel housing
901 7 -8.03   990 930 925 910 -901   imp:n=1    $ OD
905 7 -8.03   905 -925               imp:n=1    $ taper
910 7 -8.03   920 -910               imp:n=1    $ ID
c
c -- Air gap for SINRD detectors (sec. 3)
```

```
c void for now, use air in Fugen file from Holly (mat 3? or
4?)
930 3 -0.0011455  970 950 -930
                  715 #711 #712 740 #741 #742
                  781 #781 #782 #725 #726 #727  imp:n=1
931 3 -0.0011455  950 -970  523  514
                  740 #741 781 #781 #725 #726 #727  imp:n=1
932 3 -0.0011455  950 -970 -533 -524
                  740 781 #725 #726 #727  imp:n=1
933 3 -0.0011455  950 -970 -513  534
                  740 #742 781 #782 #725 #726 #727   imp:n=1
c
c -- Cd liner for PNAR (see sec. 3)
950  9950 -8.65  910  965 -950            imp:n=1
9501 9950 -8.65  910 -950 960 -965        imp:n=1
951   9950 -8.65   910 -960 -950   521   512 #725 #726 #727
imp:n=1
952   9950 -8.65   910 -960 -950 -531 -522 #725 #726 #727
imp:n=1
953   9950 -8.65   910 -960 -950 -511   532 #725 #726 #727
imp:n=1
c
c fill windows in Cd liner with air
954 3 -0.0011455  910 -950 -960  511 -512     imp:n=1
955 3 -0.0011455  910 -950 -960 -521  522     imp:n=1
956 3 -0.0011455  910 -950 -960  531 -532     imp:n=1
c 957 3 -0.0011455  920 -950 -960  511 -512     imp:n=1
c 958 3 -0.0011455  920 -950 -960 -521  522     imp:n=1
c 959 3 -0.0011455  920 -950 -960  531 -532     imp:n=1
c
c -- Polyethylene region ... verify material & density
990 9990 -0.96  910 925 930 630 #631 #632 830 #831 #832
              -990 imp:n=1
c
c -- Region outside of detector
995 9920 -1.0     -995 901 920          imp:n=1
996 0           920 995 -996 imp:n=1
999 0           996 920                imp:n=0
c -----
c
c ------ section 1, PNAR w/o Cd ------
c ---- hole for FFM ... rotate 120 deg. for 3 FFM's
630 0 -630 fill=630 imp:n=1
631 like 630 but TRCL=931
632 like 630 but TRCL=932
```

```
c
c -- PNAR, no Cd FC
635 9942 -2.7     640      u=630 imp:n=1   $ Al
640 9941 -10.97    650 -640 u=630 imp:n=1   $ U
650 0                -650 u=630 imp:n=1   $ void
c
c ------ section 2, Ion Chambers for PG ------
c ---- hole for IC ... rotate 120 deg. for 3 FFM's
830 0 -830 fill=830 imp:n=1
831 like 830 but TRCL=931
832 like 830 but TRCL=932
c
c -- Ion Chamber
835 9942 -2.7     840      u=830 imp:n=1   $ Al
840 0                -840 u=830 imp:n=1   $ void
c
c ------ section 3, SINRD Gd, Gd+Hf & Cd for PNAR ------
c ---- windows for Gd+Hf
c -- Gd+Hf screen for window 1
510 3 -0.0011455   513 -514  950 -965  #725 #726 #727 imp:n=1
$ Air
515 3 -0.0011455   513 -514  965 -970 #725 #726 #727 imp:n=1
$ Air
c 515 9943 -7.9     513 -514  965 -970  imp:n=1    $ Gd
c -- Gd+Hf screen for window 2
520 3 -0.0011455  -523 524  950 -965 #725 #726 #727 imp:n=1
$ Air
525 3 -0.0011455  -523 524  965 -970 #725 #726 #727 imp:n=1
$ Air
c 525 9943 -7.9     -523 524  965 -970  imp:n=1    $ Gd
c -- Gd+Hf screen for window 3
530 3 -0.0011455  533 -534  950 -965 #725 #726 #727 imp:n=1
$ Air
535 3 -0.0011455  533 -534  965 -970 #725 #726 #727 imp:n=1
$ Air
c 535 9943 -7.9     533 -534  965 -970  imp:n=1    $ Gd
c
c ---- hole for bare FC ... rotate 120 deg. for 3 FFM's
710 0   -715 fill=710 imp:n=1
711 like 710 but TRCL=931
712 like 710 but TRCL=932
c
c -- Bare FC
715 9942 -2.7   720 u=710 imp:n=1   $ Al
720 9941 -10.97  730 -720 u=710 imp:n=1   $ U
```

```
730 0               -730 u=710 imp:n=1   $ void
725 9950 -8.65 711 -712 950 imp:n=1
726 9950 -8.65 713 -714 950 imp:n=1
727 9950 -8.65 716 -717 950 imp:n=1
c
c ---- hole for Cd FC ... rotate 120 deg. for 3 FFM's
740 0   -740 fill=740 imp:n=1
741 like 740 but TRCL=931
742 like 740 but TRCL=932
c
c -- Cd covered FC
745 9950 -8.65  750      u=740 imp:n=1   $ Cd
750 9942 -2.7   760 -750 u=740 imp:n=1   $ Al
760 9941 -10.97  770 -760 u=740 imp:n=1   $ U
770 0               -770 u=740 imp:n=1   $ void
c
c ---- hole for FFM / PNAR w/Cd  ... rotate 120 deg. for 3
FC's
780 0   -781 fill=780 imp:n=1
781 like 780 but TRCL=931
782 like 780 but TRCL=932
c
c -- FFM / PNAR w/Cd Fission Chamber
783 9940 -2.52    784  u=780 imp:n=1       $ B4C
786 9950 -8.65    -784 783 u=780 imp:n=1   $Cd
787 9990 -0.96    -783 782 u=780 imp:n=1   $Poly
784 9942 -2.7     785 -782 u=780 imp:n=1   $ Al
785 9941 -10.97    790 -785 u=780 imp:n=1   $ U
790 0                 -790 u=780 imp:n=1   $ void
c ------------------ End Detector Cells -------------------
--
c AHWR model
c  cell cards
c
104 2 -6.55 -104 105 -920 imp:n=1
107 2 -6.55 -107 108 -920 imp:n=1
110 2 -6.55 -110 111 -920 imp:n=1
113 2 -6.55 -113 114 -920 imp:n=1
116 2 -6.55 -116 117 -920 imp:n=1
119 2 -6.55 -119 120 -920 imp:n=1
201 2 -6.55 -201 202 -920 imp:n=1
204 2 -6.55 -204 205 -920 imp:n=1
207 2 -6.55 -207 208 -920 imp:n=1
210 2 -6.55 -210 211 -920 imp:n=1
213 2 -6.55 -213 214 -920 imp:n=1
```

```
216 2 -6.55 -216 217 -920 imp:n=1
219 2 -6.55 -219 220 -920 imp:n=1
222 2 -6.55 -222 223 -920 imp:n=1
225 2 -6.55 -225 226 -920 imp:n=1
228 2 -6.55 -228 229 -920 imp:n=1
231 2 -6.55 -231 232 -920 imp:n=1
234 2 -6.55 -234 235 -920 imp:n=1
301 2 -6.55 -301 302 -920 imp:n=1
304 2 -6.55 -304 305 -920 imp:n=1
307 2 -6.55 -307 308 -920 imp:n=1
310 2 -6.55 -310 311 -920 imp:n=1
313 2 -6.55 -313 314 -920 imp:n=1
316 2 -6.55 -316 317 -920 imp:n=1
319 2 -6.55 -319 320 -920 imp:n=1
322 2 -6.55 -322 323 -920 imp:n=1
325 2 -6.55 -325 326 -920 imp:n=1
328 2 -6.55 -328 329 -920 imp:n=1
331 2 -6.55 -331 332 -920 imp:n=1
334 2 -6.55 -334 335 -920 imp:n=1
337 2 -6.55 -337 338 -920 imp:n=1
340 2 -6.55 -340 341 -920 imp:n=1
343 2 -6.55 -343 344 -920 imp:n=1
346 2 -6.55 -346 347 -920 imp:n=1
349 2 -6.55 -349 350 -920 imp:n=1
352 2 -6.55 -352 353 -920 imp:n=1
401 2 -6.55 -401 402 -920 imp:n=1
404 2 -6.55 -404 405 -920 imp:n=1
407 2 -6.55 -407 408 -920 imp:n=1
410 2 -6.55 -410 411 -920 imp:n=1
413 2 -6.55 -413 414 -920 imp:n=1
416 2 -6.55 -416 417 -920 imp:n=1
419 2 -6.55 -419 420 -920 imp:n=1
422 2 -6.55 -422 423 -920 imp:n=1
425 2 -6.55 -425 426 -920 imp:n=1
428 2 -6.55 -428 429 -920 imp:n=1
431 2 -6.55 -431 432 -920 imp:n=1
434 2 -6.55 -434 435 -920 imp:n=1
437 2 -6.55 -437 438 -920 imp:n=1
440 2 -6.55 -440 441 -920 imp:n=1
443 2 -6.55 -443 444 -920 imp:n=1
446 2 -6.55 -446 447 -920 imp:n=1
449 2 -6.55 -449 450 -920 imp:n=1
452 2 -6.55 -452 453 -920 imp:n=1
455 2 -6.55 -455 456 -920 imp:n=1
458 2 -6.55 -458 459 -920 imp:n=1
```

```
461 2 -6.55 -461 462 -920 imp:n=1
464 2 -6.55 -464 465 -920 imp:n=1
467 2 -6.55 -467 468 -920 imp:n=1
470 2 -6.55 -470 471 -920 imp:n=1
105 1 -10.48 -105 -920 imp:n=1
108 1 -10.48 -108 -920 imp:n=1
111 1 -10.48 -111 -920 imp:n=1
114 1 -10.48 -114 -920 imp:n=1
117 1 -10.48 -117 -920 imp:n=1
120 1 -10.48 -120 -920 imp:n=1
202 1 -10.48 -202 -920 imp:n=1
205 1 -10.48 -205 -920 imp:n=1
208 1 -10.48 -208 -920 imp:n=1
211 1 -10.48 -211 -920 imp:n=1
214 1 -10.48 -214 -920 imp:n=1
217 1 -10.48 -217 -920 imp:n=1
220 1 -10.48 -220 -920 imp:n=1
223 1 -10.48 -223 -920 imp:n=1
226 1 -10.48 -226 -920 imp:n=1
229 1 -10.48 -229 -920 imp:n=1
232 1 -10.48 -232 -920 imp:n=1
235 1 -10.48 -235 -920 imp:n=1
302 1 -10.48 -302 -920 imp:n=1
305 1 -10.48 -305 -920 imp:n=1
308 1 -10.48 -308 -920 imp:n=1
311 1 -10.48 -311 -920 imp:n=1
314 1 -10.48 -314 -920 imp:n=1
317 1 -10.48 -317 -920 imp:n=1
320 1 -10.48 -320 -920 imp:n=1
323 1 -10.48 -323 -920 imp:n=1
326 1 -10.48 -326 -920 imp:n=1
329 1 -10.48 -329 -920 imp:n=1
332 1 -10.48 -332 -920 imp:n=1
335 1 -10.48 -335 -920 imp:n=1
338 1 -10.48 -338 -920 imp:n=1
341 1 -10.48 -341 -920 imp:n=1
344 1 -10.48 -344 -920 imp:n=1
347 1 -10.48 -347 -920 imp:n=1
350 1 -10.48 -350 -920 imp:n=1
353 1 -10.48 -353 -920 imp:n=1
402 1 -10.48 -402 -920 imp:n=1
405 1 -10.48 -405 -920 imp:n=1
408 1 -10.48 -408 -920 imp:n=1
411 1 -10.48 -411 -920 imp:n=1
414 1 -10.48 -414 -920 imp:n=1
```

```
417 1 -10.48 -417 -920 imp:n=1
420 1 -10.48 -420 -920 imp:n=1
423 1 -10.48 -423 -920 imp:n=1
426 1 -10.48 -426 -920 imp:n=1
429 1 -10.48 -429 -920 imp:n=1
432 1 -10.48 -432 -920 imp:n=1
435 1 -10.48 -435 -920 imp:n=1
438 1 -10.48 -438 -920 imp:n=1
441 1 -10.48 -441 -920 imp:n=1
444 1 -10.48 -444 -920 imp:n=1
447 1 -10.48 -447 -920 imp:n=1
450 1 -10.48 -450 -920 imp:n=1
453 1 -10.48 -453 -920 imp:n=1
456 1 -10.48 -456 -920 imp:n=1
459 1 -10.48 -459 -920 imp:n=1
462 1 -10.48 -462 -920 imp:n=1
465 1 -10.48 -465 -920 imp:n=1
468 1 -10.48 -468 -920 imp:n=1
471 1 -10.48 -471 -920 imp:n=1
601 2 -6.55 -601 imp:n=1
602 2 -6.55 -602 imp:n=1
603 2 -6.55 -603 imp:n=1
900 9920 -1 -922 104 107 110 113 116 119 201 204 207 210 213
216 219 222 225
          228 231 234 301 304 307 310 313 316 319 322 325
328 331 334 337
          340 343 346 349 352 401 404 407 410 413 416 419
422 425 428 83
          431 434 437 440 443 446 449 452 455 458 461 464
467 470 601 602 603
          imp:n=1
902 0 -921 104 107 110 113 116 119 201 204 207 210 213 216
219 222 225
          228 231 234 301 304 307 310 313 316 319 322 325
328 331 334 337
          340 343 346 349 352 401 404 407 410 413 416 419
422 425 428 83
          431 434 437 440 443 446 449 452 455 458 461 464
467 470 601 602 603
          imp:n=1
83  5 -15.1 -83 imp:n=1
c
c    Fill assembly
```

```
c
************************************************************
*****************
c
c  SURFACE CARDS
c
c
************************************************************
*****************
c
c ----------------- Begin Detector Surfaces ---------------
-----
c Note: #'s <=502 define the FA and the FA region from Holly
Trellue
c       #'s 6XX refer to detectors in section 1
c       #'s 7XX refer to detectors in section 2
c       #'s 8XX refer to detectors in section 3
c       #'s 9XX refer to global detector housing
c
c
83 rcc 0 0 9.425 0 0 3.15 0.45
c --------------- Global ---------------
c -- concentric cylinders around FA
901 rcc   0 0 -5       0 0 59.0   26.365      $ Stainless
steel outer OD
905 trc   0 0 44.04    0 0 9.96   6.33 9  $ Stainless steel
taper ID
910 rcc   0 0 -5       0 0 49.04  6.56    $ Stainless steel
inner OD - .23 cm thick
920 rcc   0 0 -11      0 0 133.0   6.33    $ water gap
921 rcc   0 0 70 0 0 52 6.33
922 rcc   0 0 -11 0 0 81 6.33
925 trc   0 0 44.04    0 0 9.96   6.6475  9.3175    $ taper
of detector
930 rcc   0 0 -4.6825  0 0 31.6825 26.135 $ air in section 3
(t=0.23
950 rcc   0 0 -4.6825  0 0 31.6825 6.61 $ Cd liner for PNAR
sec. 3 - 0.5 mm thick
960 rcc   0 0 4.6975   0 0 15.145  7.1275 $ Hf window opening
(see sec. 3)
965 rcc   0 0 4.3975   0 0 15.745  7.1275 $ Hf window screen
(see sec. 3)
c change 970 from Gd foil to Air
970 rcc   0 0 4.3975   0 0 15.745  7.13   $ Gd foil for Gd+Hf
window(see sec. 3)
```

```
990 rcc   0 0 27       0 0 26.6825 19.365 $ PolyEth
995 rpp  -30 30 -30 30 -11 70     $ water
996 rpp  -40 40 -40 40 -15 80   $outside world
c
c -- Planes to define Gd+Hf windows
c - window 1
511 P   0 0 0   0 0 1    .4764  .8792 0    $ edge 1 of window
opening
512 P   0 0 0   0 0 1    .2002  .9798 0    $ edge 2 of window
opening
513 P   0 0 0   0 0 1    .5373  .8434 0    $ edge 1 of Gd+Hf
screen
514 P   0 0 0   0 0 1    .1304  .9914 0    $ edge 2 of Gd+Hf
screen
c - window 2
521 P   0 0 0   0 0 1   -.9996 -.0270 0    $ edge 1 of window
opening
522 P   0 0 0   0 0 1   -.9486 -.3165 0    $ edge 2 of window
opening
523 P   0 0 0   0 0 1   -.9990  .0436 0    $ edge 1 of Gd+Hf
screen
524 P   0 0 0   0 0 1   -.9239 -.3827 0    $ edge 2 of Gd+Hf
screen
c - window 3
531 P   0 0 0   0 0 1    .5232 -.8522 0    $ edge 1 of window
opening
532 P   0 0 0   0 0 1    .7484 -.6633 0    $ edge 2 of window
opening
533 P   0 0 0   0 0 1    .4617 -.8870 0    $ edge 1 of Gd+Hf
screen
534 P   0 0 0   0 0 1    .7934 -.6088 0    $ edge 2 of Gd+Hf
screen
c
c ------------------------------------------------------------
---
c                          SECTION 1
c ------------------------------------------------------------
---
c -- concentric cylinders for PNAR FC, no Cd  (OD's)in section
1
c    cylinders centered at a radial distance of 10.57cm from
z-axis
630  rcc  0  10.57  41.13   0  0  11.52  1.2700    $ Aluminum
640  rcc  0  10.57  45.13   0  0   6.35  1.1700    $ 0.8um
U235
```

```
650  rcc  0  10.57  45.13   0  0   6.35  1.169867   $ Void
c
c ------------------------------------------------------------
---
c                          SECTION 2
c ------------------------------------------------------------
---
c -- concentric cylinders for Ion Chamber (OD's)in section 2
c    cylinders centered at a radial distance of 8.0cm from
z-axis
830 rcc   0 -8.0 32.0   0 0 6.2   1.2700    $ Al
840 rcc   0 -8.0 32.1   0 0 6.0   1.16992   $ Void
c 830 rcc   5.1423 6.1284 32.0   0 0 6.2   1.2700    $ Al
c 840 rcc   5.1423 6.1284 32.1   0 0 6.0   1.169867   $ Void
c
c ------------------------------------------------------------
---
c                          SECTION 3
c ------------------------------------------------------------
---
c -- concentric cylinders for Gd+Hf FC's (OD's)in section 3
c    cylinders centered at a radial distance of 8.4cm from
z-axis
715 rcc   5.402 -6.437 6.555   0 0 11.55   1.2700   $ Al
720 rcc   5.402 -6.437 7.825   0 0  6.35   1.1700   $ 0.8um
U235
730 rcc   5.402 -6.437 7.825   0 0  6.35   1.169867  $ Void
711 rcc   5.000 -6.000 6.555   0 0 11.55   2.0  $Cd inner
712 rcc   5.000 -6.000 6.455   0 0 11.75   2.1  $cd outer
713 rcc   2.700 7.330 6.555 0 0 11.55 2.0
714 rcc   2.700 7.330 6.455 0 0 11.75 2.1
716 rcc   -7.700 -1.330 6.555 0 0 11.55 2.0
717 rcc   -7.700 -1.330 6.455 0 0 11.75 2.1
c
c -- concentric cylinders for Cd covered FC (OD's)in section
3
c    cylinders centered at a radial distance of 8.22cm from
z-axis
740 rcc   -5.2822 -6.296 6.355      0 0 11.95  1.4690    $
2mm Cd (plus liner)
750 rcc   -5.2822 -6.296 6.555     0 0 11.55  1.2700    $ Al
760 rcc   -5.2822 -6.296 7.825      0 0 6.35   1.1700    $
0.8um U235
770 rcc   -5.2822 -6.296 7.825     0 0 6.35   1.169867   $
void
```

```
c
c -- boron carbide & cd
c
c -- concentric cylinders for FFM / PNAR w/Cd FC's (OD's)in
section 3
c    cylinders centered at a radial distance of 12.9cm from
z-axis
781  rcc  0  -12.9  2.730   0  0  19.15   5.0000    $ B4C
782  rcc  0  -12.9  6.555   0  0  11.55   1.2700    $ Aluminum
783  rcc  0  -12.9  4.830   0  0  14.95   3.0000    $ Poly
784  rcc  0  -12.9  4.730   0  0  15.15   3.1       $ cd
785  rcc  0  -12.9  7.825   0  0   6.35   1.1700    $ 0.8um
U235
790  rcc  0  -12.9  7.825   0  0   6.35   1.169867   $ Void
791  py   -11.4
792  py   -11.3
c ------------------ End Detector Surfaces ---------------
-----
c
c    Pellet
104  c/z 0.000 -1.265 0.54
107  c/z 1.096 -0.633 0.54
110  c/z 1.096 0.633 0.54
113  c/z 0.000 1.265 0.54
116  c/z -1.096 0.633 0.54
119  c/z -1.096 -0.632 0.54
201  c/z 0.000 -2.530 0.54
204  c/z 1.265 -2.191 0.54
207  c/z 2.191 -1.265 0.54
210  c/z 2.530 0.000 0.54
213  c/z 2.191 1.265 0.54
216  c/z 1.265 2.191 0.54
219  c/z 0.000 2.530 0.54
222  c/z -1.265 2.191 0.54
225  c/z -2.191 1.265 0.54
228  c/z -2.530 0.000 0.54
231  c/z -2.191 -1.265 0.54
234  c/z -1.265 -2.191 0.54
301  c/z 0.000 -3.795 0.54
304  c/z 1.298 -3.566 0.54
307  c/z 2.439 -2.907 0.54
310  c/z 3.287 -1.898 0.54
313  c/z 3.737 -0.659 0.54
316  c/z 3.737 0.659 0.54
319  c/z 3.287 1.898 0.54
```

```
322  c/z 2.439 2.907 0.54
325  c/z 1.298 3.566 0.54
328  c/z 0.000 3.795 0.54
331  c/z -1.298 3.566 0.54
334  c/z -2.439 2.907 0.54
337  c/z -3.287 1.898 0.54
340  c/z -3.737 0.659 0.54
343  c/z -3.737 -0.659 0.54
346  c/z -3.287 -1.898 0.54
349  c/z -2.439 -2.907 0.54
352  c/z -1.298 -3.566 0.54
401  c/z 0.930 -4.974 0.54
404  c/z 2.115 -4.597 0.54
407  c/z 3.172 -3.942 0.54
410  c/z 4.038 -3.049 0.54
413  c/z 4.660 -1.972 0.54
416  c/z 5.000 -0.776 0.54
419  c/z 5.038 0.467 0.54
422  c/z 4.772 1.682 0.54
425  c/z 3.843 3.292 0.54
428  c/z 2.924 4.130 0.54
431  c/z 1.828 4.718 0.54
434  c/z 0.622 5.022 0.54
437  c/z -0.622 5.022 0.54
440  c/z -1.828 4.718 0.54
443  c/z -2.924 4.130 0.54
446  c/z -3.843 3.292 0.54
449  c/z -4.772 1.682 0.54
452  c/z -5.038 0.467 0.54
455  c/z -5.000 -0.776 0.54
458  c/z -4.660 -1.972 0.54
461  c/z -4.038 -3.049 0.54
464  c/z -3.172 -3.942 0.54
467  c/z -2.115 -4.597 0.54
470  c/z -0.930 -4.974 0.54
105  c/z 0.000 -1.265 0.4255
108  c/z 1.096 -0.633 0.4255
111  c/z 1.096 0.633 0.4255
114  c/z 0.000 1.265 0.4255
117  c/z -1.096 0.633 0.4255
120  c/z -1.096 -0.632 0.4255
202  c/z 0.000 -2.530 0.4255
205  c/z 1.265 -2.191 0.4255
208  c/z 2.191 -1.265 0.4255
211  c/z 2.530 0.000 0.4255
```

```
214  c/z 2.191 1.265 0.4255
217  c/z 1.265 2.191 0.4255
220  c/z 0.000 2.530 0.4255
223  c/z -1.265 2.191 0.4255
226  c/z -2.191 1.265 0.4255
229  c/z -2.530 0.000 0.4255
232  c/z -2.191 -1.265 0.4255
235  c/z -1.265 -2.191 0.4255
302  c/z 0.000 -3.795 0.4255
305  c/z 1.298 -3.566 0.4255
308  c/z 2.439 -2.907 0.4255
311  c/z 3.287 -1.898 0.4255
314  c/z 3.737 -0.659 0.4255
317  c/z 3.737 0.659 0.4255
320  c/z 3.287 1.898 0.4255
323  c/z 2.439 2.907 0.4255
326  c/z 1.298 3.566 0.4255
329  c/z 0.000 3.795 0.4255
332  c/z -1.298 3.566 0.4255
335  c/z -2.439 2.907 0.4255
338  c/z -3.287 1.898 0.4255
341  c/z -3.737 0.659 0.4255
344  c/z -3.737 -0.659 0.4255
347  c/z -3.287 -1.898 0.4255
350  c/z -2.439 -2.907 0.4255
353  c/z -1.298 -3.566 0.4255
402  c/z 0.930 -4.974 0.4255
405  c/z 2.115 -4.597 0.4255
408  c/z 3.172 -3.942 0.4255
411  c/z 4.038 -3.049 0.4255
414  c/z 4.660 -1.972 0.4255
417  c/z 5.000 -0.776 0.4255
420  c/z 5.038 0.467 0.4255
423  c/z 4.772 1.682 0.4255
426  c/z 3.843 3.292 0.4255
429  c/z 2.924 4.130 0.4255
432  c/z 1.828 4.718 0.4255
435  c/z 0.622 5.022 0.4255
438  c/z -0.622 5.022 0.4255
441  c/z -1.828 4.718 0.4255
444  c/z -2.924 4.130 0.4255
447  c/z -3.843 3.292 0.4255
450  c/z -4.772 1.682 0.4255
453  c/z -5.038 0.467 0.4255
456  c/z -5.000 -0.776 0.4255
```

```
459  c/z -4.660 -1.972 0.4255
462  c/z -4.038 -3.049 0.4255
465  c/z -3.172 -3.942 0.4255
468  c/z -2.115 -4.597 0.4255
471  c/z -0.930 -4.974 0.4255
601  box 0.200 -4.395 -1 0.000 -1.201 0 -0.400 0.000 0 0 0 2
602  box 3.707 2.371 -1 1.040 0.601 0 0.200 -0.346 0 0 0 2
603  box -3.906 2.025 -1 -1.040 0.600 0 0.200 0.346 0 0 0 2
900  rcc 0.0 0.0 -11.0 0.0 0.0 133.0  5.6
c

c
************************************************************
******************
c
c  DATA CARDS
c
c
************************************************************
******************
c
c ----- Fugen FA source -----
c sdef rad=d1   ext=d2   pos=fcel=d3   cel=d4   axs 0 0 1
par=sf   TR 999
sdef rad=d1 ext=d2 pos=0 0 11.0   axs=0 0 1    par=sf
si1 0 0.05
sp1 -21 1
si2 -.15 .15
sp2 0 1
c
c kcode 1000 1.0 100 1100
c ksrc  0 -1.265 30
c       1.096 -0.633 30
c       1.096 0.633 30
c       0 1.265 30
c       -1.096 0.633 30
c       -1.096 -0.633 30
c
nps 5E6
dbcn 101
prdmp -15 -120 1
print
c
c
c ******************************************
```

```
c                      TALLIES
c ****************************************
c
c ----------------------------------
c  SECTION 1
c  FFM (for PNAR NO Cd)
c ----------------------------------
f6404:n   (640<630)
fc6404 FFM Tally, No Cd for PNAR 1 (sec. 1)
fm6404    (-1 9941 -6)
sd6404    1
tf6404    1
fq6404    f m
c
f6414:n  (640<631)
fc6414 FFM Tally, No Cd for PNAR 2 (sec. 1)
fm6414    (-1 9941 -6)
sd6414    1
tf6414    1
fq6414    f m
c
f6424:n  (640<632)
fc6424 FFM Tally, No Cd for PNAR 3 (sec. 1)
fm6424    (-1 9941 -6)
sd6424    1
tf6424    1
fq6424    f m
c
c ----------------------------------
c  SECTION 2
c ----------------------------------
c turn these off, not set up for ion chambers yet
c f864:n   (860<830) (860<831) (860<832) t
c fc864 Ion Chambers tally (sec. 2)
c fm864    (-1 9941 -6)
c sd864    1 1 1 1
c tf864    4
c fq864    f m
c
c ----------------------------------
c  SECTION 3
c  FFM (for PNAR and SINRD WITH Cd)
c ----------------------------------
c  *** Bare 1 ***
f7204:n   (720<710)
```

```
fc7204 Bare Tally for SINRD 1 (sec. 3)
fm7204    (-1 9941 -6)
sd7204    1
tf7204    1
fq7204    f m
c
c  *** Bare 2 ***
f7214:n   (720<711)
fc7214 Bare Tally for SINRD 2 (sec. 3)
fm7214    (-1 9941 -6)
sd7214    1
tf7214    1
fq7214    f m
c
c  *** Bare 3 ***
f7224:n   (720<712)
fc7224 Bare Tally for SINRD 3 (sec. 3)
fm7224    (-1 9941 -6)
sd7224    1
tf7224    1
fq7224    f m
c
c *** Cd 1 ***
f7604:n   (760<740)
fc7604 Cd Tally for SINRD 1 (sec. 3)
fm7604    (-1 9941 -6)
sd7604    1
tf7604    1
fq7604    f m
c
c *** Cd 2 ***
f7614:n   (760<741)
fc7614 Cd Tally for SINRD 2 (sec. 3)
fm7614    (-1 9941 -6)
sd7614    1
tf7614    1
fq7614    f m
c
c *** Cd 3 ***
f7624:n   (760<742)
fc7624 Cd Tally for SINRD 3 (sec. 3)
fm7624    (-1 9941 -6)
sd7624    1
tf7624    1
fq7624    f m
```

```
c
c *** FFM & PNAR w/Cd 1 ***
f7904:n   (785<780)
fc7904 FFM 1 Tally in FC U
fm7904    (-1 9941 -6)
sd7904    1
tf7904    1
fq7904    f m
c f7902:n (781.1<780)
c fc7902 FFM 1 Tally on outside b4c
c e7902  0.00000001 80log 10
c fs7902    781.2 781.3
c sd7902    1 1 1
c c7902     0 1
c tf7902    1
c fq7902    f m
c f7802:n (784.1<780)
c fc7802 FFM 1 Tally on outside cd
c e7802  0.00000001 80log 10
c fs7802    784.2 784.3
c sd7802    1 1 1
c c7802    0 1
c tf7802    1
c fq7802    f m
c f7702:n (783.1<780)
c fc7702 FFM 1 Tally on inside cd
c e7702  0.00000001 80log 10
c fs7702   783.2 783.3
c sd7702    1 1 1
c c7702   0 1
c tf7702    1
c fq7702    f m
c f7602:n (782.1<780)
c fc7602 FFM 1 Tally on Al outside
c e7602  0.00000001 80log 10
c fs7602   782.2 782.3
c sd7602    1 1 1
c tf7602    1
c fq7602    f m
c
c *** FFM & PNAR w/Cd 2 ***
f7914:n   (785<781)
fc7914 FFM Tally for SINRD, PNAR w/Cd 2 (sec. 3)
fm7914    (-1 9941 -6)
sd7914    1
```

```
tf7914    1
fq7914    f m
c f7912:n (781.1<781)
c fc7912 FFM 2 Tally on outside b4c
c e7912  0.00000001 80log 10
c fs7912    781.2 781.3
c sd7912    1 1 1
c c7912  0 1
c f7812:n (784.1<781)
c fc7812 FFM 2 Tally on outside cd
c e7812  0.00000001 80log 10
c fs7812    784.2 784.3
c sd7812    1 1 1
c c7812   0 1
c f7712:n (783.1<781)
c fc7712 FFM 2 Tally on inside cd
c e7712  0.00000001 80log 10
c fs7712   783.2 783.3
c sd7712    1 1 1
c c7712  0 1
c f7612:n (782.1<781)
c fc7612 FFM 1 Tally on Al outside
c e7612  0.00000001 80log 10
c fs7612   782.2 782.3
c sd7612    1 1 1
c
c *** FFM & PNAR w/Cd 3 ***
f7924:n   (785<782)
fc7924 FFM Tally for SINRD, PNAR w/Cd 3 (sec. 3)
fm7924    (-1 9941 -6)
sd7924    1
tf7924    1
fq7924    f m
c f7922:n (781.1<782)
c fc7922 FFM 3 Tally on outside b4c
c e7922  0.00000001 80log 10
c fs7922    781.2 781.3
c sd7922    1 1 1
c c7922  0 1
c f7822:n (784.1<782)
c fc7822 FFM 3 Tally on outside cd
c e7822  0.00000001 80log 10
c fs7822    784.2 784.3
c sd7822    1 1 1
c c7822  0 1
```

```
c f7722:n (783.1<782)
c fc7722 FFM 3 Tally on inside cd
c e7722  0.00000001 80log 10
c fs7722   783.2 783.3
c sd7722    1 1 1
c c7722  0 1
c f7622:n (782.1<782)
c fc7622 FFM 1 Tally on Al outside
c e7622  0.00000001 80log 10
c fs7622   782.2 782.3
c sd7622    1 1 1
c
c
c OPTIMIZE ON TOTAL FISSION RATE
c f4:n (640 640 720 760 760 790 790)
c fm4  (-1 9941 -6)
c sd4   1
c
c  ------------------------------------------------------
-
c                      VARIANCE REDUCTION
c  ------------------------------------------------------
-
c ----- NOT USING VARIANCE REDUCTION for now -----
c CUT:n 2j 0 0
c FCL:n 12j 1 5j 1 6j 1 7j 1 7j 1 6j 1 91j
c WWG 4 0
c WWP:n  5 3 5 0 -1
c
c MESH geom cyl   origin 0 0 -50   axs 0 0 1   vec 0 -1 0
ref 0 0 22
c     imesh 6.999 19.1 50   iints 1 1 7
c     jmesh 40 49.9 94.1 105 145    jints 1 3 1 3 1
c     kmesh 1   kints 1
c  ------------------------------------------------------
-
c
c
*********************************************************
c  MATERIAL CARDS
c
*********************************************************
c
c ----------------- Begin Detector System -----------------
---
```

```
c  Material 9920 is Water
m9920       1001.70c 2.0
            8016.70c 1.0
mt9920      lwtr.60t
c
c Material 9940 is boron carbide (density = 2.52 g/cc)
m9940     5010 0.16
          5011 0.64
          6000. 0.2
          nlib=.70c
c Material 9939 is enriched boron (natural density around
2.4 g/cc)
m9939     5010 0.9
          5011 0.1
          nlib=.70c
c  Material 9941 is UO2 in FC (density = 10.97 g/cc)
m9941     92234 -0.008899
          92235 -0.820161
          92236 -0.003794
          92238 -0.047356
           8016 -0.119781
          nlib=.70c
c
c  Material 9942 is Aluminum  (density = 2.70 g/cc)
m9942     13027 1.0
          nlib=.70c
c
c  Material 9943 is NATURAL Gadolinium (density = 7.9 g/cc)
m9943    64152 0.0020
         64154 0.0218
         64155 0.1480
         64156 0.2047
         64157 0.1565
         64158 0.2484
         64160 0.2186
         nlib=.70c
c
c  Material 9949 is NATURAL Hf (density = -13.31 g/cm3)
m9949    72174 0.00162
         72176 0.05206
         72177 0.18606
         72178 0.27297
         72179 0.13629
         72180 0.35100
         nlib=.70c
```

```
c
c  Material 9950 is NATURAL Cadmium (density = 8.65 g/cc)
m9950   48106 0.01250
        48108 0.00890
        48110 0.12490
        48111 0.12800
        48112 0.24130
        48113 0.12220
        48114 0.28730
        48116 0.07490
        nlib=.70c
c
c  Material 9990 is polyethylene (density = 0.96 g/cc)
m9990       1001.70c 2.0
            6000.70c 1.0
mt9990      poly.10t
c  material 9980 is zr2
m9980    8016   0.006796
        24000   0.001743
        26000   0.001623
        28000   0.000772
        40000   0.978381
        50000   0.010686
c
c ----- transformations -----
c -- rotation 1 for detectors
*TR931 0 0 0    120 210 90      30 120 90   90 90 0
c -- rotation 2 for detectors
*TR932 0 0 0   -120 -30 90   -210 -120 90   90 90 0
c -- translation of FA in fuel assembly ... verify trans. <
available gap
c     uncomment only one of the following TR999 cases, for
the desired
c    orientation of the FA in the detector.
*TR999 0 0 0  $ no translation, i.e., centered (full gap) -
- pos. 0
c *TR999 0 1.399 0  $ minimize gap, 0 deg                  -
- pos. 1
c *TR999 0 1.000 0  $ small gap, 0 deg                     -
- pos. 2
c *TR999 0 0.500 0  $ medium gap, 0 deg                    -
- pos. 3
c *TR999 1.2116 0.6995 0  $ minimize gap, 30 deg           -
- pos. 4
```

```
c *TR999 0.8660 0.5000 0  $ small gap, 30 deg             -
- pos. 5
c *TR999 0.4330 0.2500 0  $ medium gap, 30 deg            -
- pos. 6
c *TR999 0.6995 1.2116 0  $ minimize gap, 60 deg          -
- pos. 7
c *TR999 0.5000 0.8660 0  $ small gap, 60 deg             -
- pos. 8
c *TR999 0.2500 0.4330 0  $ medium gap, 60 deg            -
- pos. 9
c ------------------ End Detector System ------------------
---
c    Material cards
c kcode  50000 1.0 30 130
c ksrc   -0.9333  -0.9333
c          -2.6 -3.9
c         0.9333  -0.9333
c          2.6 -3.9
c         -0.9333  0.9333
c          -2.6 3.9
c         0.9333  0.9333
c          2.6 3.9
c
c  zircaloy-2
m2
       40090.70c   -0.5055
       40091.70c   -0.1102
       40092.70c   -0.1685
       40094.70c   -0.1708
       40096.70c   -0.0275
       26054.70c -7.965e-5   26056.70c -0.00123822 26057.70c
-2.835e-5
       26058.70c -3.78e-6
       50112.70c   -0.00014065      50114.70c   -0.00009425
50115.70c -5.22e-5
       50116.70c   -0.00210685       50117.70c   -0.0011136
50118.70c -0.0035119
       50119.70c   -0.0012441        50120.70c   -0.00472555
50122.70c -0.00067135
       50124.70c -0.00083955
       24050.70c   -4.345e-5
       24052.70c   -8.379e-4
       24053.70c   -9.5e-5
       24054.70c   -2.365e-5
       28058.70c   -3.4135e-4
```

```
       28060.70c   -1.305e-4
       28061.70c   -5.65e-6
       28062.70c   -1.795e-5
       28064.70c   -4.55e-6
       72176.70c   -5.206e-6
       72177.70c   -1.8606e-5
       72178.70c   -2.7297e-5
       72179.70c   -1.3629e-5
       72180.70c   -3.51e-5
c
c  Zr2.5Nb
m6
       40090.70c   -0.5016
       40091.70c   -0.1094
       40092.70c   -0.1672
       40094.70c   -0.1695
       40096.70c   -0.0273
       41093.70c   -0.025
c
c   light water
m4    1001.70c  -0.111898     $ Fresh Water
      8016.70c  -0.88597021
      8017.70c  -0.00035524
mt4    lwtr.10t
c  air
m3      6000.70c  -0.000124
        7014.70c  -0.755268
        8016.70c  -0.231781
c        18000.70c  -0.012827
c
c  stainless steel
m7  26054.70c -0.00029225 26056.70c -0.0045877   26057.70c -
0.00010595
      26058.70c -0.0000141  40090.70c -0.50375   40091.70c -
0.109855
      40092.70c -0.167916   40094.70c -0.17017   40096.70c -
0.027415
      50112.70c -0.00015423
      50114.70c -0.00010494 50115.70c -0.00005406  50116.70c
-0.00231186
      50117.70c -0.00122112 50118.70c -0.003851    50119.70c
-0.0013658
      50120.70c -0.00518    50122.70c -0.00073617  50124.70c
-0.00092061
c m1 is 3.19% uranium in the fuel
```

```
m1
       8016.70c   -11.8535
      92234.70c   -0.0240
      92235.70c   -2.8119
      92236.70c   -0.0129
      92238.70c   -84.5611
c m8 is du in the fuel
m8
       8016.70c   -11.8495
      92234.70c   -0.0012
      92235.70c   -0.1763
      92236.70c   -0.0008
      92238.70c   -87.9722
m5
      98252.70c -1
```

APPENDIX B

Photon Sensitivity Simulation Base Case Input Decks

MCNPX Input file:

```
julia eigenbrodt fuel pin sensitivity simulations BASE
10    10 -10.02      -10  3 -4             imp:n=1 $region 1
11    11 -10.02  +10 -11  3 -4             imp:n=1 $region 2
12    12 -10.02  +11 -12  3 -4             imp:n=1 $region 3
13    13 -10.02  +12 -13  3 -4             imp:n=1 $region 4
14    14 -10.02  +13 -2   3 -4             imp:n=1 $region 5
2     2  -6.55   -1   2  3 -4             imp:n=1 $clad
3     3  -0.7157 -5   6 -7  8  1  3 -4    imp:n=1 $water
999   0          +5:-6:+7:-8:+4:-3        imp:n=0

1     cz   0.475    $Clad OD
2     cz   0.418    $fuel OD
*3    pz   0.0      $bottom
*4    pz  10.0      $top
*5    px   0.6618
*6    px  -0.6618
*7    py   0.6618
*8    py  -0.6618
10    cz   0.2159
11    cz   0.3238
12    cz   0.3777
13    cz   0.4046

kcode 1000 1.0 30 400
ksrc  0.0 0.0 5.0
m10   92234.72c  -0.000306
      92235.72c  -0.035258
      92236.72c  -0.000162
      92238.72c  -0.845728
       8016.72c  -0.118546
m11   92234.72c  -0.000306
      92235.72c  -0.035258
      92236.72c  -0.000162
      92238.72c  -0.845728
       8016.72c  -0.118546
m12   92234.72c  -0.000306
```

```
       92235.72c  -0.035258
       92236.72c  -0.000162
       92238.72c  -0.845728
        8016.72c  -0.118546
m13    92234.72c  -0.000306
       92235.72c  -0.035258
       92236.72c  -0.000162
       92238.72c  -0.845728
        8016.72c  -0.118546
m14    92234.72c  -0.000306
       92235.72c  -0.035258
       92236.72c  -0.000162
       92238.72c  -0.845728
        8016.72c  -0.118546
m2     40000.66c -98.193
       24000.50c  -0.10
       26000.50c  -0.20
       28000.50c  -0.007
       50000.40c  -1.500
m3     1001.71c    0.667
       8016.71c    0.333
       5010.71c    0.000100
       5011.71c    0.000400
mt3    lwtr.15t
```

Monteburns input file:

```
Calvert Cliffs
UNSU
5                !Number of MCNP Materials to Burn
10               !MCNP Material "m" Numbers
11               !MCNP Material "m" Numbers
12               !MCNP Material "m" Numbers
13               !MCNP Material "m" Numbers
14               !MCNP Material "m" Numbers
1.465334         !Volume of Cells Containing the Materials
1.828899         !Volume of Cells Containing the Materials
1.186895         !Volume of Cells Containing the Materials
0.660927         !Volume of Cells Containing the Materials
0.347061         !Volume of Cells Containing the Materials
0.0016006        !Power in MWt
-200.0           !Q-value for Fission
0                !Total Number of Days Burned
55               !Number of Outer Burn Steps
10               !Number of Inner Burn Steps
1                !Number of Predictor Steps
```

```
0                  !Step to Restart After
pwru               !ORIGEN2 Library
/usr/local/origen-2.2/libs  !Location of ORIGEN2 Library
0.005              !Fractional Importance Limit
0                  !Flag for Intermediate keff Calculations
34                 !Number of Automatic Tally Isotopes
92234.72c
92235.72c
92236.72c
92238.72c
93237.72c
94238.72c
94239.72c
94240.72c
94241.72c
94242.72c
95241.72c
95243.72c
55134.72c
55137.72c
60148.72c
62149.72c
63154.72c
63155.72c
64155.72c
40091.72c
43099.72c
54131.72c
55133.72c
60143.72c
61149.72c
62153.72c
63153.72c
44106.72c
47510.72c
51125.72c
58144.72c
62151.72c
62152.72c
63152.72c
34
92234.72c
92235.72c
92236.72c
92238.72c
```

93237.72c
94238.72c
94239.72c
94240.72c
94241.72c
94242.72c
95241.72c
95243.72c
55134.72c
55137.72c
60148.72c
62149.72c
63154.72c
63155.72c
64155.72c
40091.72c
43099.72c
54131.72c
55133.72c
60143.72c
61149.72c
62153.72c
63153.72c
44106.72c
47510.72c
51125.72c
58144.72c
62151.72c
62152.72c
63152.72c
34
92234.72c
92235.72c
92236.72c
92238.72c
93237.72c
94238.72c
94239.72c
94240.72c
94241.72c
94242.72c
95241.72c
95243.72c
55134.72c
55137.72c

60148.72c
62149.72c
63154.72c
63155.72c
64155.72c
40091.72c
43099.72c
54131.72c
55133.72c
60143.72c
61149.72c
62153.72c
63153.72c
44106.72c
47510.72c
51125.72c
58144.72c
62151.72c
62152.72c
63152.72c
34
92234.72c
92235.72c
92236.72c
92238.72c
93237.72c
94238.72c
94239.72c
94240.72c
94241.72c
94242.72c
95241.72c
95243.72c
55134.72c
55137.72c
60148.72c
62149.72c
63154.72c
63155.72c
64155.72c
40091.72c
43099.72c
54131.72c
55133.72c
60143.72c

61149.72c
62153.72c
63153.72c
44106.72c
47510.72c
51125.72c
58144.72c
62151.72c
62152.72c
63152.72c
34
92234.72c
92235.72c
92236.72c
92238.72c
93237.72c
94238.72c
94239.72c
94240.72c
94241.72c
94242.72c
95241.72c
95243.72c
55134.72c
55137.72c
60148.72c
62149.72c
63154.72c
63155.72c
64155.72c
40091.72c
43099.72c
54131.72c
55133.72c
60143.72c
61149.72c
62153.72c
63153.72c
44106.72c
47510.72c
51125.72c
58144.72c
62151.72c
62152.72c
63152.72c

Monteburns feed file:

```
TimeStep             Feed#PowFr             mat#BeginAndEnd(-
1=previous)RemovalGroup#FractionF.P.Removed
 (i4) (f8.2), (f7.3) (i4)(i4)  grams/day(2f8.1)(i4)(f7.3)
   1   15.00  1.000  10   0     0.0     0.0   0  0.000 0 0.00
0 0.00
                     11   0     0.0     0.0   0  0.000 0 0.00
0 0.00
                     12   0     0.0     0.0   0  0.000 0 0.00
0 0.00
                     13   0     0.0     0.0   0  0.000 0 0.00
0 0.00
                     14   0     0.0     0.0   0  0.000 0 0.00
0 0.00
   2   15.00  1.000  10   0     0.0     0.0   0  0.000 0 0.00
0 0.00
                     11   0     0.0     0.0   0  0.000 0 0.00
0 0.00
                     12   0     0.0     0.0   0  0.000 0 0.00
0 0.00
                     13   0     0.0     0.0   0  0.000 0 0.00
0 0.00
                     14   0     0.0     0.0   0  0.000 0 0.00
0 0.00
   3  425.00  1.000  10   0     0.0     0.0   0  0.000 0 0.00
0 0.00
                     11   0     0.0     0.0   0  0.000 0 0.00
0 0.00
                     12   0     0.0     0.0   0  0.000 0 0.00
0 0.00
                     13   0     0.0     0.0   0  0.000 0 0.00
0 0.00
                     14   0     0.0     0.0   0  0.000 0 0.00
0 0.00
   4   20.00  0.000  10   0     0.0     0.0   0  0.000 0 0.00
0 0.00
                     11   0     0.0     0.0   0  0.000 0 0.00
0 0.00
                     12   0     0.0     0.0   0  0.000 0 0.00
0 0.00
                     13   0     0.0     0.0   0  0.000 0 0.00
0 0.00
                     14   0     0.0     0.0   0  0.000 0 0.00
0 0.00
```

```
   5   15.00  1.000  10   0     0.0     0.0   0  0.000 0 0.00
0 0.00
                     11   0     0.0     0.0   0  0.000 0 0.00
0 0.00
                     12   0     0.0     0.0   0  0.000 0 0.00
0 0.00
                     13   0     0.0     0.0   0  0.000 0 0.00
0 0.00
                     14   0     0.0     0.0   0  0.000 0 0.00
0 0.00
   6   15.00  1.000  10   0     0.0     0.0   0  0.000 0 0.00
0 0.00
                     11   0     0.0     0.0   0  0.000 0 0.00
0 0.00
                     12   0     0.0     0.0   0  0.000 0 0.00
0 0.00
                     13   0     0.0     0.0   0  0.000 0 0.00
0 0.00
                     14   0     0.0     0.0   0  0.000 0 0.00
0 0.00
   7  425.00  1.000  10   0     0.0     0.0   0  0.000 0 0.00
0 0.00
                     11   0     0.0     0.0   0  0.000 0 0.00
0 0.00
                     12   0     0.0     0.0   0  0.000 0 0.00
0 0.00
                     13   0     0.0     0.0   0  0.000 0 0.00
0 0.00
                     14   0     0.0     0.0   0  0.000 0 0.00
0 0.00
   8  495.00  0.000  10   0     0.0     0.0   0  0.000 0 0.00
0 0.00
                     11   0     0.0     0.0   0  0.000 0 0.00
0 0.00
                     12   0     0.0     0.0   0  0.000 0 0.00
0 0.00
                     13   0     0.0     0.0   0  0.000 0 0.00
0 0.00
                     14   0     0.0     0.0   0  0.000 0 0.00
0 0.00
   9   15.00  1.000  10   0     0.0     0.0   0  0.000 0 0.00
0 0.00
                     11   0     0.0     0.0   0  0.000 0 0.00
0 0.00
```

```
                    12   0     0.0     0.0   0  0.000 0 0.00
0 0.00
                    13   0     0.0     0.0   0  0.000 0 0.00
0 0.00
                    14   0     0.0     0.0   0  0.000 0 0.00
0 0.00
  10   15.00  1.000  10   0     0.0     0.0   0  0.000 0 0.00
0 0.00
                    11   0     0.0     0.0   0  0.000 0 0.00
0 0.00
                    12   0     0.0     0.0   0  0.000 0 0.00
0 0.00
                    13   0     0.0     0.0   0  0.000 0 0.00
0 0.00
                    14   0     0.0     0.0   0  0.000 0 0.00
0 0.00
  11  425.00  1.000  10   0     0.0     0.0   0  0.000 0 0.00
0 0.00
                    11   0     0.0     0.0   0  0.000 0 0.00
0 0.00
                    12   0     0.0     0.0   0  0.000 0 0.00
0 0.00
                    13   0     0.0     0.0   0  0.000 0 0.00
0 0.00
                    14   0     0.0     0.0   0  0.000 0 0.00
0 0.00
  12  365.00  0.000  10   0     0.0     0.0   0  0.000 0 0.00
0 0.00
                    11   0     0.0     0.0   0  0.000 0 0.00
0 0.00
                    12   0     0.0     0.0   0  0.000 0 0.00
0 0.00
                    13   0     0.0     0.0   0  0.000 0 0.00
0 0.00
                    14   0     0.0     0.0   0  0.000 0 0.00
0 0.00
  13  365.00  0.000  10   0     0.0     0.0   0  0.000 0 0.00
0 0.00
                    11   0     0.0     0.0   0  0.000 0 0.00
0 0.00
                    12   0     0.0     0.0   0  0.000 0 0.00
0 0.00
                    13   0     0.0     0.0   0  0.000 0 0.00
0 0.00
```

```
                    14   0     0.0     0.0   0  0.000 0 0.00
0 0.00
  14  900.00  0.000  10   0     0.0     0.0   0  0.000 0 0.00
0 0.00
                    11   0     0.0     0.0   0  0.000 0 0.00
0 0.00
                    12   0     0.0     0.0   0  0.000 0 0.00
0 0.00
                    13   0     0.0     0.0   0  0.000 0 0.00
0 0.00
                    14   0     0.0     0.0   0  0.000 0 0.00
0 0.00
  15  195.00  0.000  10   0     0.0     0.0   0  0.000 0 0.00
0 0.00
                    11   0     0.0     0.0   0  0.000 0 0.00
0 0.00
                    12   0     0.0     0.0   0  0.000 0 0.00
0 0.00
                    13   0     0.0     0.0   0  0.000 0 0.00
0 0.00
                    14   0     0.0     0.0   0  0.000 0 0.00
0 0.00
  16  900.00  0.000  10   0     0.0     0.0   0  0.000 0 0.00
0 0.00
                    11   0     0.0     0.0   0  0.000 0 0.00
0 0.00
                    12   0     0.0     0.0   0  0.000 0 0.00
0 0.00
                    13   0     0.0     0.0   0  0.000 0 0.00
0 0.00
                    14   0     0.0     0.0   0  0.000 0 0.00
0 0.00
  17  925.00  0.000  10   0     0.0     0.0   0  0.000 0 0.00
0 0.00
                    11   0     0.0     0.0   0  0.000 0 0.00
0 0.00
                    12   0     0.0     0.0   0  0.000 0 0.00
0 0.00
                    13   0     0.0     0.0   0  0.000 0 0.00
0 0.00
                    14   0     0.0     0.0   0  0.000 0 0.00
0 0.00
  18  900.00  0.000  10   0     0.0     0.0   0  0.000 0 0.00
0 0.00
```

```
                    11   0     0.0     0.0   0  0.000 0 0.00
0 0.00
                    12   0     0.0     0.0   0  0.000 0 0.00
0 0.00
                    13   0     0.0     0.0   0  0.000 0 0.00
0 0.00
                    14   0     0.0     0.0   0  0.000 0 0.00
0 0.00
  19  900.00  0.000  10   0     0.0     0.0   0  0.000 0 0.00
0 0.00
                    11   0     0.0     0.0   0  0.000 0 0.00
0 0.00
                    12   0     0.0     0.0   0  0.000 0 0.00
0 0.00
                    13   0     0.0     0.0   0  0.000 0 0.00
0 0.00
                    14   0     0.0     0.0   0  0.000 0 0.00
0 0.00
  20  900.00  0.000  10   0     0.0     0.0   0  0.000 0 0.00
0 0.00
                    11   0     0.0     0.0   0  0.000 0 0.00
0 0.00
                    12   0     0.0     0.0   0  0.000 0 0.00
0 0.00
                    13   0     0.0     0.0   0  0.000 0 0.00
0 0.00
                    14   0     0.0     0.0   0  0.000 0 0.00
0 0.00
  21  950.00  0.000  10   0     0.0     0.0   0  0.000 0 0.00
0 0.00
                    11   0     0.0     0.0   0  0.000 0 0.00
0 0.00
                    12   0     0.0     0.0   0  0.000 0 0.00
0 0.00
                    13   0     0.0     0.0   0  0.000 0 0.00
0 0.00
                    14   0     0.0     0.0   0  0.000 0 0.00
0 0.00
  22  900.00  0.000  10   0     0.0     0.0   0  0.000 0 0.00
0 0.00
                    11   0     0.0     0.0   0  0.000 0 0.00
0 0.00
                    12   0     0.0     0.0   0  0.000 0 0.00
0 0.00
```

```
                    13   0     0.0     0.0   0  0.000 0 0.00
0 0.00
                    14   0     0.0     0.0   0  0.000 0 0.00
0 0.00
  23  900.00  0.000  10   0     0.0     0.0   0  0.000 0 0.00
0 0.00
                    11   0     0.0     0.0   0  0.000 0 0.00
0 0.00
                    12   0     0.0     0.0   0  0.000 0 0.00
0 0.00
                    13   0     0.0     0.0   0  0.000 0 0.00
0 0.00
                    14   0     0.0     0.0   0  0.000 0 0.00
0 0.00
  24  900.00  0.000  10   0     0.0     0.0   0  0.000 0 0.00
0 0.00
                    11   0     0.0     0.0   0  0.000 0 0.00
0 0.00
                    12   0     0.0     0.0   0  0.000 0 0.00
0 0.00
                    13   0     0.0     0.0   0  0.000 0 0.00
0 0.00
                    14   0     0.0     0.0   0  0.000 0 0.00
0 0.00
  25  900.00  0.000  10   0     0.0     0.0   0  0.000 0 0.00
0 0.00
                    11   0     0.0     0.0   0  0.000 0 0.00
0 0.00
                    12   0     0.0     0.0   0  0.000 0 0.00
0 0.00
                    13   0     0.0     0.0   0  0.000 0 0.00
0 0.00
                    14   0     0.0     0.0   0  0.000 0 0.00
0 0.00
  26  900.00  0.000  10   0     0.0     0.0   0  0.000 0 0.00
0 0.00
                    11   0     0.0     0.0   0  0.000 0 0.00
0 0.00
                    12   0     0.0     0.0   0  0.000 0 0.00
0 0.00
                    13   0     0.0     0.0   0  0.000 0 0.00
0 0.00
                    14   0     0.0     0.0   0  0.000 0 0.00
0 0.00
```

```
  27  900.00  0.000  10   0     0.0     0.0   0  0.000 0 0.00
0 0.00
                     11   0     0.0     0.0   0  0.000 0 0.00
0 0.00
                     12   0     0.0     0.0   0  0.000 0 0.00
0 0.00
                     13   0     0.0     0.0   0  0.000 0 0.00
0 0.00
                     14   0     0.0     0.0   0  0.000 0 0.00
0 0.00
  28  900.00  0.000  10   0     0.0     0.0   0  0.000 0 0.00
0 0.00
                     11   0     0.0     0.0   0  0.000 0 0.00
0 0.00
                     12   0     0.0     0.0   0  0.000 0 0.00
0 0.00
                     13   0     0.0     0.0   0  0.000 0 0.00
0 0.00
                     14   0     0.0     0.0   0  0.000 0 0.00
0 0.00
  29  900.00  0.000  10   0     0.0     0.0   0  0.000 0 0.00
0 0.00
                     11   0     0.0     0.0   0  0.000 0 0.00
0 0.00
                     12   0     0.0     0.0   0  0.000 0 0.00
0 0.00
                     13   0     0.0     0.0   0  0.000 0 0.00
0 0.00
                     14   0     0.0     0.0   0  0.000 0 0.00
0 0.00
  30  900.00  0.000  10   0     0.0     0.0   0  0.000 0 0.00
0 0.00
                     11   0     0.0     0.0   0  0.000 0 0.00
0 0.00
                     12   0     0.0     0.0   0  0.000 0 0.00
0 0.00
                     13   0     0.0     0.0   0  0.000 0 0.00
0 0.00
                     14   0     0.0     0.0   0  0.000 0 0.00
0 0.00
  31  900.00  0.000  10   0     0.0     0.0   0  0.000 0 0.00
0 0.00
                     11   0     0.0     0.0   0  0.000 0 0.00
0 0.00
```

```
                    12   0     0.0     0.0   0  0.000 0 0.00
0 0.00
                    13   0     0.0     0.0   0  0.000 0 0.00
0 0.00
                    14   0     0.0     0.0   0  0.000 0 0.00
0 0.00
  32  900.00  0.000  10   0     0.0     0.0   0  0.000 0 0.00
0 0.00
                    11   0     0.0     0.0   0  0.000 0 0.00
0 0.00
                    12   0     0.0     0.0   0  0.000 0 0.00
0 0.00
                    13   0     0.0     0.0   0  0.000 0 0.00
0 0.00
                    14   0     0.0     0.0   0  0.000 0 0.00
0 0.00
  33  900.00  0.000  10   0     0.0     0.0   0  0.000 0 0.00
0 0.00
                    11   0     0.0     0.0   0  0.000 0 0.00
0 0.00
                    12   0     0.0     0.0   0  0.000 0 0.00
0 0.00
                    13   0     0.0     0.0   0  0.000 0 0.00
0 0.00
                    14   0     0.0     0.0   0  0.000 0 0.00
0 0.00
  34  150.00  0.000  10   0     0.0     0.0   0  0.000 0 0.00
0 0.00
                    11   0     0.0     0.0   0  0.000 0 0.00
0 0.00
                    12   0     0.0     0.0   0  0.000 0 0.00
0 0.00
                    13   0     0.0     0.0   0  0.000 0 0.00
0 0.00
                    14   0     0.0     0.0   0  0.000 0 0.00
0 0.00
  35  900.00  0.000  10   0     0.0     0.0   0  0.000 0 0.00
0 0.00
                    11   0     0.0     0.0   0  0.000 0 0.00
0 0.00
                    12   0     0.0     0.0   0  0.000 0 0.00
0 0.00
                    13   0     0.0     0.0   0  0.000 0 0.00
0 0.00
```

```
                    14   0     0.0     0.0   0  0.000 0 0.00
0 0.00
  36  900.00  0.000  10   0     0.0     0.0   0  0.000 0 0.00
0 0.00
                    11   0     0.0     0.0   0  0.000 0 0.00
0 0.00
                    12   0     0.0     0.0   0  0.000 0 0.00
0 0.00
                    13   0     0.0     0.0   0  0.000 0 0.00
0 0.00
                    14   0     0.0     0.0   0  0.000 0 0.00
0 0.00
  37  900.00  0.000  10   0     0.0     0.0   0  0.000 0 0.00
0 0.00
                    11   0     0.0     0.0   0  0.000 0 0.00
0 0.00
                    12   0     0.0     0.0   0  0.000 0 0.00
0 0.00
                    13   0     0.0     0.0   0  0.000 0 0.00
0 0.00
                    14   0     0.0     0.0   0  0.000 0 0.00
0 0.00
  38  900.00  0.000  10   0     0.0     0.0   0  0.000 0 0.00
0 0.00
                    11   0     0.0     0.0   0  0.000 0 0.00
0 0.00
                    12   0     0.0     0.0   0  0.000 0 0.00
0 0.00
                    13   0     0.0     0.0   0  0.000 0 0.00
0 0.00
                    14   0     0.0     0.0   0  0.000 0 0.00
0 0.00
  39  900.00  0.000  10   0     0.0     0.0   0  0.000 0 0.00
0 0.00
                    11   0     0.0     0.0   0  0.000 0 0.00
0 0.00
                    12   0     0.0     0.0   0  0.000 0 0.00
0 0.00
                    13   0     0.0     0.0   0  0.000 0 0.00
0 0.00
                    14   0     0.0     0.0   0  0.000 0 0.00
0 0.00
  40  900.00  0.000  10   0     0.0     0.0   0  0.000 0 0.00
0 0.00
```

```
                    11   0     0.0     0.0   0  0.000 0 0.00
0 0.00
                    12   0     0.0     0.0   0  0.000 0 0.00
0 0.00
                    13   0     0.0     0.0   0  0.000 0 0.00
0 0.00
                    14   0     0.0     0.0   0  0.000 0 0.00
0 0.00
  41  900.00  0.000  10   0     0.0     0.0   0  0.000 0 0.00
0 0.00
                    11   0     0.0     0.0   0  0.000 0 0.00
0 0.00
                    12   0     0.0     0.0   0  0.000 0 0.00
0 0.00
                    13   0     0.0     0.0   0  0.000 0 0.00
0 0.00
                    14   0     0.0     0.0   0  0.000 0 0.00
0 0.00
  42  900.00  0.000  10   0     0.0     0.0   0  0.000 0 0.00
0 0.00
                    11   0     0.0     0.0   0  0.000 0 0.00
0 0.00
                    12   0     0.0     0.0   0  0.000 0 0.00
0 0.00
                    13   0     0.0     0.0   0  0.000 0 0.00
0 0.00
                    14   0     0.0     0.0   0  0.000 0 0.00
0 0.00
  43  900.00  0.000  10   0     0.0     0.0   0  0.000 0 0.00
0 0.00
                    11   0     0.0     0.0   0  0.000 0 0.00
0 0.00
                    12   0     0.0     0.0   0  0.000 0 0.00
0 0.00
                    13   0     0.0     0.0   0  0.000 0 0.00
0 0.00
                    14   0     0.0     0.0   0  0.000 0 0.00
0 0.00
  44  900.00  0.000  10   0     0.0     0.0   0  0.000 0 0.00
0 0.00
                    11   0     0.0     0.0   0  0.000 0 0.00
0 0.00
                    12   0     0.0     0.0   0  0.000 0 0.00
0 0.00
```

```
                    13   0     0.0     0.0   0  0.000 0 0.00
0 0.00
                    14   0     0.0     0.0   0  0.000 0 0.00
0 0.00
  45  900.00  0.000  10   0     0.0     0.0   0  0.000 0 0.00
0 0.00
                    11   0     0.0     0.0   0  0.000 0 0.00
0 0.00
                    12   0     0.0     0.0   0  0.000 0 0.00
0 0.00
                    13   0     0.0     0.0   0  0.000 0 0.00
0 0.00
                    14   0     0.0     0.0   0  0.000 0 0.00
0 0.00
  46  900.00  0.000  10   0     0.0     0.0   0  0.000 0 0.00
0 0.00
                    11   0     0.0     0.0   0  0.000 0 0.00
0 0.00
                    12   0     0.0     0.0   0  0.000 0 0.00
0 0.00
                    13   0     0.0     0.0   0  0.000 0 0.00
0 0.00
                    14   0     0.0     0.0   0  0.000 0 0.00
0 0.00
  47  150.00  0.000  10   0     0.0     0.0   0  0.000 0 0.00
0 0.00
                    11   0     0.0     0.0   0  0.000 0 0.00
0 0.00
                    12   0     0.0     0.0   0  0.000 0 0.00
0 0.00
                    13   0     0.0     0.0   0  0.000 0 0.00
0 0.00
                    14   0     0.0     0.0   0  0.000 0 0.00
0 0.00
  48  950.00  0.000  10   0     0.0     0.0   0  0.000 0 0.00
0 0.00
                    11   0     0.0     0.0   0  0.000 0 0.00
0 0.00
                    12   0     0.0     0.0   0  0.000 0 0.00
0 0.00
                    13   0     0.0     0.0   0  0.000 0 0.00
0 0.00
                    14   0     0.0     0.0   0  0.000 0 0.00
0 0.00
```

```
  49  950.00  0.000  10   0     0.0     0.0   0  0.000 0 0.00
0 0.00
                     11   0     0.0     0.0   0  0.000 0 0.00
0 0.00
                     12   0     0.0     0.0   0  0.000 0 0.00
0 0.00
                     13   0     0.0     0.0   0  0.000 0 0.00
0 0.00
                     14   0     0.0     0.0   0  0.000 0 0.00
0 0.00
  50  900.00  0.000  10   0     0.0     0.0   0  0.000 0 0.00
0 0.00
                     11   0     0.0     0.0   0  0.000 0 0.00
0 0.00
                     12   0     0.0     0.0   0  0.000 0 0.00
0 0.00
                     13   0     0.0     0.0   0  0.000 0 0.00
0 0.00
                     14   0     0.0     0.0   0  0.000 0 0.00
0 0.00
  51  900.00  0.000  10   0     0.0     0.0   0  0.000 0 0.00
0 0.00
                     11   0     0.0     0.0   0  0.000 0 0.00
0 0.00
                     12   0     0.0     0.0   0  0.000 0 0.00
0 0.00
                     13   0     0.0     0.0   0  0.000 0 0.00
0 0.00
                     14   0     0.0     0.0   0  0.000 0 0.00
0 0.00
  52  900.00  0.000  10   0     0.0     0.0   0  0.000 0 0.00
0 0.00
                     11   0     0.0     0.0   0  0.000 0 0.00
0 0.00
                     12   0     0.0     0.0   0  0.000 0 0.00
0 0.00
                     13   0     0.0     0.0   0  0.000 0 0.00
0 0.00
                     14   0     0.0     0.0   0  0.000 0 0.00
0 0.00
  53  900.00  0.000  10   0     0.0     0.0   0  0.000 0 0.00
0 0.00
                     11   0     0.0     0.0   0  0.000 0 0.00
0 0.00
```

```
                      12   0     0.0     0.0   0  0.000 0 0.00
0 0.00
                      13   0     0.0     0.0   0  0.000 0 0.00
0 0.00
                      14   0     0.0     0.0   0  0.000 0 0.00
0 0.00
  54  900.00  0.000  10   0     0.0     0.0   0  0.000 0 0.00
0 0.00
                      11   0     0.0     0.0   0  0.000 0 0.00
0 0.00
                      12   0     0.0     0.0   0  0.000 0 0.00
0 0.00
                      13   0     0.0     0.0   0  0.000 0 0.00
0 0.00
                      14   0     0.0     0.0   0  0.000 0 0.00
0 0.00
  55  900.00  0.000  10   0     0.0     0.0   0  0.000 0 0.00
0 0.00
                      11   0     0.0     0.0   0  0.000 0 0.00
0 0.00
                      12   0     0.0     0.0   0  0.000 0 0.00
0 0.00
                      13   0     0.0     0.0   0  0.000 0 0.00
0 0.00
                      14   0     0.0     0.0   0  0.000 0 0.00
0 0.00
  0                 ! # of feed specs
  0                 ! # of removal
```